Application of Ultrasound in Regeneration of Adsorbents

by

Hooman Daghooghi-Mobarakeh

A Dissertation Presented in Partial Fulfillment
of the Requirements for the Degree
Doctor of Philosophy

Approved June 2021 by the
Graduate Supervisory Committee:

Patrick E. Phelan, Chair
Ronald Calhoun
Shuguang Deng
Liping Wang
Robert Y. Wang

ARIZONA STATE UNIVERSITY

August 2021

ABSTRACT

Desorption processes are an important part of all processes which involve utilization of solid adsorbents such as adsorption cooling, sorption thermal energy storage, and drying and dehumidification processes and are inherently energy-intensive. Here, how those energy requirements can be reduced through the application of ultrasound for three widely used adsorbents namely zeolite 13X, activated alumina and silica gel is investigated. To determine and justify the effectiveness of incorporating ultrasound from an energy-savings point of view, an approach of constant overall input power of 20 and 25 W was adopted. To measure the extent of the effectiveness of using ultrasound, the ultrasonic-power-to-total power ratios of 0.2, 0.25, 0.4 and 0.5 were investigated and the results compared with those of no-ultrasound (heat only) at the same total power. Duplicate experiments were performed at three nominal frequencies of 28, 40 and 80 kHz to observe the influence of frequency on regeneration dynamics. Regarding moisture removal, application of ultrasound results in higher desorption rate compared to a non-ultrasound process. A nonlinear inverse proportionality was observed between the effectiveness of ultrasound and the frequency at which it is applied. Based on the variation of desorption dynamics with ultrasonic power and frequency, three mechanisms of reduced adsorbate adsorption potential, increased adsorbate surface energy and enhanced mass diffusion are proposed. Two analytical models that describe the desorption process were developed based on the experimental data from which novel efficiency metrics were proposed, which can be employed to justify incorporating ultrasound in regeneration and drying processes.

"An experiment is a question which science poses to Nature, and a measurement is the recording of Nature's answer."

- MAX PLANCK

To Mom and Dad for showing me what love, forgiveness and support truly mean

To Behnaz for her unconditional love and support

ACKNOWLEDGEMENT

The author gratefully acknowledges the invaluable advice and continual guidance of Dr. Patrick Phelan. There is no way I could have accomplished this goal of mine without the support and mentorship I have received from him. Thank you, Pat!

I would also like to thank Dr. Liping Wang, Dr. Robert Wang, Dr. Ronald Calhoun, and Dr. Shuguang Deng for their support and guidance.

TABLE OF CONTENTS

Page

LIST OF TABLES

LIST OF FIGURES

Figure Page

Figure Page

Figure Page

NOMENCLATURE

α	Energy ratio	(-)
α_p	Acoustic attenuation in porous media	dB cm^{-1}
α_s	Acoustic attenuation in solid	dB cm^{-1}
α_v	Acoustic attenuation in void	dB cm^{-1}
σ_{ads}	Adsorption-induced stress	Pa
ε_{ads}	Adsorption-induced strain	(-)
ϵ	Porosity	(-)
δ	Acoustic displacement	
δ_f	Acoustic diffusivity	m^2 s^{-1}
Λ	Mean free path	µm
μ	Dimensionless moisture removed	(-)
ν_g	Kinematic viscosity	m^2 s^{-1}
η	Thermal efficiency	(-)
$\eta_{\Delta t}$	Constant time thermal efficiency	(-)
η_p	Constant power thermal efficiency	(-)
ρ_s	Adsorbent density	kg m^{-3}
θ	Phase angle	Rad
Θ	Surface coverage	(-)
ΔH_{ads}	Enthalpy of desorption	kJ kg^{-1}
$\Delta m_{removed,US}$	Mass of adsorbate removed with ultrasound	g

$\Delta m_{removed,non\ US}$	Mass of adsorbate removed without ultrasound	g
Δt	Time period	s
γ	Surface energy	eV
A	Adsorption Potential	J
A_s	Material specific coefficient	$m^{-3}\ s^4$
b	Klingenberg factor	Pa
C_0	Speed of sound	$m\ s^{-1}$
C_f	Heat capacity rate	$W\ K^{-1}$
C_s	Specific heat capacity	$kJ\ kg^{-1}\ K^{-1}$
D	Grain diameter	m
d	Molecule effective diameter	nm
d_p	Pore diameter	nm
D_{ADM}	Diffusivity of advective-diffusive model	$m^2\ s^{-1}$
D_{app}	Apparent diffusivity	$m^2\ s^{-1}$
D_s	Surface diffusivity	$m^2\ s^{-1}$
$D_{s,\infty}$	Surface diffusivity at infinite temperature	$m^2\ s^{-1}$
D_T	Total diffusivity	$m^2\ s^{-1}$
E_{ac}	Activation energy	J
E	Young modulus	Pa
f_{US}	Ultrasonic frequency	Hz
h_w	Enthalpy	$kJ\ kg^{-1}$
k_0	Intrinsic permeability	m^2

k	Permeability	m^2
k_B	Boltzmann constant	$J\ K^{-1}$
k_n	Knudsen number	(-)
I	Ultrasonic intensity	$W\ m^{-2}$
I_{rms}	Root mean square current	A
MR	Moisture ratio	(-)
m_{dry}	Mass of dry sample	g
$m_{measured}$	Measured mass	g
m_w	Mass of removed moisture	g
P	Pressure	kPa
P_s	Saturation pressure	kPa
P_{total}	Total power	W
P_{TH}	Thermal power	W
P_{US}	Ultrasonic power	W
R	Ideal gas constant	$J\ mol^{-1}\ K^{-1}$
T	Temperature	K
T_{reg}	Regeneration temperature	°C
TH	Thermal	(-)
UDE	Ultrasonic desorption enhancement	(-)
$UDEE$	Ultrasonic desorption efficiency enhancement	(-)
US	Ultrasound	(-)
V_{rms}	Root mean square voltage	V

1. INTRODUCTION

1.1 Motivation

Desiccants consisting of solid porous materials are increasingly gaining attention for various applications including thermal energy storage, adsorption cooling, dehumidification processes, water purification, desalination, and water harvesting [1]–[6]. The inherent temporal and intermittent nature of solar radiation makes thermal energy storage (TES) an essential element in many solar thermal energy systems. In addition, increasing awareness of environmental issues related to thermal systems calls for higher thermal efficiency by utilizing/storing byproduct waste heat. Mainly, there are three types of thermal storage: sensible, latent and sorption. Amongst thermal energy storage systems, sorption thermal storage is more favorable as it has much higher energy storage density compared to the other types of thermal storage, a remarkable temperature rise, and the capability of long-term storage over seasonal variation in ambient temperature [1], [7]–[11]. Additionally, adsorption cooling systems can utilize lower-grade heat than common heat-driven cycles, and incorporate environmentally friendly refrigerants such as H_2O, NH_3, H_2, CO_2, hydrocarbons, etc. [12], [13].

The dehydration of industrial gases is a an essential process to prevent undesired condensation and ice formation, solid hydrate formation, hydrolysis and corrosion [14]–[16]. The dehydration and drying processes of industrial gases such as natural gas, compressed air, nitrogen and oxygen, that is, reducing the water vapor content of the industrial gases to a satisfactory level, are considered energy intensive [17], [18]. It's estimated that about 0.5 Quads of energy was used just for natural gas and compressed air drying in 2019 in the U.S., out of a total industrial primary energy consumption of 32.5

Quads which corresponds to about 1.5% to total industrial primary energy consumption [19], [20].

Currently, industrial gas dehydration is achieved by means of condensation, liquid desiccants, and solid desiccants [16], [21]. Condensation dehydration is achieved either by reducing the temperature of the gas below the dewpoint (saturation temperature corresponding to the desired moisture content) and reheating the gas or by decreasing the pressure using expansion valves (Joule-Thompson effect). Compared to desiccant dehydration, condensation dehydration is the most energy-intensive drying process except for very high gas pressures (> 20 MPa) [21]. Liquid-desiccant dehydration is achieved by bubbling the gas through a liquid that has high affinity for water vapor. The water vapor is removed from the gas by absorption. Liquid desiccants offer the least energy-intensive drying process, however they cannot deliver the 'bone dry' gas required in some applications such as cryogenics. Commercially available liquid desiccants are either highly corrosive such as lithium chloride and lithium bromide, or prone to contamination such as glycols [16], [22]. In addition, there is the major health concern of droplet/vapor carry over associated with dehydration using liquid desiccants [23]. Solid desiccant dehumidification is achieved by passing moist gas through a packed bed containing adsorbent. Since adsorbents have high affinity for water vapor, the water vapor is adsorbed on the surface of the desiccant to a certain degree, after which the material becomes saturated and needs to be regenerated. Solid desiccant dehydration energy intensity is higher than dehydration using liquid desiccants, but much lower than dehydration by condensation [24]. Despite their higher energy intensity, solid desiccants are often preferable to liquid desiccants in

drying processes as they can deliver much higher levels of dryness and require much simpler reactors [14], [15], [25], [26].

One of the significant drawbacks of using desiccant materials in desiccant-integrated systems is the lengthy and energy-inefficient process of regeneration of the material, which calls for novel and more efficient desorption processes instead of conventional regeneration processes namely direct heating and application of hot air [27]. In recent years researchers have attempted to resolve the issue of inefficiencies caused by inadequate heat and mass transfer in desiccant materials by introducing alternative energy sources to assist in the desorption process along with low-grade heating [28], [29]. One such energy source is *ultrasound* [27], [30]–[33]. Ultrasound has been used to not only assist desorption of adsorbates in sorption cooling and dehumidification, but also desorption of many other chemicals as well as the drying of food, clothing and wood [34]–[45]. The use of ultrasound on adsorbents has been recently studied as a means of overcoming insufficient heat and mass transfer during the regeneration of the adsorbents [27], [30], [33]. Conventional heating of adsorbents is the primary contributor to the long time required for regeneration and the energy-consuming nature of the desorption process. In the relatively sparse amount of research available on ultrasonic regeneration, there have been investigations on the effect of the input power and frequency of the sound waves as well as on how the impact of those variables differ under different thermal power input, e.g., regeneration temperature [27], [30], [33]. Zhang et al. [30] investigated the effects of different levels of ultrasonic power and regeneration temperature on moisture removal from silica gel and found that higher ultrasonic power and regeneration temperature results in higher desorption. Zhang et al. [33], on the other hand, investigated the effects of ultrasonic frequency on moisture

removal from silica gel. They reported that with an increase in ultrasonic frequency desorption decreases. These studies have attributed numerous theories on ultrasonic interaction with silica gel for a fundamental explanation as to why desorption is enhanced. But, as discussed later, the fundamental mechanisms behind why the application of ultrasound improves desorption are still not clear.

1.2. Ultrasound

Sound is a form of energy transferred by pressure variations in air, water, or elastic media. Displacement of a particle from its mean path position in a medium leads to sudden alteration in pressure. During restoration of the particle's original position, it passes the disturbance to the other particles. Ultrasound is an oscillating sound pressure wave with a frequency greater than the human hearing range and has wide range of scientific, engineering, industrial, chemical, medical, and biological applications [46]. Ultrasound devices operate with frequencies from 20 kHz up to several gigahertz. Because of its pressure-alternating and displacement-inducing nature, ultrasound can be utilized to enhance mass and heat transfer. Thus, ultrasound is employed in applications that could benefit from microscale transport enhancement. These applications include, but are not limited to systems involving sorption process, heat exchangers, drying, welding and so on [47]–[51].

1.3. Conceptualization of Ultrasound-Enhanced Desorption

In recent years there have been several efforts to conceptualize the principle of ultrasound-enhanced desorption. This improved desorption process can be described using heat and mass transfer governing relations while also incorporating ultrasonication effects into them to analyze this improvement [52].

In the literature, there are several contributing factors cited proposing why improved desorption occurs due to the introduction of an acoustic field, but the most common factor discussed in previous studies is *surface cavitation* [35], [52]–[57]. An illustration of these mechanisms is provided in Fig. 1. The alternating, locally established compressions and rarefactions induced by ultrasound waves at the surface of the adsorbent material subject the solid-gas interface to successive negative and positive pressures.

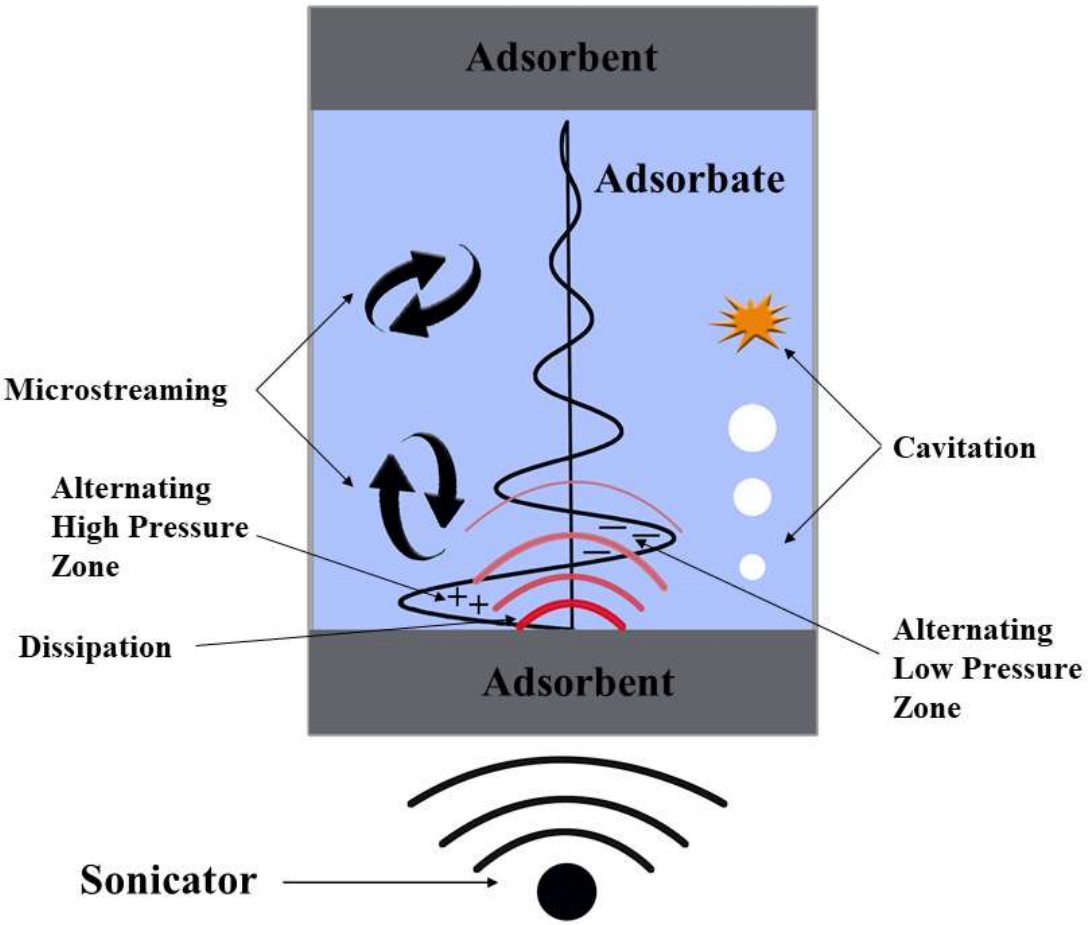

Figure 1. Illustration of the ultrasound-induced mechanisms.

Experimentally, it has been shown that the effect of expansion dominates that of compression at the adsorbent/fluid interface, which results in surface cavitation that breaks

the boundary layer and overcomes the adsorption forces (van der Waals and electrostatic forces) [53].

Another important effect of ultrasound that improves desorption that has been discussed is ultrasonic-induced, locally established partial vacuum. When an adsorbent is under ultrasonic radiation, a pulsating partial vacuum is created at the same frequency as the ultrasonic field that in turn reduces the gas pressure at the gas-solid interface and enhances vapor transport by canceling or prevailing over the present adsorption field and thus promoting surface evaporation [35], [53], [55]. Based on findings from previous studies, another factor shown to play a significant role in ultrasound-assisted desorption is circulating fluid currents. Induced by high-intensity ultrasonic radiation at the adsorbent surface, circulating currents enhance desorption of adsorbate from the surface [58]. The movement of the adsorbate molecules is achieved when acoustic forces dominate the viscous and surface forces allowing molecules to move more freely. This phenomenon is also reported as *microstreaming*, which occurs at the desiccant material surface resulting in a reduction in the diffusion boundary layer hence an increase in diffusion and mass transfer [54].

Another explanation proposed is that the alternating pressure creates local vapor bubbles, which force liquid molecules to move around forming currents [35]. It has also been postulated that the flow of the fluid in porous media is accelerated in an ultrasonic field [35], [59]. Turbulence is another factor contributing to ultrasonic-enhanced desorption.

Turbulence induced at the gas phase will partially reduce the gas pressure and consequently increase the diffusivity at the gas-solid interface [53].

Viscosity and diffusivity are important factors governing the heat and mass transfer and must be considered in any discussion of enhanced desorption. Ultrasonic radiation reduces the adsorbate viscosity, which will have the effect of increasing its diffusivity [60], [61]. The temperature rise due to dissipation of ultrasonic energy is a controversial factor. In some studies, the application of ultrasonic waves has been considered as a contributing factor to enhanced mass transfer, while in others dismissed as a contributing factor compared to others [53], [61].

1.4. Research Objectives

Although utilization of ultrasound in regeneration of adsorbents proved to be beneficial [30], [33], at this point, it seems the precise mechanisms by which ultrasound enhances desorption from porous media are not firmly established [48]. Many theories have been proposed, however some contradict each other, and some appear to be material specific. In addition, ultrasonic-enhanced regeneration hasn't been analyzed from an efficiency point of view. Also, the real-life application of ultrasound-assisted regeneration requires further investigation. This work focuses on addressing the issues mentioned above through realization of the objectives specified below:

- Improve fundamental understanding of solid (adsorbent)/fluid (adsorbent) thermophysics subject to ultrasonication.
- Investigate the effects of ultrasonic variables, i.e. power and frequency, on the regeneration process.
- Investigate the feasibility of ultrasound-assisted regeneration of adsorption pairs from an energy-savings point of view.

- Investigate the effects of ultrasonication on regeneration temperature for low-grade heat utilization through adsorption thermal energy storage, adsorption cooling and drying processes.

2. EXPERIMENTAL SETUP AND PROCEDURE

To investigate the ultrasound-assisted regeneration of adsorption pairs, an experimental setup that could utilize thermal power with or without ultrasound to regenerate adsorbents is designed. The input to the setup is either thermal power or thermal power along with ultrasonic power while the total input power remains constant. Basically, two regenerative variables, i.e. regeneration temperature and mass of desorbed adsorbate, are measured at the same time. The measured temperature and mass of desorbed adsorbate enable the comparison and justification of ultrasound-assisted regeneration versus heat-only regeneration.

2.1. Experimental System Design

The main components of the experimental equipment used in this study are the desorption bed, an ultrasonic transducer, a function generator (Siglent Technologies SDG1032X) , a high frequency-low slew rate amplifier (AALABSYSTEMS A-303), a cartridge heater, and a power supply (PROTEK P6000). A detailed schematic of the experimental setup is shown in Fig. 2. The bed is of hollow cylindrical shape machined out of aluminum 6061 rod. The ultrasonic transducers used are of low-heat piezoceramic type procured from APC INTERNATIONAL. Incorporating a combination of function generator and amplifier instead of fixed power - frequency ultrasonic generator makes it possible to drive the transducer at any desirable power level and frequency. The desorption bed is attached to the transducer with resin epoxy. A detailed photo of the experimental setup is also provided in Fig. 4. Three widely used adsorbents namely zeolite 13X, activated alumina and silica gel were investigated.

Drying of the zeolite 13X, activated alumina and silica gel samples was achieved by heating them in an oven at 280 °C, 280 °C and 120 °C respectively and measuring the mass until no change in mass was observed.

The drying process of the sample was validated using a vacuum oven. The mass of the dried sample was controlled to be 48.31 ± 0.01 g in all experiments. The dried zeolite 13X, activated alumina and silica gel samples were then saturated to 27%, 20% and 34% moisture ratio (*MR*) using an ultrasonic humidifier respectively. During the saturation stage, the relative humidity and the temperature of the feed flow were controlled at 95%-100% and 20 °C respectively using a Honeywell HIH-6130 temperature and relative humidity sensor. The moisture ratio *MR*, representing the mass of adsorbate adsorbed by adsorbent, is used to describe the desorption process and is defined as:

$$MR = \frac{M_{measured} - M_{dry}}{M_{dry}} \quad (1)$$

where $M_{measured}$ is the measured mass of the sample during the experiment and M_{dry} the measured mass of the dry sample. The resonant frequency of the transducers was determined using an oscilloscope (Rigol DS 1054Z) and a shunt resistor. The ultrasonic transducer and the shunt resistor were connected in series and with the help of four voltage probes, the impedance of the transducer based on the voltages across the transducer and across the shunt resistor was calculated. The resonant frequency corresponds to the lowest impedance (also the phase difference between the voltage and current is zero) [62].

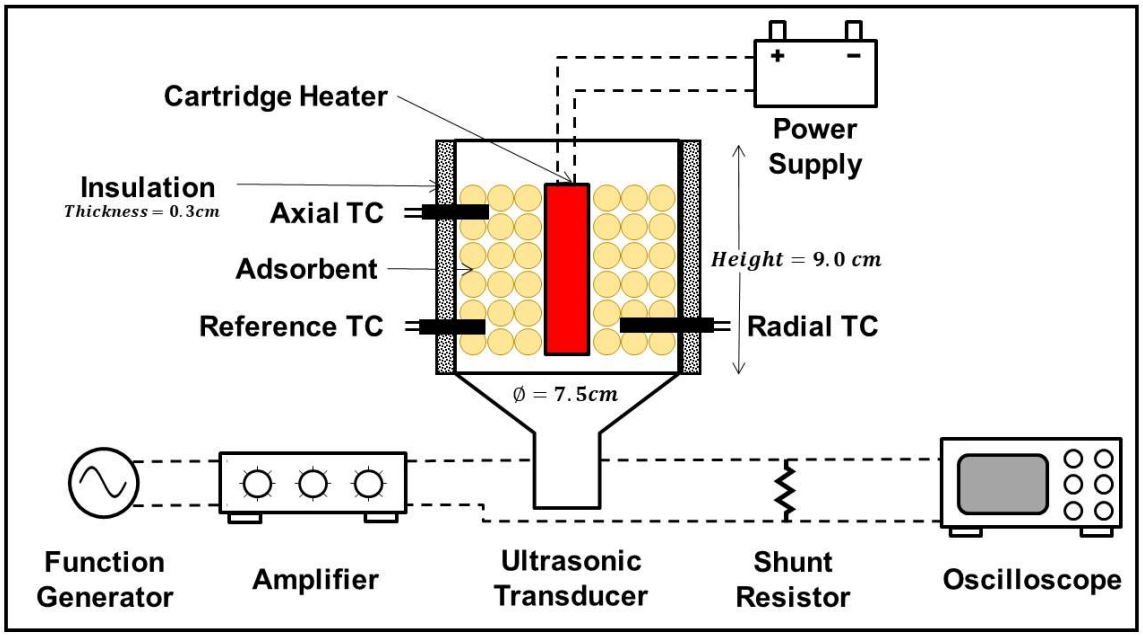

Figure 2. Schematic diagram of the experimental setup.

The resonant frequencies of the unloaded transducers provided by the supplier, 28 kHz (APC 90-4040), 40 kHz (APC 90-4050), and 80 kHz (APC 90-4040) kHz were validated and the resonant frequency of the transducer-bed assembly was measured to be 24.3, 31.5, and 75.5 kHz for the zeolite sample, 24.1, 31.2, and 75.1 kHz for the activated alumina sample, and 31.8 kHz for the silica gel sample respectively. The impedance variation and the resonant frequency of the loaded 28 kHz transducer-bed assembly for the zeolite sample is shown in Fig. 3. Identically, for each frequency, experiments at two levels of total power (P_{Total} = 20 and 25 W) were carried out. The experimental ultrasonic (P_{US}) – thermal power (P_{TH}) combinations are presented in Table 1. Thermal power was regulated through a power supply connected to the cartridge heater. The ultrasonic power was regulated using a shunt resistor, an oscilloscope and voltage probes. The ultrasonic power was determined as:

$$P_{US} = V_{rms}\, I_{rms}\, \cos\theta \tag{2}$$

where V_{rms} is the root mean square value of voltage across the transducer, I_{rms} the root mean square value of alternating current passing through the transducer, and θ the phase angle between the voltage and current.

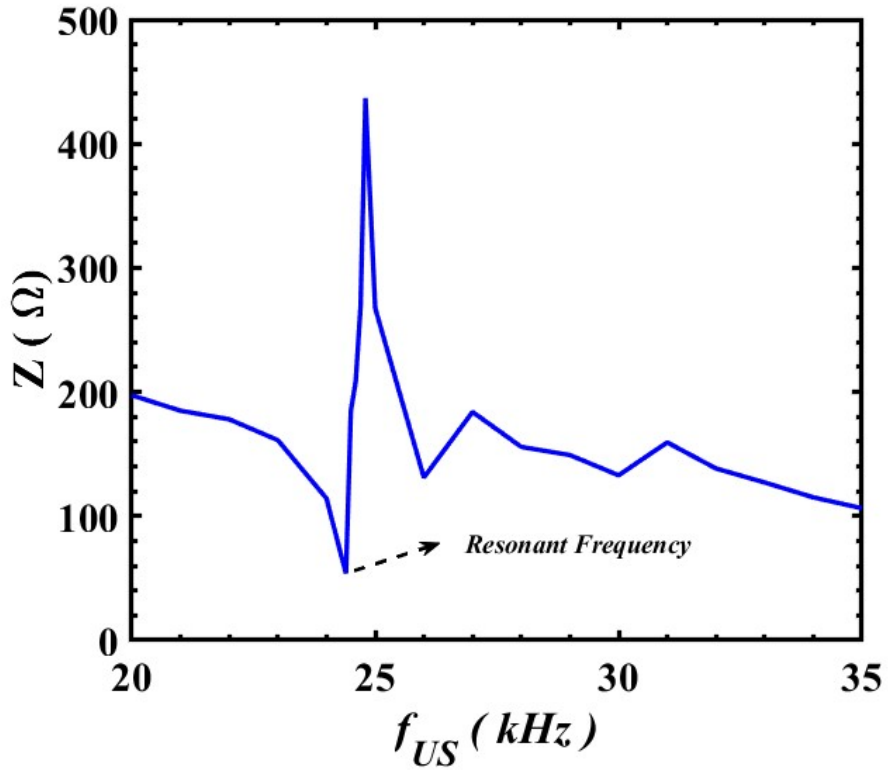

Figure 3. Impedance variation and the resonant frequency of the zeolite-loaded 28 kHz transducer-bed assembly

Since adsorbents are poor heat conductors, the regeneration temperature was measured at several different locations using OMEGA T type thermocouples (wire diameter = 0.571 mm), referred to as reference, axial, and radial temperatures, and a NATIONAL INSTRUMENTS data acquisition device NI 9212. The experimental period is limited to 50 minutes and the mass and temperatures are measured at 5-minute intervals. For each measurement, all wires are disconnected from the bed and the mass of the bed is measured using an electronic scale (My Weigh SCMIM01) with a capacity of 1000 ±0.01 g.

Table 1.Experimental ultrasonic-thermal power combinations.

P_{Total} (W)	P_{TH} (W)	P_{US} (W)	P_{US}/P_{Total} (-)
20	20	0	0
20	15	5	0.25
20	10	10	0.50
25	25	0	0
25	20	5	0.20
25	15	10	0.40

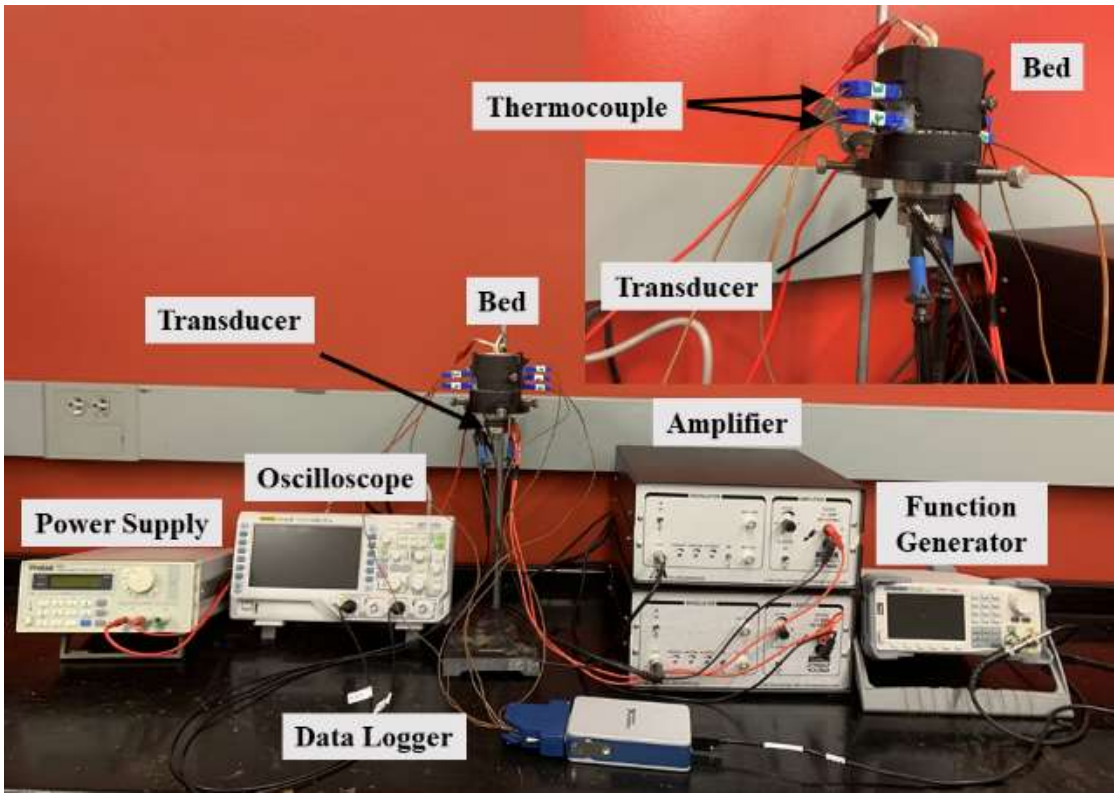

Figure 4. Detailed photo of the experimental setup.

2.2. Desorption Metrics

2.2.1. Ultrasonic Desorption Enhancement

The ultrasonic desorption enhancement *UDE* indicates the percent improvement in removing the adsorbate using ultrasound compared to a heat-only desorption process and is defined as:

$$UDE = \frac{\Delta m_{removed,US} - \Delta m_{removed,non\ US}}{\Delta m_{removed,non\ US}} \quad (3)$$

where $\Delta m_{removed,US}$ is the mass of adsorbate removed in a desorption process involving ultrasound and $\Delta m_{removed,non\ US}$ is the mass of adsorbate removed in a heat-only desorption process.

2.2.2. Ultrasonic Desorption Efficiency Enhancement

The ultrasonic desorption efficiency enhancement *UDEE* is an indicator of the amount of energy saved in desorbing adsorbate from adsorbent by using ultrasound compared to a heat-only desorption process and is defined as:

$$UDEE = \frac{\frac{P_{Total}\,\Delta t}{\Delta m_{removed,non\ US}} - \frac{P_{Total}\,\Delta t}{\Delta m_{removed,US}}}{\frac{P_{Total}\,\Delta t}{\Delta m_{removed,non\ US}}} \quad (4)$$

where Δt is the total time of the experiment (50 minutes). The common numerator $P_{Total}\Delta t$ was not cancelled to keep the universality and a sense of specific energy in the equation.

2.3. Uncertainty Analysis

2.3.1. Measured and Calculated Variables

The thermocouple-data acquisition device was calibrated using a HONEYWELL HIH 6130 silicon bandgap temperature sensor with an accuracy of ±1.0°C. The accuracies of the mass and temperature measurements are provided in Table 2. The uncertainties of the calculated variables were determined using [63]

$$w_f = ({w_1}^2(\frac{\partial f}{\partial x_1})^2 + {w_2}^2(\frac{\partial f}{\partial x_2})^2 + {w_3}^2(\frac{\partial f}{\partial x_3})^2 + \cdots)^{0.5} \quad (5)$$

where w_f is the uncertainty of the calculated variable $f(x_1, x_2, x_3, \ldots)$ and w_1, w_2, w_3, ... the uncertainties involved in the measured variables $x_1, x_2, x_3, \ldots$ respectively. For instance, the uncertainty associated with the calculated variable *MR* is obtained using

$$w_{MR} = \sqrt{w_{m_{measured}}^2(\frac{1}{m_{dry}})^2 + w_{m_{dry}}^2(\frac{m_{measured}}{m_{dry}^2})^2} \quad (6)$$

Table 2.Accuracy of measured variables.

Measured variable	Accuracy	Unit
Temperature	±1.0	°C
Mass	±0.01	g
Voltage	2	%
Phase angle	0.1	minute

The maximum values of uncertainty of the calculated variables are provided in Table 3.

Table 3.Maximum values of uncertainty for calculated variables.

Calculated variable	Maximum uncertainty	unit
MR	±0.21	%
T_{reg}	±1.7	°C
UDE	±0.45	%
UDEE	±1.98	%

2.3.2 Sensible Heat Loss

To minimize the effects of sensible heat losses, the desorption bed was fully insulated. However, some amount of heat loss is unavoidable and should be taken into consideration in interpreting the experimental results. To investigate the amount of heat losses and for the purpose of comparing the sensible heat loss to the heat gained by the zeolite, the worst case heat loss, i.e., the maximum temperature rise (15 W thermal power and 10 W of

ultrasound at a nominal frequency of 80 kHz) is considered. Since the bed is a short, thick cylinder, the effect of curvature can be neglected, and the periphery is regarded as a vertical surface [64]. The top surface of the bed is treated as a horizontal surface.

Assuming natural convection from the horizontal and vertical surfaces and using the known temperatures of the insulation surface and the ambient, the heat transfer coefficients for vertical and horizontal surfaces are determined to vary between 0.24 - 5.72 W m^{-2} K^{-1} and 6.51 - 11.3 W m^{-2} K^{-1} throughout the experiment, respectively. The total average heat loss for the entire period of the experiment is ~1.8 W corresponding to 7.2% of the total input power.

2.3.3. Bed Size and Input Power Proportionality

Since this work is a comparative study that evaluates and justifies the energy-saving characteristic of ultrasound–assisted versus heat-only desorption and considering that the sensible heat losses are taken into account, the size of the desorption bed is not of importance. However, to realize the real–time applicability of the study, the amounts of input power are proportional to the bed size. The specific cooling power of the adsorption-based cooling systems are reported to be about 200 - 600 W kg^{-1} [65], [66], so the 20 and 25 W of total input power corresponding to specific desorbing input powers of 327 and 410 W kg^{-1} respectively, are comparable.

3. ULTRASOUND-ASSISTED REGENERATION OF ZEOLITE/WATER ADSORPTION PAIR

3.1. Zeolite 13X

The zeolite 13X beads used in this study were procured from SORBENT SYSTEMS IMPAK Inc. The physical properties and specifications provided by the supplier are presented in Table 4.

Table 4. Physical Properties of zeolite 13X

Bead diameter (mm)	3 - 5
Pore diameter (nm)	1.3
Specific surface area (m^2/g)	726
Porous volume (ml/g)	0.25
Density (kg/m^3)	689

Zeolite 13X is porous crystalline alumina silicate with maximum water adsorption capacity of 12% - 36% by mass [66], [67]. As a desiccant material, zeolite 13X has various applications including sorption cooling [65], [66], [68]–[70] and thermal storage [71]–[73]. Wang et al. [69] reported the adsorption enthalpy of the zeolite-water pair to be about 3300 - 4200 kJ kg^{-1} and the regeneration temperature to be about 250 – 300 °C. The high values of adsorption enthalpy and regeneration temperature of the zeolite/water pair, compared to other adsorption pairs like silica gel/water or activated carbon/ammonia, makes it both a curse and a blessing for sorption cooling and thermal storage applications, respectively.

3.2. Moisture Ratio

Figure 5 shows the measured reduction in moisture ratio (i.e. desorption) of zeolite 13X for all six power combinations and at all three ultrasonic frequencies, including no applied ultrasound (heat-only).

It can be observed from the figure that with constant power level, replacing some portion of thermal power with ultrasound enhances moisture removal from the adsorbent. In previous studies [36], [71], [74], the ultrasound was added to the thermal power such that the total power increased from the heat-only experiments to the ones with ultrasound. Although this approach confirms that applying ultrasound enhances desorption, the fact that heat-only and ultrasound-assisted experiments were not performed with the same level of total power makes it impossible to justify the use of ultrasound in terms of energy savings. The novelty of the present study is the *constancy of total power in both heat-only and ultrasound-integrated experiments* that justifies the use of ultrasound to enhance the desorption process. Since the total input power is constant, the enhancement in desorption must be ultrasound related.

The highest moisture ratio in this study is 27% meaning that the total mass of adsorbed water is 13.04 g. Using water molar mass and Avogadro's number, there are a total of 4.36×10^{23} water molecules present. Assuming a monolayer adsorptive distribution (water molecules tend to adhere to the zeolite surfaces rather than to other water molecules) and considering a water molecule effective radius of 0.097 nm, the total surface occupied by water molecules is $\sim 12.64 \times 10^3$ m^2. The mass of dry zeolite sample is 48.31 g and using the sample's specific area of 726 m^2/g, the total surface of the zeolite sample is 35.07×10^3 m^2. The average *surface coverage* is therefore obtained as

$$Surface\ coverage = \frac{A_{water,Total}}{A_{zeolite,Total}} = \frac{12.64 \times 10^3}{35.07 \times 10^3} = 0.36 = 36\% \quad (7)$$

In case of multilayer adsorption of water molecules resulting in water cluster formation (which usually occurs in hydrophobic adsorbents), the size of the water molecule

accumulation is reported not to exceed a pentamer [75]–[77]. Considering both monolayer and multilayer adsorptive distribution scenarios, we can confidently conclude that neither bulk liquid nor bulk-imitating liquid clusters exist in our sample.

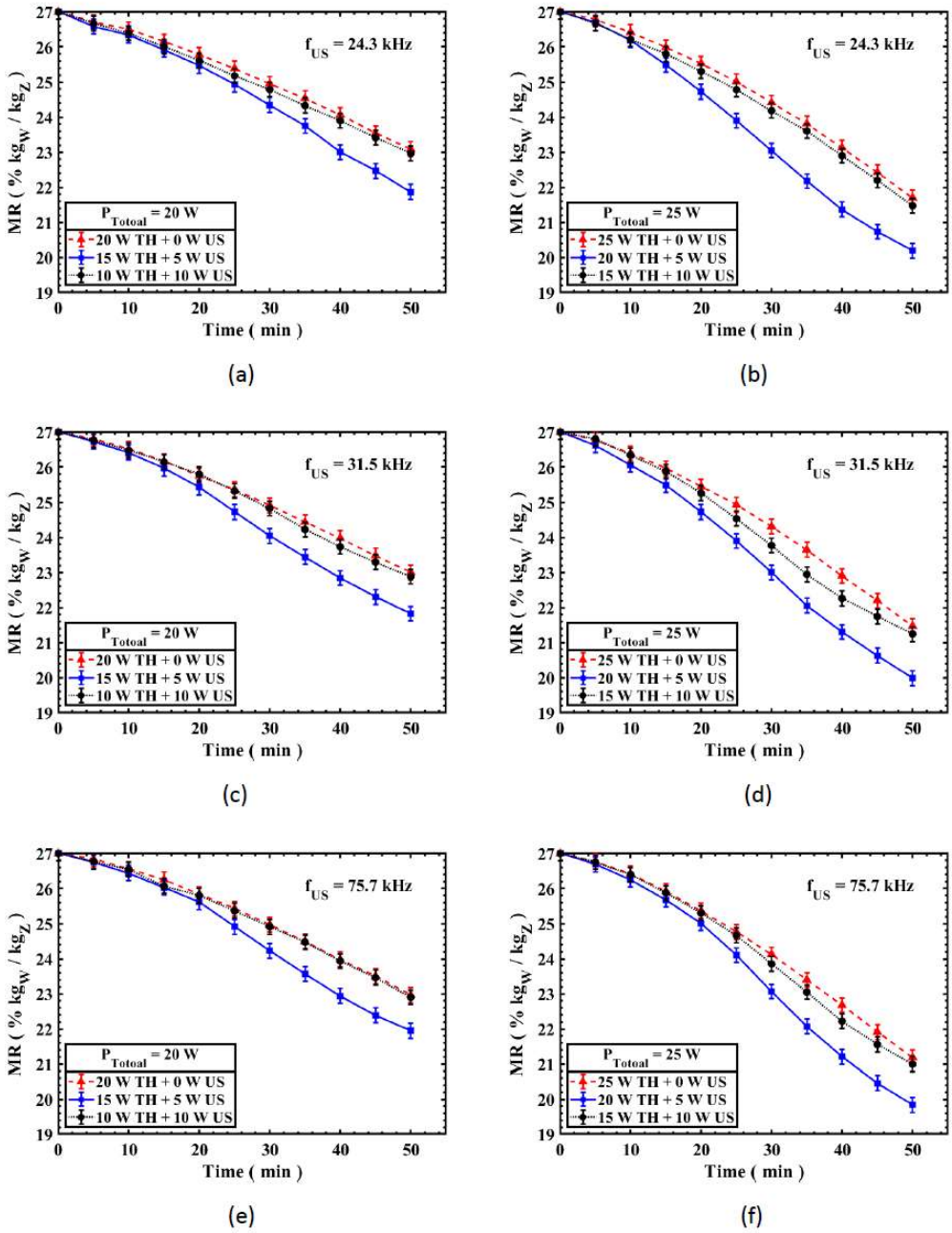

Figure 5. Desorption curves for zeolite / water. (a) at 24.3 kHz and 20 W; (b) at 24.3 kHz and 25 W; (c) at 31.5 kHz and 20 W;(d) at 31.5 kHz and 25W; (e) at 75.7 kHz and 20 W; (f) at 75.7 kHz and 25 W.

In the absence of bulk liquid or liquid film, the effects of ultrasonication involving liquid including the viscosity effect, capillary effect, sonic currents, microstreaming, circulating flow and surface cavitation can be disregarded. The observed ultrasound-assisted enhancement in desorption is therefore perhaps due to ultrasound-induced establishment of local partial vacuum and alternating zones of compression and rarefaction resulting in enhanced mass diffusivity. Another potential mechanism worth mentioning is the effect of turbulence. The ultrasound-triggered pressure alteration causes turbulence resulting in an increase in mass diffusivity where viscous diffusion is the mode of transport. The same effect is observed in Henry's constant in acoustic fields [57].

3.2.1. Effect of Ultrasonic Power

Although ultrasonic radiation apparently improves the desorption process, the amount of ultrasonic power to be used in order to achieve the highest desorption at the lowest total power input is of major concern. A closer look at Fig. 5 reveals that at any frequency, for the 20-W total power experiments, the highest desorption was achieved with a power combination of 15 W thermal power and 5 W of ultrasonic power, i.e., a ratio of ultrasonic-to-total power of $P_{US}/P_{Total} = 0.25$. In addition, with an increase in this power ratio to 0.50, there is still a slight enhancement in desorption compared to the heat-only experiment, but it is relatively insignificant. The same trend, regardless of variation in frequency, can be observed for the 25-W total power experiments. The greatest enhancement in desorption occurred at a power combination of 20 W thermal and 5 W of ultrasonic power ($P_{US}/P_{Total} = 0.20$). Again, at a higher $P_{US}/P_{Total} = 0.40$, there is a modest improvement in desorption over the heat-only experiment. This suggests that there is an optimal value for P_{US}/P_{Total} resulting in maximal adsorbate removal per constant total power.

3.2.2. Effect of Ultrasonic Frequency

The values of ultrasonic desorption enhancement *UDE* relative to heat-only desorption are plotted in Fig. 6. It can be concluded from the figure that for any total power level and with any ultrasonic – thermal power combination, with an increase in ultrasonic frequency f_{US}, the ultrasonic desorption enhancement decreases. The same trend of deterioration in desorption enhancement with an increase in f_{US} has been observed in some previous studies [33]. The reduction is somehow proportional to the increase in f_{US}. With a slight shift from 24.3 kHz to 31.5 kHz, there is a slight drop in *UDE*. However, with an increase from 24.3 kHz to 75.7 kHz, there is a significant reduction in *UDE*. The inverse proportionality between f_{US} and *UDE* in some ways appears to confirm the ultrasound-induced desorption improvement through partial vacuum and zones of alternating pressure. At higher frequencies, the rarefication, compression, and partial vacuum are established and demolished so fast that there may not be enough time for the mass-transfer-enhancing effects to be fully developed. The same phenomena can be observed in ultrasonic-induced cavitation when acoustic-induced cavitation bubbles explode prematurely at higher frequencies [78], [79].

3.3. Regeneration Temperature

Figure 6 shows the average regeneration temperature, taken as the average of the three thermocouples shown in Figs. 2 and 3, for all experiments. For all three frequencies and both total power levels, ultrasound-enhanced experiments showed higher temperatures than the non-ultrasonic ones. Specifically, at almost any frequency, the highest temperature was observed at the lower value of P_{US}/P_{Total} meaning that the temperature is not solely

dictated by the thermal power and there are other factors contributing to the temperature rise.

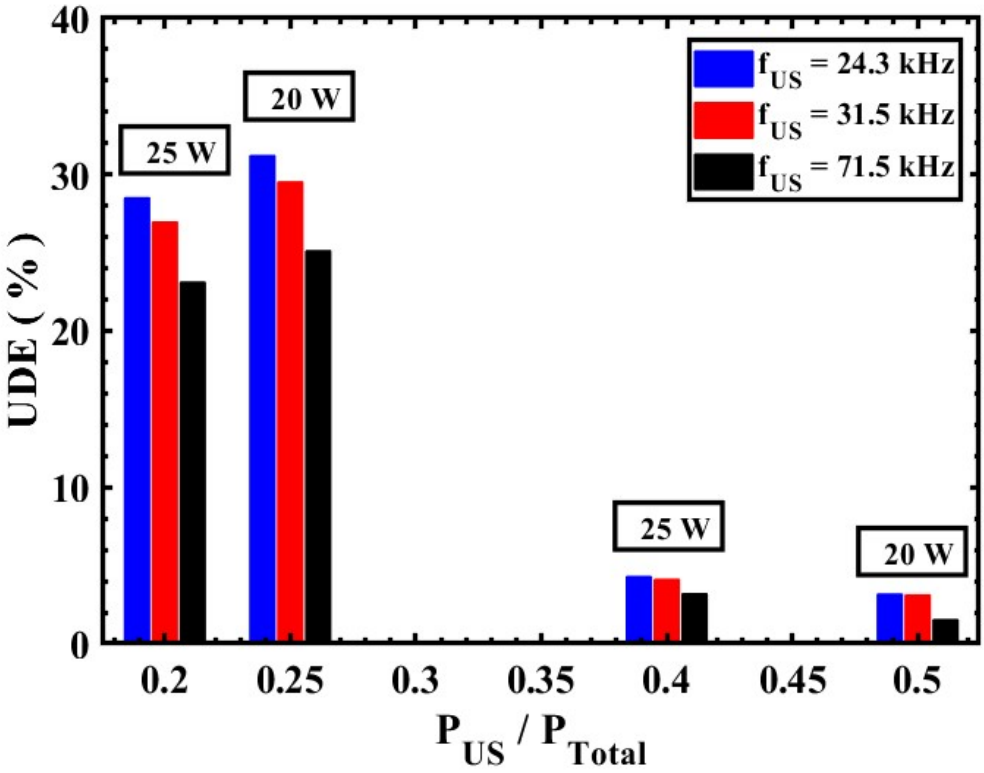

Figure 6.Ultrasonic desorption enhancement for zeolite/water at different frequencies and total power levels. The uncertainty of the UDE is provided in Table 3.

One such factor could be the fact that zeolite 13X, being a porous medium with low thermal conductivity (about 0.1 - 0.6 W m^{-1} $°C^{-1}$) [71], has poor heat transfer capability so using ultrasound enhances the heat transfer in the medium [80]–[83]. Another reason could be the radially uniform dissipation of ultrasonic waves increasing the temperature rather than relying solely on radial heat conduction from the cartridge heater. The latter cannot be the sole contributor to the temperature rise, as the highest temperature was not observed at higher P_{US}/P_{Total}.

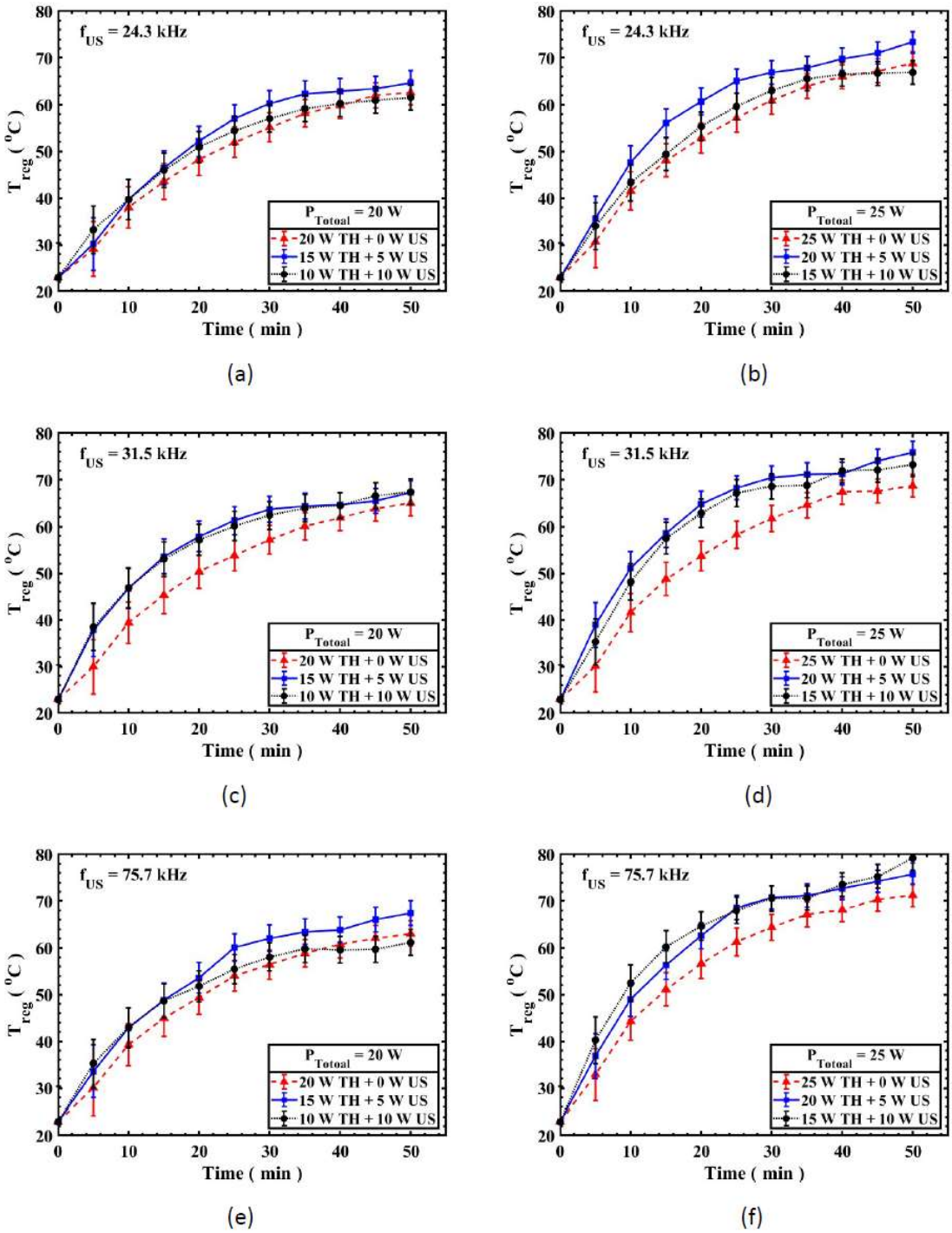

Figure 7. Desorption curves for zeolite / water. (a) at 24.3 kHz and 20 W; (b) at 24.3 kHz and 25 W; (c) at 31.5 kHz and 20 W;(d) at 31.5 kHz and 25W; (e) at 75.7 kHz and 20 W; (f) at 75.7 kHz and 25 W.

3.4. Ultrasonic Desorption Efficiency Enhancement

The ultrasonic desorption efficiency enhancement *UDEE* indicates the amount of energy saved when a portion of thermal power is replaced with ultrasonic power while the total power remains constant. Figure 7 shows the percent energy saved for both power levels (20 and 25 W) and at all three levels of frequency. Regarding the ultrasonic frequency f_{US}, there is a general downward trend in *UDEE* with an increase in f_{US}. As can be seen from the figure, there is no distinguishable trend in *UDEE* with regard to P_{US}/P_{Total}, other than that an optimal value of P_{US}/P_{Total} is apparent that maximizes *UDEE*. The most efficient desorption process was achieved at $P_{US}/P_{Total} = 0.25$.

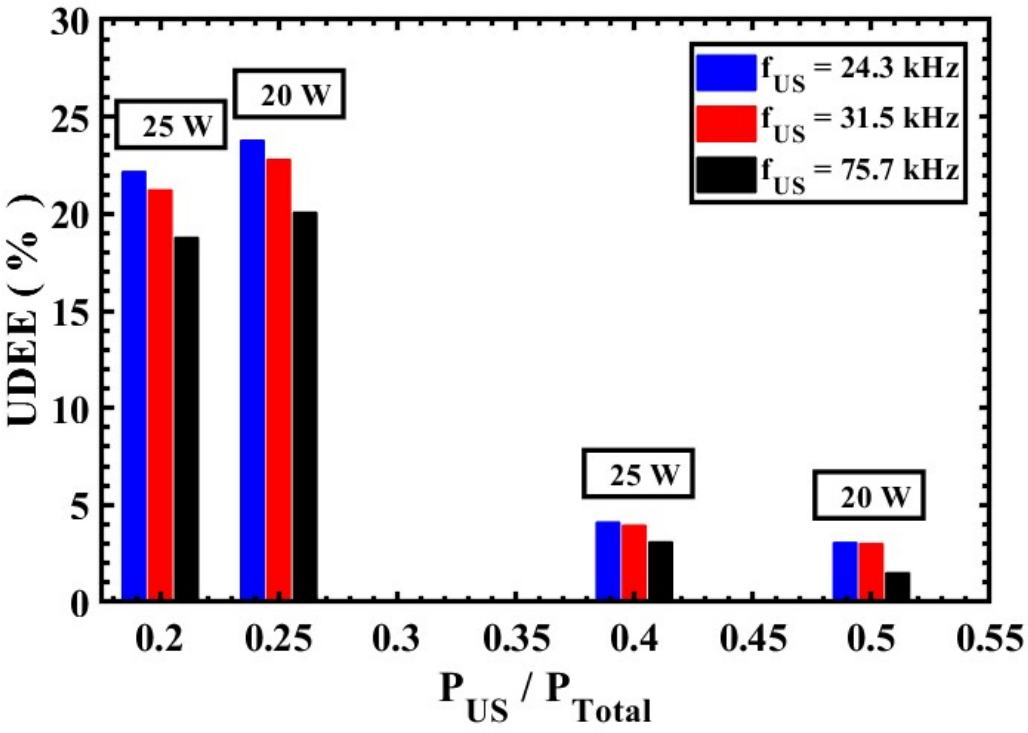

Figure 8. Ultrasonic desorption efficiency enhancement for zeolite/water at different frequencies and total power levels. The uncertainty of the UDEE is provided in Table 3.

In addition, with an increase in this ratio, the efficiency drops drastically meaning that there is an optimal ratio of P_{US}/P_{Total} resulting in the highest desorption efficiency enhancement.

3.5. Desorption Speed

In general, it is beneficial to reduce the time required for desorption. To investigate the effect of incorporating ultrasound on the desorption speed (i.e., on the time required for desorption), the elapsed times needed for ultrasound-assisted and heat-only regeneration processes to reach the same amount of remaining adsorbed moisture are compared. To do so, for each power level, the water content of the adsorbent at the end of the heat-only experiment (50 min) is considered as the reference value. Then the time needed to reach the same water content in ultrasound-assisted regeneration with the same total power input, is determined. The elapsed times for the most effective frequency (24.3 kHz) are presented in Table 5. The shortest desorption times are observed at P_{US}/P_{Total} = 0.2 and 0.25 with 23.8% and 18.4% shorter regeneration processes, respectively. Shifting toward higher P_{US}/P_{Total}, the improvements in desorption time decreases drastically as expected.

Table 5. Elapsed regeneration time at 24.3 kHz ultrasonic frequency.

Total power (W)	Power ratio	Final moisture ratio (%)	Time (min)
20	0.00	23.09	50.0
	0.25		40.8
	0.50		48.4
25	0.00	21.70	50.0
	0.20		38.1
	0.40		48.3

3.6. Ultrasonication-Induced Deterioration

To propose ultrasound as an alternative energy source for regeneration, it is essential to investigate its potential deteriorating and eroding effects. Although the previous investigations on the subject apparently contradict each other, they suggest that the eroding effects of ultrasonication are associated with its cavitation-inducing nature [84]–[87]. However, the deteriorating effects of ultrasound on a number of porous materials have been investigated and no significant changes in their sorption capabilities were reported [4], [34], [88]. In this study, in the absence of bulk liquid, there was no worrisome ultrasound-induced cavitation to be accounted for; however, a BET analysis on a sample after 12 cycles of ultrasonication was carried out to verify the stability of the sample under sonication. BET analysis based on the Brunauer–Emmett–Teller theory of multilayer adsorption of gas molecules on a solid surface is technique for the measurement of the specific surface area of materials [89]. The results of the BET analysis for the sample before and after sonication are presented in Table 6. There is a negligible decrease in BET-specific surface area, porous volume and pore width that should not affect the adsorption capacity of the sample.

Table 6. BET analysis of the zeolite sample before and after ultrasonication

Characteristic	Before	After
Specific surface area (m^2/g)	480.4843	463.4843
Porous volume (ml/g)	0.2223	0.2136

3.7. Summary

In this study, ultrasonic-assisted desorption of water from zeolite 13X was investigated. The extent to which application of ultrasound is effective was analyzed. To do so, the effects of ultrasonic power and ultrasonic frequency on moisture removal and regeneration temperature were investigated. Comparing the moisture ratio at different ultrasonic-to-total

power ratios shows that using ultrasound at lower power ratios, i.e. 0.20 and 0.25, significantly improves desorption relative to using only heat for regeneration.

Using the newly defined metric ultrasonic desorption enhancement *UDE*, the effects of ultrasonic frequency on moisture removal were analyzed and it was concluded that the effect of ultrasound on desorption is more significant at lower frequencies. Comparing the regeneration temperature of all experiments shows that ultrasonication increases the adsorbent temperature regardless of frequency, presumably due to the heat-transfer-enhancing nature of ultrasound. Not surprisingly, at all three frequencies the highest desorption was achieved at the highest regeneration temperature. Another defined indicator, the ultrasonic desorption efficiency enhancement *UDEE*, was used to justify the use of ultrasound in moisture removal from zeolite 13X. Comparing the values of *UDEE* indicates that with an optimized ratio of ultrasonic-to-total power a ~24 % reduction in energy and time required for desorption of water from zeolite 13X can be achieved, relative to using only heat.

4. ULTRASOUND-ASSISTED REGENERATION OF ACTIVATED ALUMINA/WATER ADSORPTION PAIR

4.1. Activated Alumina

Activated alumina is porous aluminum oxide that can adsorb as much as 20% - 38 % of its mass of water [90]. As a desiccant, activated alumina has various applications including air dehumidification, industrial gases and natural gas dehydration processes, and chemical removal from water and air [68], [91]–[97]. Srivastava et al. reported the adsorption enthalpy of the activated alumina/water adsorption pair to be around 2800 - 3000 kJ/kg and the regeneration temperature to be about 250 – 300 °C [68]. The relatively high mechanical and chemical stability, acceptable adsorption capacity and exceptional porous volume of the activated alumina, compared to most other adsorbents, makes it an encouraging candidate for drying and separation applications. Like most desiccants, no matter what the application is, the pitfall of using activated alumina is the obligatory lengthy and energy-intensive process of regeneration, thus demanding faster and more energy-efficient regeneration methods beyond just conventional heating.

The activated alumina beads used in this study were procured from Delta Adsorbents Div. of Delta Enterprises, Inc. The physical properties and specifications provided by the supplier are presented in Table 7.

Table 7. Physical properties of activated alumina

Bead diameter (mm)	3.175
Pore diameter (nm)	~ 4.8
Specific surface area (m^2/g)	350
Porous volume (ml/g)	0.5
Density (kg/m^3)	769

4.2. Moisture Ratio

The variation of the activated alumina moisture content with time for all experiments is presented in Fig. 9. It can be inferred from the figure that at all three frequencies and power levels, integration of ultrasound while the total power input remains unchanged improves the regeneration process of activated alumina. The general trend is that while the total input power to the bed is constant, exchanging smaller portions of thermal input i.e. 20 and 25% with ultrasound considerably amplifies desorption with a tradeoff between ultrasound-induced enhancement and ultrasonic power input. More specifically, applying ultrasound at lower ultrasonic-to-total power ratios of P_{US}/P_{Total} = 0.2 and 0.25 pertaining to the total power levels of P_{Total} = 25 and 20 W respectively seems to significantly enhance the desorption process compared to the no-ultrasound (i.e., heat only) desorption process at the same P_{Total}. At higher P_{US}/P_{Total} = 0.4 and 0.5, the effectiveness of incorporating ultrasound is still noticeable but not as much as at lower P_{US}/P_{Total}. The same trend was observed in ultrasound-assisted regeneration of zeolite with the exception that the highest desorption was observed at P_{US}/P_{Total} = 0.25 indicating that adsorbents are affected by ultrasound differently. Since P_{Total} is unchanged, the observed improvement must be due to ultrasonication. The initial moisture content of the activated alumina sample is 20% corresponding to 12 g of water consisting of 4.011×10^{23} water molecules. Assuming a 0.097 nm effective radius for the water molecule, the total surface area occupied by the adsorbate is 12×10^{3} m^2. The total surface area of the activated alumina sample is ~21×10^{3} m^2. Following the same reasoning from the zeolite case, the surface coverage comes out to be around 56%. This means that there is little or no accumulation of water molecules that resembles liquid so to interpret ultrasound-assisted desorption, ultrasound-induced

mechanisms entailing the liquid phase such as the viscosity effect, the capillary effect, sonic currents, microstreaming, circulating flow and surface cavitation can be neglected.

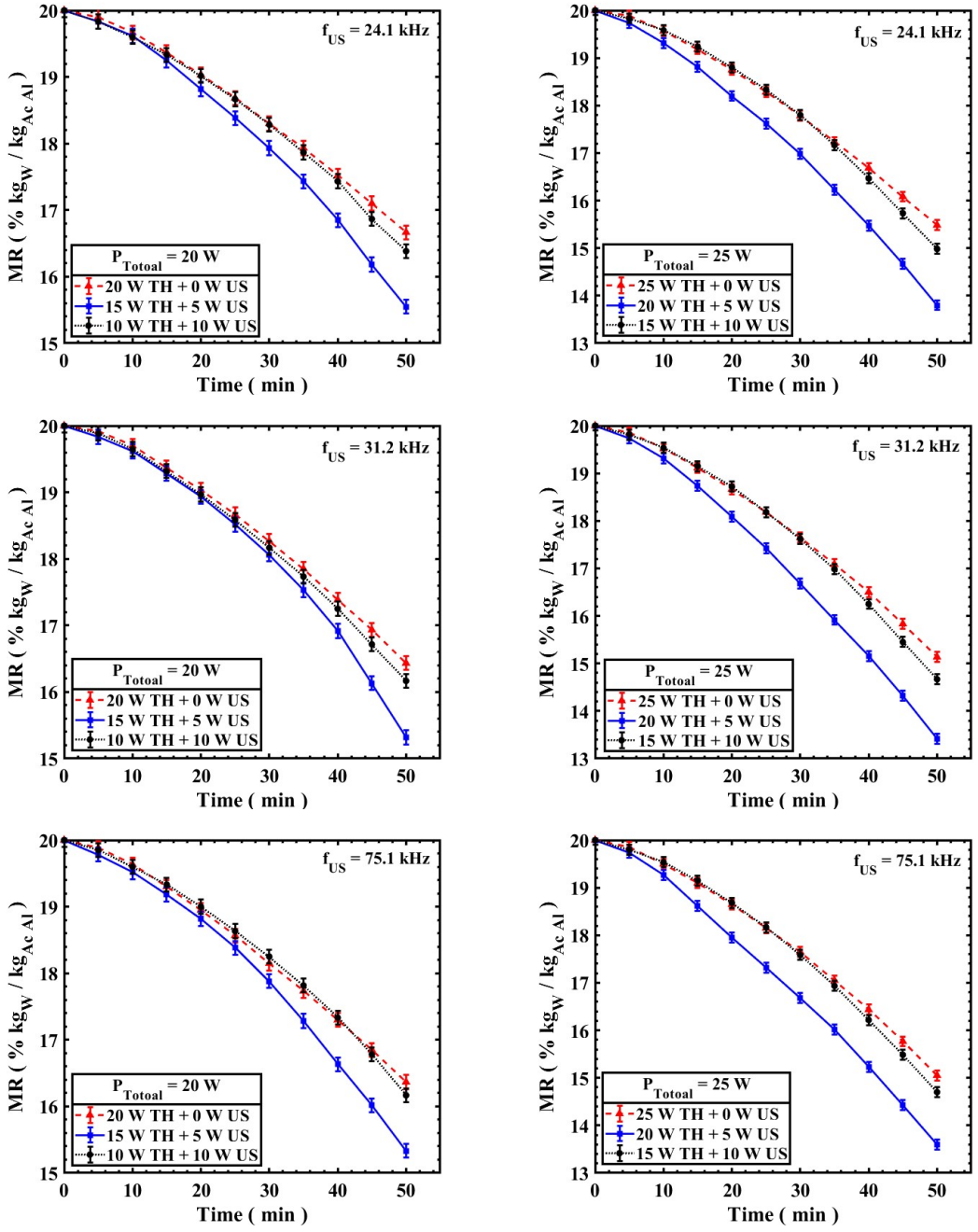

Figure 9. Desorption curves for activated alumina/water. P_{Total} =20 W (left) and P_{Total} =25 W (right). f_{US} =24.1 kHz (top), f_{US} =31.2 kHz (middle) and f_{US} =75.1 kHz (bottom).

To investigate the effect of f_{US} on the desorption process, the metric *UDE* is employed. This metric enables comparison of the amount of adsorbate removed in an ultrasonic-assisted regeneration process with that of a non-ultrasonic (heat-only) regeneration process. The variation of *UDE* with P_{US}/P_{Total} for both total power levels and all three f_{US} is presented in Fig. 10. For any P_{US}/P_{Total}, with an increase in f_{US} the value of *UDE* decreases meaning that the effectiveness of applying ultrasound is inversely proportional to f_{US}. A similar trend was observed in the literature for silica gel [33], and we reported a similar trend for zeolite 13X. Averaged over all values of P_{US}/P_{Total}, shifting f_{US} from 24.1 kHz to 31.2 kHz and 75.1 kHz results in approximately 9% and 25% drop in *UDE* value respectively, suggesting a nonlinear inverse proportionality between the effectiveness of incorporating ultrasound in the desorption process and the frequency at which ultrasound is applied.

4.3. Regeneration Temperature

Since the three thermocouples in zeolite/water regeneration temperature failed to provide axial and radial temperature gradient, it was decided to add two more thermocouples (one radial and one axial) to improve the accuracy of the measurement. The average regeneration temperature, taken as the average of the five thermocouple measurements for all six activated alumina experiments are shown in Fig. 10. For all three frequencies and both total power levels, ultrasound-enhanced experiments showed lower temperatures than the non-ultrasonic ones. Specifically, at any frequency and any power level, the lowest temperature was observed at the higher value of P_{US}/P_{Total}.

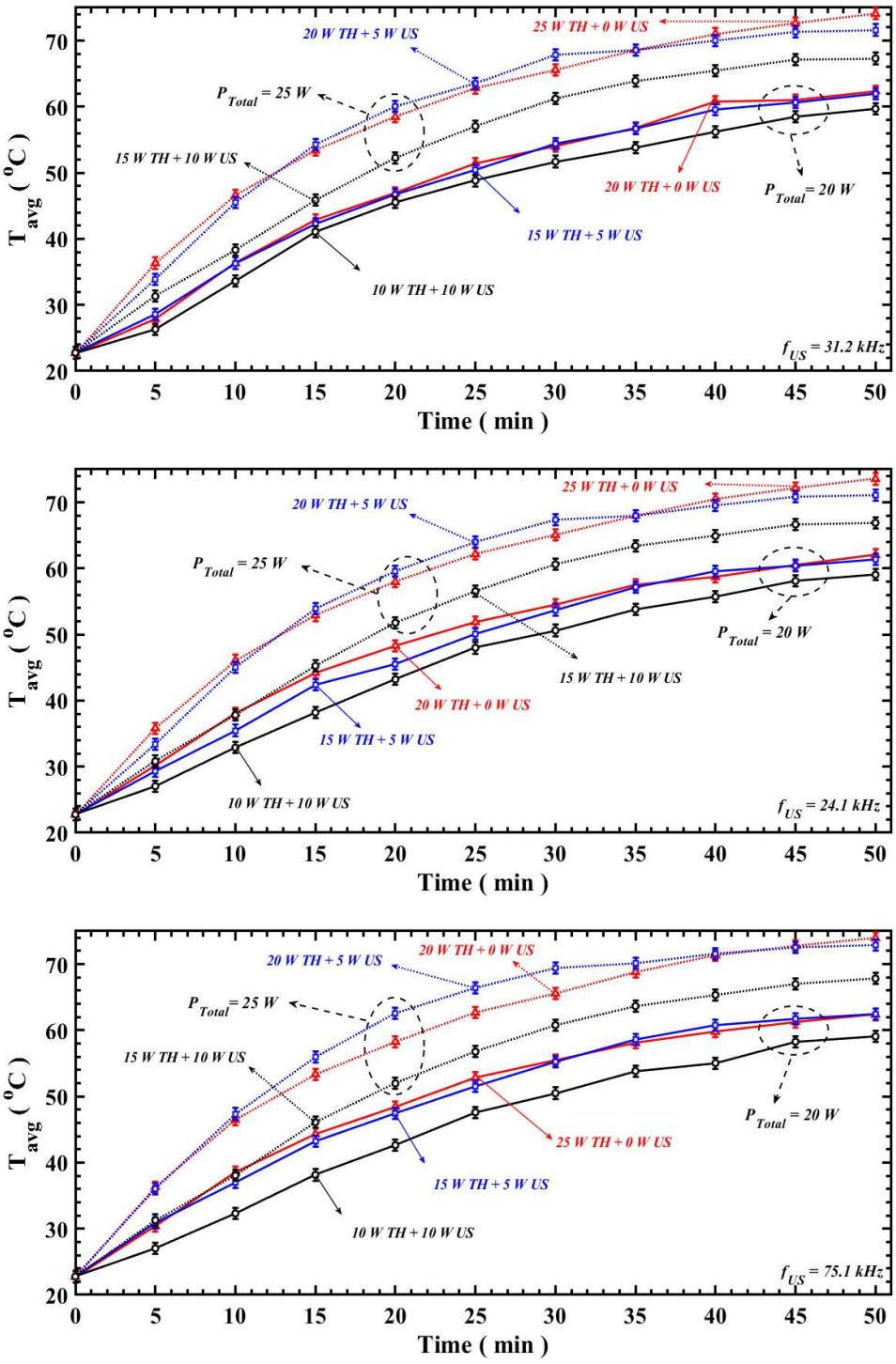

Figure 10. Average regeneration temperature for activated alumina/water. f_{US} =24.1 kHz (top), f_{US} =31.2 kHz (middle) and f_{US} =75.1 kHz (bottom).

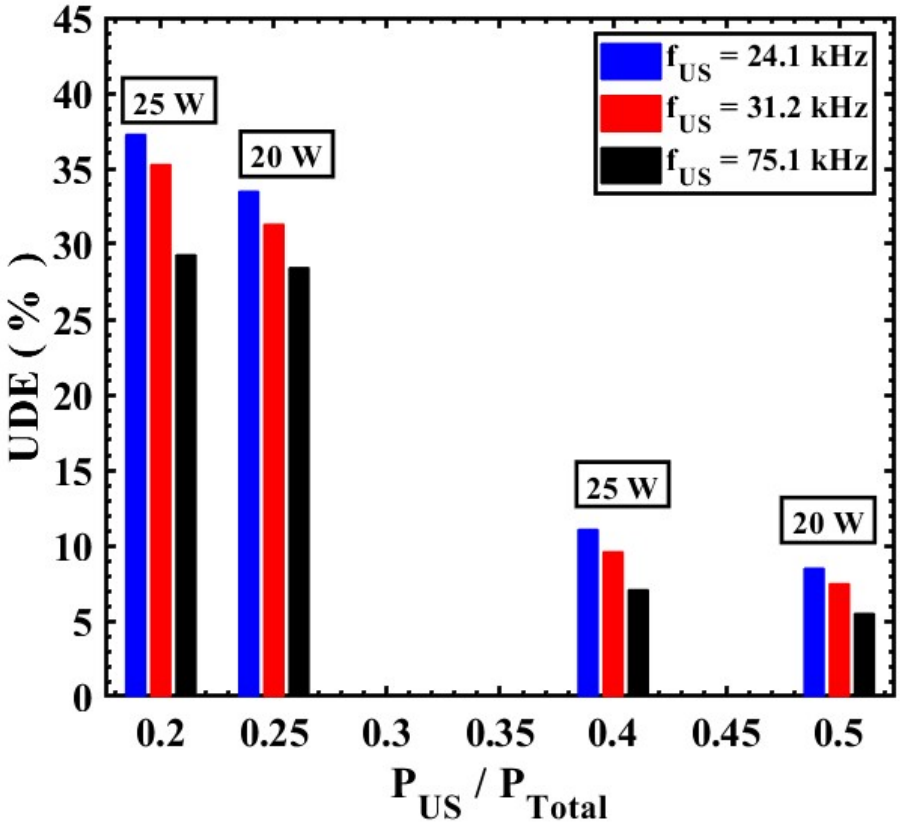

Figure 11. Ultrasonic desorption enhancement for activated alumina/water at different frequencies and total power levels. The uncertainty of the *UDE* is provided in Table 3.

In addition, regardless of frequency and power level, the temperature of adsorbent during heat-only and lower ultrasonic-to-total power ratio experiments are observed to be very close, suggesting that the temperature is not solely dictated by the thermal power and there are other factors contributing to the temperature rise. These factors have been discussed previously in section 3.3.

4.4. Ultrasonic Desorption Efficiency Enhancement

The ultrasonic desorption efficiency enhancement *UDEE* simply indicates the amount of energy saved when ultrasound is incorporated. Figure 12 shows the percent energy saved for both power levels (20 and 25 W) and at all three levels of frequency.

Regarding the ultrasonic frequency f_{US}, there is a general downward trend in *UDEE* with an increase in f_{US} suggesting that for regeneration purposes, the lower levels of frequency are desirable. As can be seen from the figure, there is a distinguishable trend in *UDEE* with regard to P_{US}/P_{Total}. The most efficient desorption process was achieved at $P_{US}/P_{Total} = 0.20$, and with an increase in this ratio, the efficiency drops drastically.

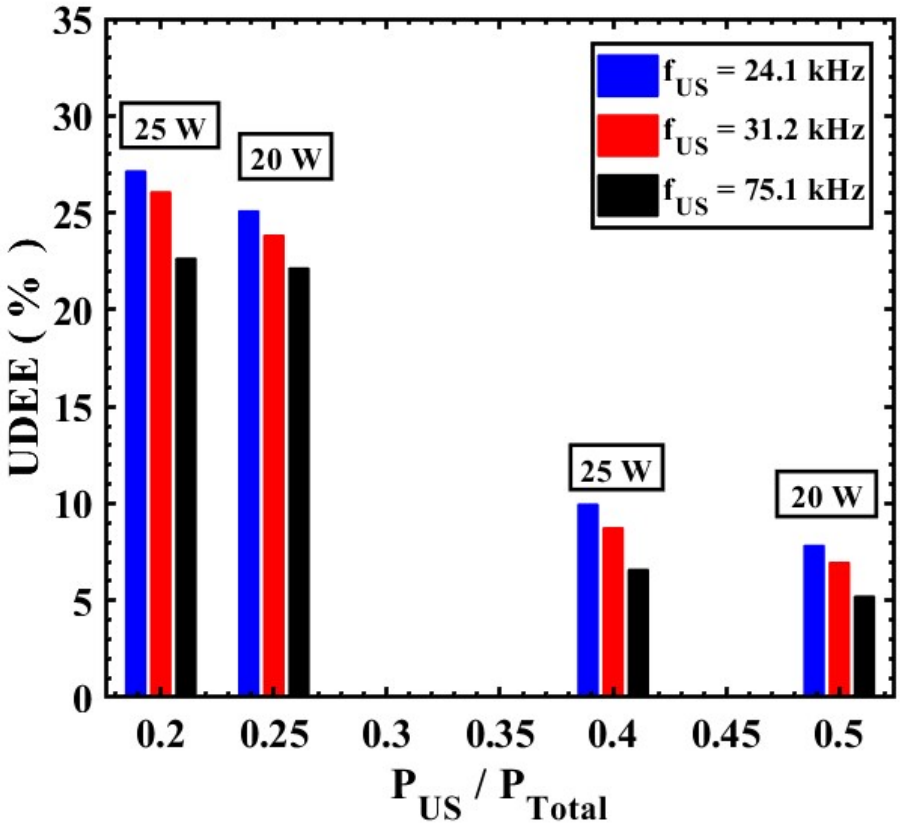

Figure 12. Ultrasonic desorption efficiency enhancement for activated alumina/water at different frequencies and total power levels. The uncertainty of the UDEE is provided in Table 3.

4.5. Summary

Ultrasound-assisted regeneration of activated alumina/water adsorption pair has been investigated. The experimental results clearly show that integration of ultrasound along

with thermal power without increasing the total input power enhances the removal of water from activated alumina relative to heat-only desorption with the same total power input.

The effectiveness of applying ultrasound is strongly influenced by the ratio of ultrasonic-to-total power and amongst the measured power ratios of 0.2, 0.25, 0.4 and 0.5, the highest desorption was observed at 0.2 power ratio corresponding to about 27% energy savings. The effect of ultrasonic frequency on moisture removal was investigated and it was concluded that increasing the frequency reduces the effectiveness of ultrasound. In terms of regeneration temperature, experimental data show that integration of ultrasound at higher power ratios, i.e. 0.4 and 0.5, considerably lowers the regeneration temperature without jeopardizing the desorption process. An ultrasound-enhanced desorption mechanism based on the effect of acoustic stress on the adsorbate surface energy was proposed and a relation between adsorbate surface energy and acoustic pressure was established.

5. ULTRASOUND-ASSISTED REGENERATION OF SILICA GEL /WATER ADSORPTION PAIR

5.1. Silica Gel

The silica gel used in this study was procured from the Delta Adsorbents Division of Delta Enterprises, Inc. The physical and porous properties provided by the manufacturer are shown in Table 8.

Table 8. Physical properties of silica gel.

Average bead diameter (mm)	3.5
Pore diameter (nm)	2-3
Specific surface area (m^2/g)	650
Density (kg/m^3)	700

5.2. Moisture Ratio

The variation of the silica gel moisture content with time for all experiments is depicted in Fig. 13. To establish the influence of ultrasound in desorption-temperature dynamics, the dimensionless moisture removal μ is defined:

$$\mu = \frac{m_{ini} - m_{measured}}{m_{ini} - m_{dry}} \tag{8}$$

where m_{ini} is the initial mass of the sample (adsorbent + adsorbate), $m_{measured}$ the measured mass of the sample and m_{dry} the mass of the dry sample. The dimensionless moisture removal μ can be easily converted to the more previously defined moisture ratio MR using

$$\mu = 1 - \frac{m_{dry}}{m_{ini} - m_{dry}}\, MR \tag{9}$$

The specific regenerating power of the silica gel-water pair is reported to be about 180-390 W_{th}/kg_{SG}, so the 20 and 25 W of total input power corresponding to specific desorbing input powers of 327 and 409 W/kg_{SG} respectively, are comparable [98], [99]. It can be inferred from Fig. 13 that at both total power levels P_{Total} = 20 or 25 W, at any value of the ratio P_{US}/P_{Total}, application of ultrasound improves the moisture removal from silica gel. The observed trend is that while the total input power to the desorption bed remains constant, replacing smaller portions of thermal power i.e., 20% (20W TH + 5W US) and 25% (15W TH + 5W US) with ultrasonic power significantly enhances moisture removal compared to the no-ultrasound desorption process at the same total power level.

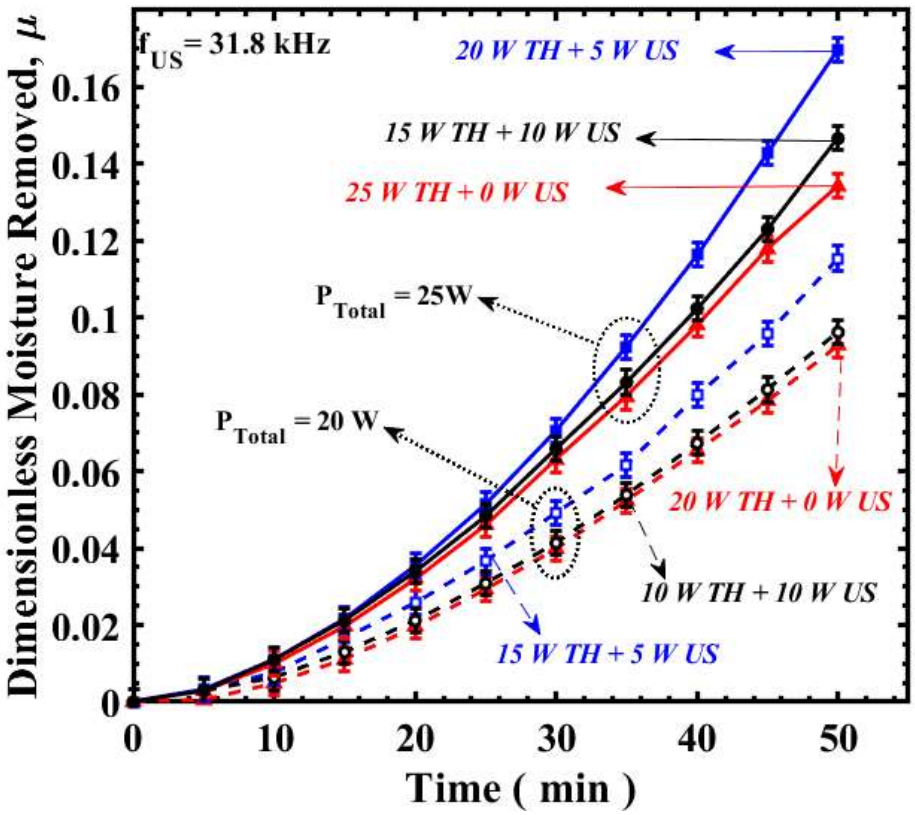

Figure 13. Variation of dimensionless moisture removed in ultrasound-assisted and heat-only regeneration of silica gel.

At higher P_{US}/P_{Total} of 40% (15W TH + 10W US) and 50% (10W TH + 10W US), the observed enhancement associated with integration of ultrasound is still perceptible, however not as significant as at lower P_{US}/P_{Total}. Since there is no increase in the total input power to the system, the observed improvement must be ultrasound-induced.

5.3. Regeneration Temperature

The variation of silica gel regeneration temperature, T_{reg}, averaged over five measured temperatures at various radial and axial locations with time is depicted in Fig. 14. The temperature of the silica gel during the regeneration process is dictated by three factors namely heat input, acoustic dissipation and ultrasonic-enhanced heat transfer [100], [101]. At any power level, the lowest regeneration temperature is observed at the highest P_{US}/P_{Total} ratio when a significant fraction (40% at 25 W total power level and 50% at 20 W total power input) of thermal power is replaced by ultrasonic power implying that the thermal input is the leading factor in controlling the regeneration temperature regime compared to ultrasonic-enhanced heat transfer and acoustic dissipation. Also, values of T_{reg} at low ultrasonic input, i.e., high thermal input and no ultrasound including heat-only input, are observed to be very close suggesting that that when a small portion (20% at P_{Total} = 25 W and 25% at P_{Total} = 20 W) of thermal power is replaced by ultrasonic power, the ultrasound-enhanced heat transfer can nearly offset the effect of the eliminated portion of the thermal input on regeneration temperature.

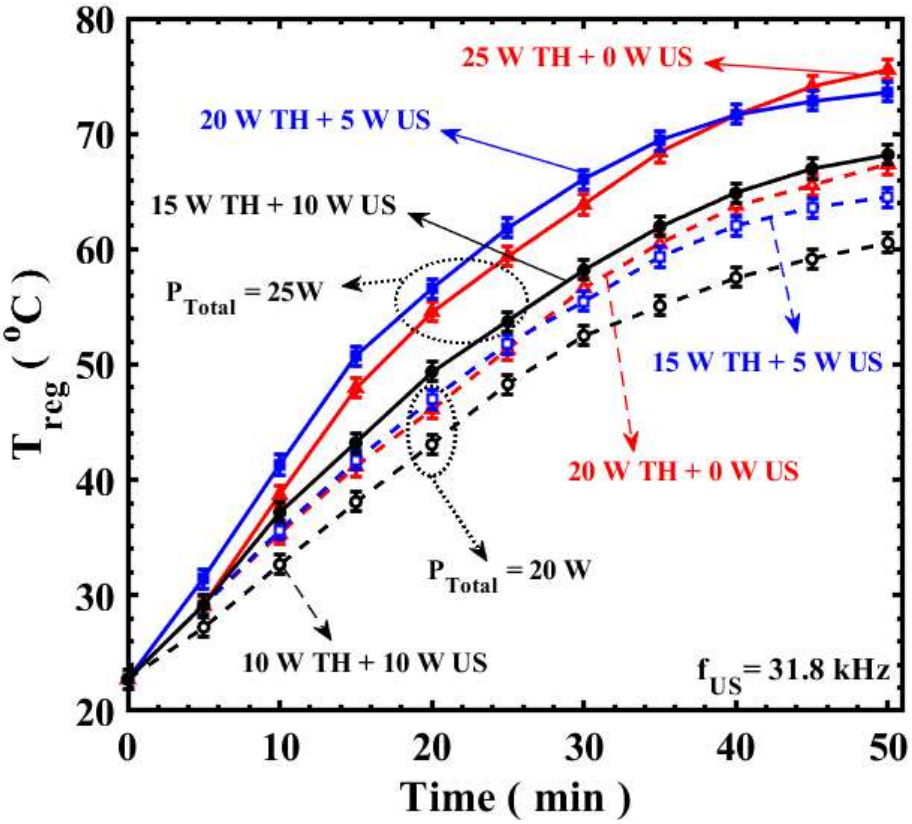

Figure 14. Measured regeneration temperature of silica gel.

5.4. Ultrasonic Desorption Efficiency Enhancement

To investigate the improved energy efficiency associated with integration of ultrasound, the metric *UDEE* is utilized. Figure 15 shows the values of *UDEE* for both power levels (20 and 25 W) and all P_{US}/P_{Total}. Regarding the dependence on P_{US}/P_{Total}, there is a general downward trend in *UDEE* with an increase in P_{US}/P_{Total}. Energy efficiency improvement ensues from the integration of ultrasound in any case, however, the highest energy saved, i.e. 26% is achieved at the lowest ultrasonic input—20% of the total input.

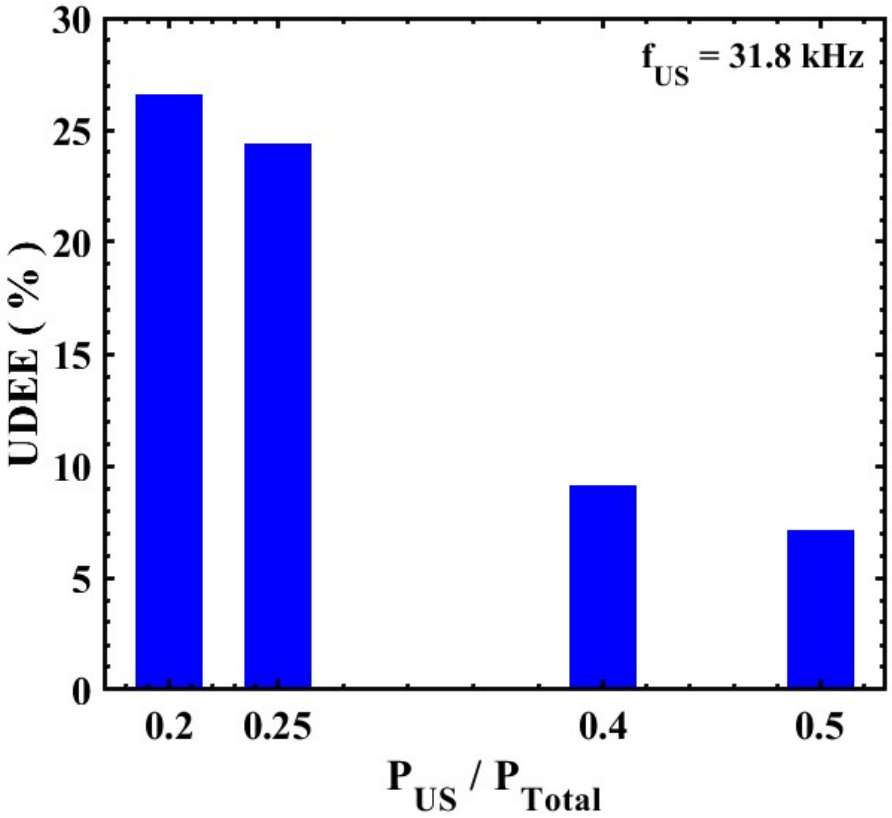

Figure 15. Ultrasonic desorption efficiency enhancement (*UDEE*) for the regeneration of silica gel. The uncertainty of *UDEE* is provided in Table 4.

5.5. Moisture Variation with Temperature

The issue with current methods of regenerating solid adsorbents is the relatively high levels of regeneration temperature requiring high thermal energy input. Utilization of low-grade thermal energy such as waste heat and solar thermal energy could potentially decrease the energy and carbon intensity of drying and dehumidification processes involving solid adsorbents. However, utilization of low-grade heat is limited by its inherent low temperature. Ultrasound, which besides temperature incorporates alternating pressure and surface energy into desorption kinetics, can alter the desorption dynamics. Figure 16 shows the variation of silica gel moisture content with regeneration temperature T_{reg}.

At both power levels, relative to heat-only regeneration, integration of ultrasound decreases the regeneration temperature. The reduction in regeneration temperature due to ultrasonication was observed in case of ultrasound-assisted regeneration of activated alumina. However, the ultrasonication resulted in an increase in ultrasound-assisted regeneration of zeolite 13X. The differences in regeneration temperature alteration because of ultrasonication in ultrasound-assisted regeneration of zeolite 13X, activated alumina and silica gel could be related to different thermal and acoustical properties of these materials. As it was mentioned earlier, the temperature regime is dictated by thermal diffusion and acoustic dissipation. The thermal diffusion depends on many factors such as thermal conductivity and bead geometry (gap volume between the beads and area of contact between beads) all of which are material-specific. Acoustic dissipation depends on various factors such as Young modulus and Poisson's ratio and geometry of pores and beads which all f them differ for different material.

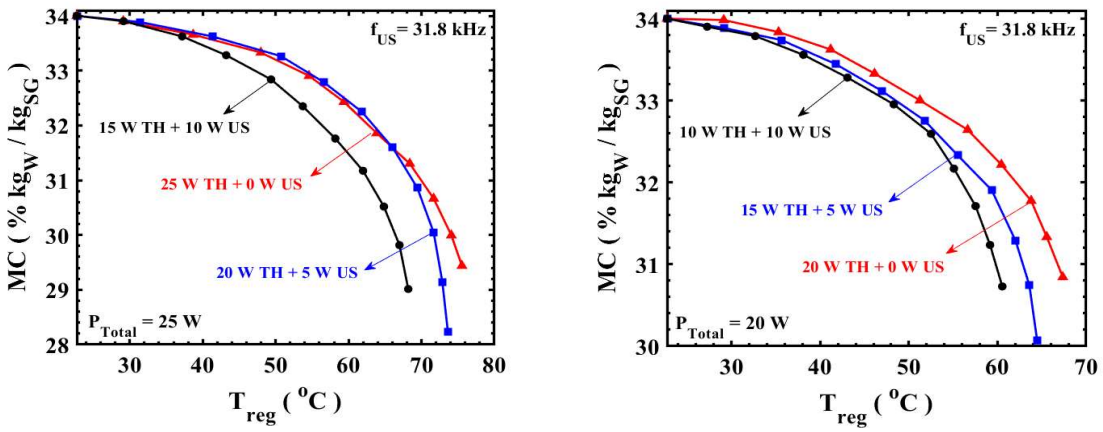

Figure 16. Moisture content variation with average regeneration temperature for silica gel, P_{Total}=20W (left) and P_{Total} =25W

Additionally, at higher P_{US}/P_{Total}, i.e., P_{US}/P_{Total} = 0.4 and 0.5, there is a noticeable drop in T_{reg}.

To investigate the effect of incorporating ultrasound on the variation of moisture content with T_{reg}, the temperatures at which ultrasound-assisted and heat-only regeneration processes reach the same amount of remaining adsorbed moisture are compared. To do so, for each power level, the water content of the adsorbent at the end of the heat-only experiment is considered as the baseline value. Then the temperature to reach the same water content in ultrasound-assisted regeneration with the same total power input, is determined. The temperatures at which the *MC* reaches the baseline value for all power ratios are presented in Table 9. The lowest T_{reg} are observed at P_{US}/P_{Total} = 0.4 and 0.5 with 9.9% and 10.6% lower T_{reg}, respectively. Shifting toward lower P_{US}/P_{Total}, the decrease in T_{reg} compared to no-ultrasound decreases drastically. It is noteworthy that at these values of P_{US}/P_{Total} the *UDEE* values are the lowest, meaning that there is a trade-off between lowering T_{reg} and lowering the regeneration energy intensity when it comes to utilization of ultrasound.

Table 9. Regeneration temperatures to reach final moisture content, where the initial moisture content is 34% for each case.

Total power (W)	P_{US}/P_{Total}	Final moisture Content (%)	T_{reg} (°C)
20	0.00	30.8	66.8
	0.25		62.8
	0.50		59.7
25	0.00	29.4	75.1
	0.20		72.4
	0.40		67.7

5.6. Summary

Regeneration of silica gel under ultrasonic radiation for application in solid desiccant industrial gas drying is investigated.

Since at each power level the total power input P_{Total} was kept constant, the results of both ultrasound-assisted and non-ultrasound regeneration processes can be compared. Analysing the values of moisture content, it can be concluded the application of ultrasound, regardless of P_{Total} or P_{US}/P_{Total} where P_{US} is the ultrasonic power, results in higher moisture removal rate. The water vapor diffusion regime in silica gel is investigated and a diffusion model that includes all likely transport modes in porous media is proposed, based on which an apparent diffusion coefficient that considers temperature and acoustic inputs is developed. Regarding the regeneration temperature, it is concluded that the regeneration temperature of the silica gel is not solely dictated by the thermal input and the ultrasound-enhanced heat transfer and acoustic dissipation noticeably contributes to the temperature rise. To appraise the energy efficiency associated with integration of ultrasound the metric ultrasonic desorption efficiency enhancement *UDEE* is used. Comparing the values of *UDEE* in ultrasound-assisted and non-ultrasound regeneration processes proves that application of ultrasound at any power level and all P_{US}/P_{Total} results in energy savings by as much as 26%. The lower P_{US}/P_{Total} are observed to be more effective in improving energy efficiency than higher P_{US}/P_{Total}. The variation of *MC* with T_{reg} is investigated and integration of ultrasound observed to lower the regeneration temperature. The highest drop in T_{reg} were achieved at highest P_{US}/P_{Total} with ~ 11% lower T_{reg}.

6. ULTRASOUND-ASSISTED REGENERATION MECHANISMS

Although the usefulness of integrating ultrasound in the regeneration process is established, the mechanisms by which ultrasound improves regeneration are still unclear. The regeneration of desiccants can be considered to consist of two processes: the detachment of the adsorbate molecule from the adsorbent surface (desorption) and transport of the detached adsorbate molecule out of the pore and eventually far from the surface (diffusion). A schematic of processes involved in regeneration of adsorbents is provided in Fig. 17. Ultrasound can potentially enhance both desorption and diffusion processes. As has been stablished earlier, in the absence of bulk liquid or liquid-mimicking molecular clusters, all ultrasound-associated enhancing mechanisms related to liquids such as acoustic cavitation, acoustic streaming and boundary layer alteration can be disregarded as an enhancement mechanism in ultrasound-assisted regeneration. Additionally, the inverse proportionality between desorption and ultrasonic frequency observed in ultrasound-assisted regeneration of zeolite 13X and activated alumina (Figs. 8 and 12), which has also been reported in the literature [33], contradicts the proposed theory of ultrasound-enhanced desorption through acoustic dissipation [52] to some degree since the acoustic attenuation coefficient is proportional to frequency. An increase in frequency should therefore lead to an increase in desorption [102]–[104], but that is contradicted by the current results. The attenuation in porous media can be thought of as an amalgamation of attenuation in the solid and void parts. The attenuation in the granular solid part α_s is defined as [105]:

$$\alpha_s = A_s D^3 f_{US}^4 \tag{10}$$

where A_s is a material-specific coefficient that depends on the elastic moduli, D the grain diameter and f the frequency of the acoustic wave. The attenuation in the void part regardless of the presence of adsorbate molecules is thermo-viscous absorption and is formulated as [46]:

$$\alpha_v = \frac{2\pi^2 \delta_f f_{US}^2}{c_0^3} \tag{11}$$

where δ_f is the fluid-specific acoustic diffusivity and c_0 the speed of sound in the fluid media. Thus, the acoustic attenuation in porous media, regardless of the order of predominance, depends on f_{US} to either the 2nd or 4th power:

$$\alpha_p \propto F(f_{US}^4, f_{US}^2) \tag{12}$$

Therefore, it appears unlikely that increased acoustic dissipation is responsible for the observed enhancements in desorption. Ultrasound basically induces a pressure change which in fluidic media results in alternating high-low pressure zones and in solids results in mechanical stress. This alternating pressure can affect the regeneration dynamics such as adsorption potential, surface energy and adsorbate diffusivity.

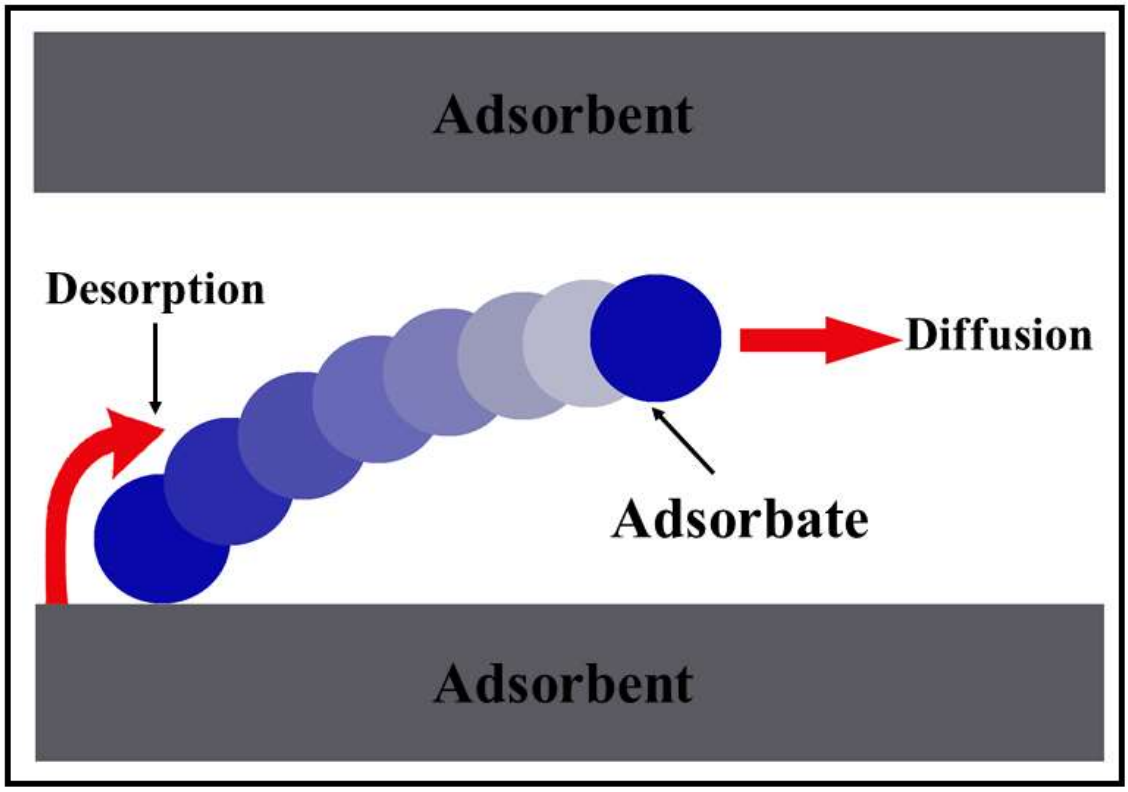

Figure 17. Regeneration process broken down to desorption and diffusion processes.

6.1. Decrease in Adsorption Potential

Considering that desorption is the reverse of the adsorption process, it can be interpreted as overcoming the adsorption potential. The adsorption potential is the energy required to move adsorbate molecules in the gas phase of pressure to a condensed state of vapor pressure [89]. Following Polanyi potential theory, the adsorption potential A is defined as [106]:

$$A = RTln(\frac{P_s}{p}) \tag{13}$$

where R is the ideal gas constant, T the temperature in Kelvin, P the pressure and P_s the adsorbate saturation pressure at T. Keeping in mind that saturation pressure is a function

of temperature *f(T)*, the adsorption potential can be rearranged as an implicit function of pressure and temperature *H*:

$$A = H(T, P) \tag{14}$$

The variation in the pressure is dictated by the ultrasound–induced alternating zones of compression and rarefaction (P_{US}) and the variation in the temperature is imposed by the thermal input (P_{TH}). Therefore, the adsorption potential can be considered as an implicit function of both ultrasonic and thermal inputs *H**:

$$A = H^*(P_{TH}, P_{US}) \tag{15}$$

A schematic diagram of the dependency of adsorption potential on both temperature and pressure is provided in Fig. 18. The implicit dependency of adsorption potential on both ultrasonic and thermal input suggests that to achieve the most efficient desorption, the ratio of ultrasonic-to-total power needs to be optimized.

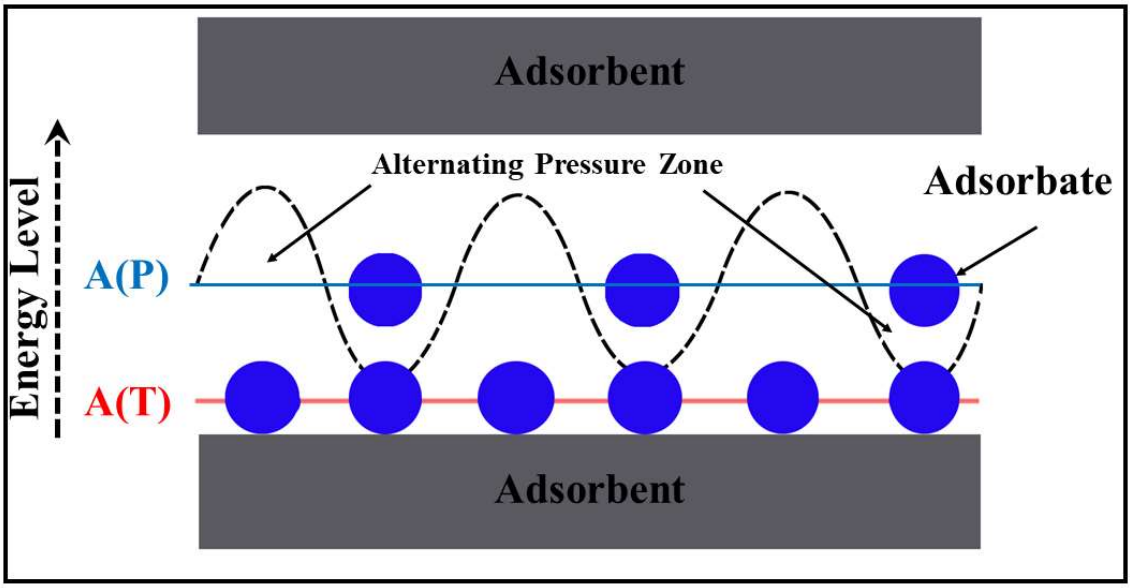

Figure 18. Change in adsorption potential due to ultrasonication.

6.2. Increase in Adsorbate Surface Energy

The adsorption-induced strain or swelling of adsorbents has been observed and investigated for a long time [107]–[115]. The adsorption-induced expansion is not due to the physical stress that is allegedly exerted on the adsorbent by the adsorbate molecules but comes about because of the relaxation of the adsorbent surface due to energy loss. During the adsorption process, both adsorbate and adsorbent molecules end up with a reduction in energy (release of the adsorption enthalpy), with the adsorbent losing its surface energy and consequently expanding. Boissiere et al. [114] investigated the expansion/contraction of the adsorbent in an adsorption-desorption cycle on porous silica and observed expansion of the adsorbent during adsorption and contraction to its initial size during desorption.

Since the contraction of the adsorbent during desorption was observed and the adsorbent retracts to its original dimension, it can be concluded that the adsorption-induced expansion and the desorption-induced contraction occur within the elastic regime and thus it yields:

$$\sigma_{ads} = E\varepsilon_{ads} \tag{16}$$

where σ_{ads} is the adsorption-induced stress on the adsorbent surface, ε_{ads} the adsorption-induced strain and E the adsorbent elastic modulus. Bangham's law states that the strain of an adsorbent ε_{ads} during the adsorption process is proportional to the reduction in its surface energy γ [116].

$$\varepsilon_{ads} \propto \Delta\gamma \tag{17}$$

Consequently, the adsorption-induced stress on the surface of the adsorbent is related to the reduction in its surface energy:

$$\frac{\sigma}{E} \propto \Delta\gamma \tag{18}$$

The ultrasonic-enhanced regeneration process may therefore potentially be explained by the mechanical effects of the ultrasound waves. The ultrasound wave passing through a medium exerts an alternating force which causes tensile/compressive stresses on the medium. Since both adsorption-induced expansion and desorption-induced contraction are reversible processes, contraction or in other words applying compressive stress on the adsorbent results in increasing its surface energy and consequently in desorption of adsorbate molecules. Figure 19 showcases the change in the surface energy of an occupied adsorption site due stress resulting from ultrasonication.

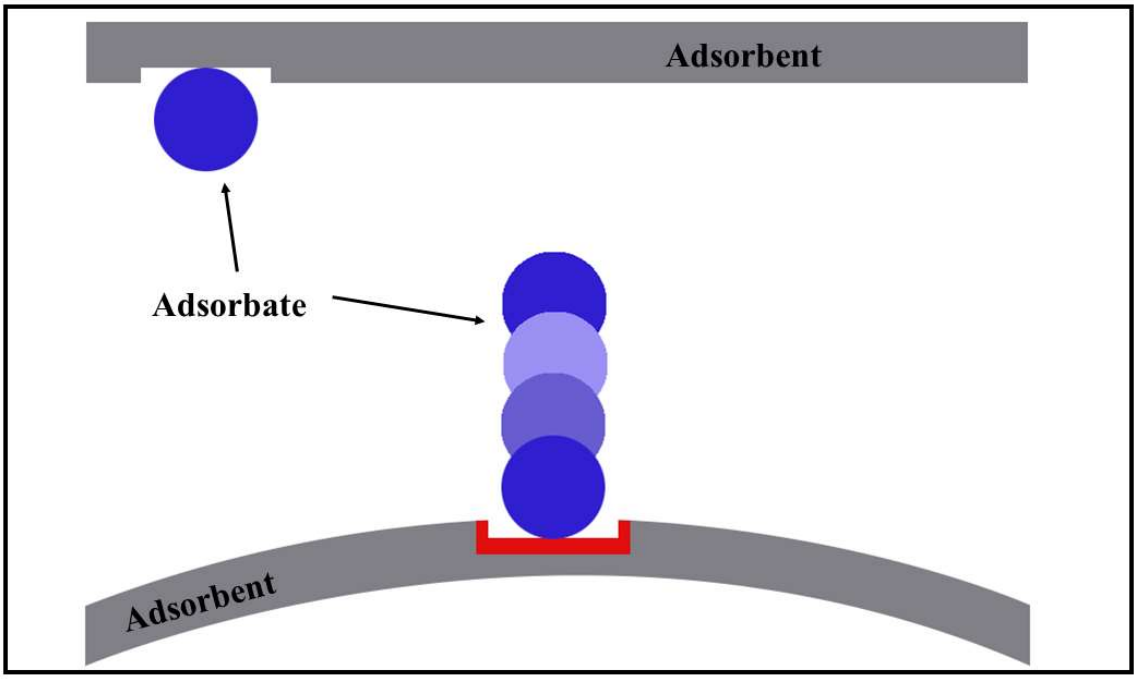

Figure 19. Increase in adsorbent surface energy due to ultrasonication.

The increase in surface energy of adsorbents due to contraction induced by ultrasound can be written as:

$$\Delta\gamma \propto \frac{\rho c \delta \omega}{E} \sin(\omega t) = \frac{\sqrt{2\rho c I}}{E} \sin(\omega t) \tag{19}$$

where ρ is the adsorbent density, c the speed of sound in the adsorbent, δ the acoustic displacement, ω the angular frequency ($\omega = 2\pi f_{US}$) and I the ultrasonic intensity. Other parameters that affect the desorption process are the temperature and pressure. The adsorption/desorption potential A depends solely on temperature and pressure since the saturation pressure varies only with temperature. So, the energy regime of the desorption process is controlled by the mechanical stress on the adsorbent surface, the pressure within its pores and its temperature. The mechanical stress (contraction) and pore pressure (in part) are dictated by the ultrasonic variables, i.e., ultrasonic power and frequency, and the temperature except for the minor acoustic dissipation effect is controlled mainly by the thermal input. Thus, the energy required for the desorption process E_{des} is an implicit function of ultrasonic power P_{US}, thermal power P_{TH}, and ultrasonic frequency f_{US}:

$$E_{des} = F(P_{US}, f_{US}, P_{TH}) \tag{20}$$

The implicit dependency of desorption energy on P_{US}, f_{US}, and P_{TH} indicates that to attain the optimal desorption, the ratio P_{US}/P_{Total} and f_{US} need to be optimized.

6.3. Enhanced Diffusion of Adsorbates

The diffusion mechanism of a single adsorbate molecule in porous media is described through Knudsen diffusion, slip diffusion, surface diffusion and viscous diffusion [117], [118]. Depending on many parameters such as adsorbent saturation degree, adsorbent pore

size, pressure and temperature, one or all of these mechanisms contribute to mass transfer either in series or parallel as shown in Fig. 20 [118]–[120]. Yao et al. reported that for porous media with pore diameter less than 200 Å which includes zeolites, activated alumina and silica gel, the ultrasound-enhanced mass transfer is due to the effect of temperature rise, induced by acoustic dissipation, on diffusivity [118]. Since the acoustic dissipation increases with an increase in frequency, ultrasound-enhanced mass transfer should therefore increase with increasing ultrasonic frequency [121]–[125]. This hypothesis, however, contradicts the experimental results of current and previous work in which the ultrasound-enhanced regeneration of silica gel, zeolite 13X and activated alumina was found to be inversely proportional to ultrasonic frequency, and with an increase in frequency the ultrasound-induced enhancement noticeably diminished [124], [125].

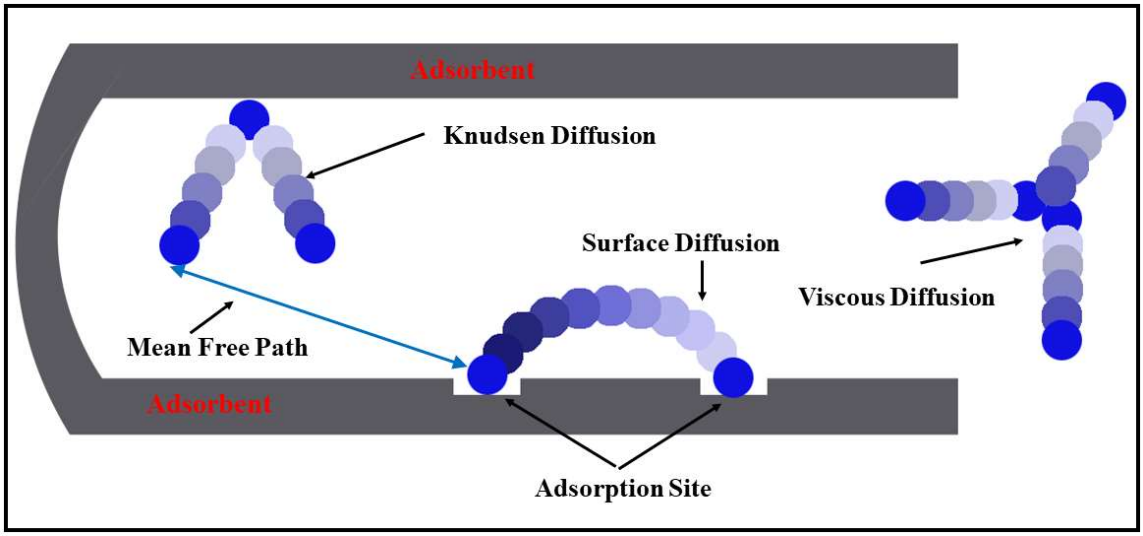

Figure 20. Various modes of diffusion in porous media.

In nano-porous materials the transport mechanism is determined using the Knudsen number k_n [117], [126]. The mean free path Λ is determined as [127]:

$$\Lambda = \frac{k_B T}{\pi\sqrt{2} P d^2} \tag{21}$$

where k_B is the Boltzmann constant, T temperature, P pressure and d the molecule effective diameter. For water molecules under normal conditions ($P = 1\ atm$ and $T = 300\ K$) the mean free path is about 0.128 μm. Considering an average pore diameter of d_p ≅ 2.5 nm for silica gel, $k_n = \Lambda / d_p \cong 50$, meaning that the probability of molecule-molecule collisions is negligible compared to molecule-wall collisions, thus justifying Knudsen diffusion [117], [126]. When the transport occurs inside relatively large pores, under ultrasonic radiation when the pressure drastically alters periodically and upon increase reduces the mean free path and consequently reduces k_n, the diffusion mechanism changes to transitional Knudsen-viscous (slip) and eventually fully viscous diffusion [117]. The advective-diffusive model (ADM) and the dusty-gas model (DGM), based on Knudsen, transition, and viscous transport modes, have been proposed to model the combined gas phase diffusion and advection in porous media.

Under atmospheric pressure and for porous media with relatively high permeabilities ($k > 10^{-13}\ m^2$), both models are in good agreement [128]. The diffusivity, D_{ADM}, based on ADM disregarding the binary transport mode is defined as [128]:

$$D_{ADM} = \frac{k_0}{\nu_g}\left(1 - \frac{b}{P}\right) RT \tag{22}$$

where k_0 is the intrinsic permeability, ν_g the gas-phase kinematic viscosity, b the Klingenberg factor (slip and Knudsen diffusion correction factor). This model, however, is more suitable for porous media of low surface area such as soil, rock and shale as it disregards surface diffusion [119], [128].

For sorbents of high surface area such as activated carbon and silica gel surface diffusion is regarded as the most important mode of transport and experimentally it has been shown that the apparent diffusivity is one order of magnitude higher than the calculated pore diffusion (surface diffusion excluded) which contributes to surface diffusion [117], [129]–[131]. Many parameters such as surface coverage, surface temperature and activation energy affect the surface diffusivity D_s which can be written as [117], [129]:

$$D_s = D_{s,\infty}(\Theta)\, e^{(-E_{ac}/RT)} \tag{23}$$

where $D_{s,\infty}(\Theta)$ is the concentration-dependent surface diffusivity at infinite temperature, Θ the surface coverage, and E_{ac} the activation energy. The activation energy E_{ac} is a fraction of the adsorption potential A [129], [132]–[134]:

$$E_{ac} = \alpha\, A \quad 0 < \alpha \leq 1 \tag{24}$$

where α is a ratio that depends on the adsorbate-adsorbent interactions.

The total diffusivity D_T that includes Knudsen, slip, viscous and surface diffusion mechanisms can thus be represented as:

$$D_T = \frac{k_0}{v_g}\left(1 - \frac{b}{P}\right) RT + D_{s,\infty}(\Theta) \exp\left[-\frac{\alpha f\left(RT ln\left(\frac{P_s}{P}\right)\right)}{RT}\right] \tag{25}$$

Under ultrasonic radiation, pressure varies periodically [135]:

$$P(t) = P_\infty + P_a \sin(\omega t) \tag{26}$$

where P_∞ is the ambient pressure, P_a the pressure amplitude, and ω the angular frequency. Substituting alternating pressure into Eq. (25) yields the apparent diffusion coefficient D_{app} in porous media under ultrasonic radiation:

$$D_{app} = \frac{k_0}{\nu_g}\left(1 - \frac{b}{P_\infty + P_a \sin(\omega t)}\right) RT + D_{s,\infty}(\Theta) \exp\left[-\frac{\alpha f\left(RT ln\left(\frac{P_s}{P_\infty + P_a \sin(\omega t)}\right)\right)}{RT}\right] \quad (27)$$

Equation (27) represents the contributions of various diffusion mechanisms–regardless of whether they are in series or parallel–and suggests the dependency of D_{app} on temperature, ultrasonic pressure and ultrasonic frequency for a given porous medium as previously observed [124], [125], [136], [137]. D_{app} increases with an increase in temperature and since the temperature rise due to the acoustic dissipation is insignificant, increases only with increasing thermal power. Additionally, the pressure alteration induced by ultrasound waves during rarefaction (low-pressure zones) results in an increase in apparent diffusivity. The magnitude of the pressure reduction P_a is proportional to the ultrasonic intensity I by a power of 0.5 [138]:

$$P_a = \sqrt{2\rho c I} \quad (28)$$

where ρ is the density of the medium and c the speed of sound. The dependency of D_{app} on the ultrasonic frequency is described through the time period of sound waves.

With an increase in frequency, the pressure alteration becomes so fast that there is not enough time for low pressure zones to effectively be established [124], [139], [140].

6.4. Contribution and Pressure Dependency of the Proposed Mechanisms

Amongst the three proposed mechanisms, decreased desorption potential and enhanced mass diffusion have theoretical equations that suggest their dependency on alternating pressure. To investigate the sensitivity of the proposed mechanisms with respect to a change in pressure, the derivate method is utilized:

$$\Delta Y = \frac{dY}{dX}\,\Delta X \tag{29}$$

where ΔY is the change in the dependent variable Y and ΔX is the change in the dependent variable X. Here we define the alternating pressure, Π, induced by ultrasonication as:

$$\Pi = P_\infty + P_a \sin(\omega t) \tag{30}$$

For the decreased desorption potential, the change in A_{des} as a result of a change in Π is obtained by:

$$\Delta A_{des} = \frac{dA_{des}}{d\Pi}\Delta\Pi = \left(RT\,\frac{1}{\Pi}\right)\Delta\Pi \tag{31}$$

The change in A_{des} due to a change in Π relative to the value of A_{des} is determined as:

$$\frac{\Delta A_{des}}{A_{des}} = \frac{RT\frac{\Delta\Pi}{\Pi}}{RT ln\left(\frac{P_s}{\Pi}\right)} = \frac{\Delta\Pi}{\Pi ln\left(\frac{P_s}{\Pi}\right)} \tag{32}$$

As for the enhanced diffusion, the change in D_{app} as a result of a change in Π is obtained by:

$$\Delta D_{app} = \frac{dD_{ap}}{d\Pi}\Delta\Pi = \left[\frac{bk_0RT}{\nu_g}\,\frac{1}{\Pi^2} + D_{s,\infty}(\theta,T)\,\frac{\alpha}{P_s}\,\frac{1}{\Pi^{1-\alpha}}\right]\Delta\Pi \tag{33}$$

Considering $\Pi \sim 10^5$, $\alpha \sim 0.65$, $\frac{1}{\Pi^2} \sim 10^{-10}$ and $\frac{1}{\Pi^{1-\alpha}} \sim 10^{-1.75}$, the first term of the derivative can be dropped from the equation. Also, since the surface diffusion is considered the most important mode of transport, the change in D_{app} due to a change in Π relative to the value of D_{app} is determined as:

$$\frac{\Delta D_{ap}}{D_{app}} = \frac{D_{s,\infty}(\theta,T)\frac{\alpha}{P_S}\frac{1}{\Pi^{1-\alpha}}\Delta\Pi}{D_{s,\infty}(\theta,T)\left(\frac{P_S}{\Pi}\right)^{-\alpha}} = \frac{\alpha\Pi^{(2\alpha-1)}}{P_S{}^{(1+\alpha)}}\Delta\Pi \tag{34}$$

To evaluate the pressure change due to ultrasonication, it's necessary to establish the medium in which alternating pressure occurs. Whether the medium is moist air or a cluster of water molecules makes a big difference in the amplitude of the alternating pressure and consequently the extent by which it affects the proposed mechanisms. The change in pressure due to ultrasonication for P_{US} =10 W can be determined using Eq. (28). Considering air acoustic properties at T_{reg} = 40 °C, ΔΠ is about 2070 Pa translating to 1.1% and 3.2% change in A_{des} and D_{app}, respectively. For bulk liquid water, considering water acoustic properties at T_{reg} = 40 °C, ΔΠ is about 98900 Pa translating to 52% and 118 % change in A_{des} and D_{app}, respectively. Considering enhancement magnitudes observed in regeneration of adsorbents, it can be concluded that ultrasound enhances regeneration by acting on the interface of air/water rather than each of them alone. Also, comparing the changes in A_{des} and D_{app} due to the change in pressure indicates that the change in D_{app} is significantly larger than the change in A_{des} regardless of the medium, suggesting that D_{app} contributes more to the ultrasound-enhanced regeneration.

6.5. Summary

Amongst the proposed mechanisms behind ultrasound-assisted regeneration, based on the inverse proportionality between f_{US} and *UDEE*, acoustic dissipation as a sole mechanism is refuted. Additionally, due to the absence of bulk liquid or bulk-liquid-imitating adsorbate molecule clusters, postulated mechanisms such as acoustic cavitation, microstreaming and acoustic streaming are rejected. Evolving from the alternating pressure associated with ultrasonication, three mechanisms of reduced adsorbate adsorption potential, increased adsorbate surface energy and enhanced mass diffusion are proposed and the implicit dependency of ultrasound-enhanced regeneration on ultrasonic parameters is postulated. Investigating the variation of reduced adsorbate adsorption potential and enhanced mass diffusion with the change in pressure using the derivative method reveals that the medium at which ultrasound acts is not either air or water but both of them to different extent. Also, for the same amount of pressure change, the magnitude of change in enhanced mass diffusion is considerably higher than that of reduced adsorbate adsorption potential pointing out the possibility of enhanced mass diffusion being the key mechanism in ultrasound-enhanced regeneration.

7. REGENERATION EFFICIENCY IN ADSORPTION THERMAL ENERGY STORAGE

Sorption thermal energy storage (TES) seems to be an auspicious solution to overcome the issues of intermittent energy sources and waste heat recovery. Sorption TES systems involve both desorption and adsorption processes and work on the principle of releasing and capturing the enthalpy of adsorption (adsorption potential) of an adsorption pair. During the charging stage (desorption), the adsorbent is regenerated and the adsorbate is desorbed. In the course of discharging (adsorption), the adsorbate is reintroduced to the adsorbent and gets adsorbed by the adsorbent. A schematic diagram of a sorption TES is provided in Fig. 21.

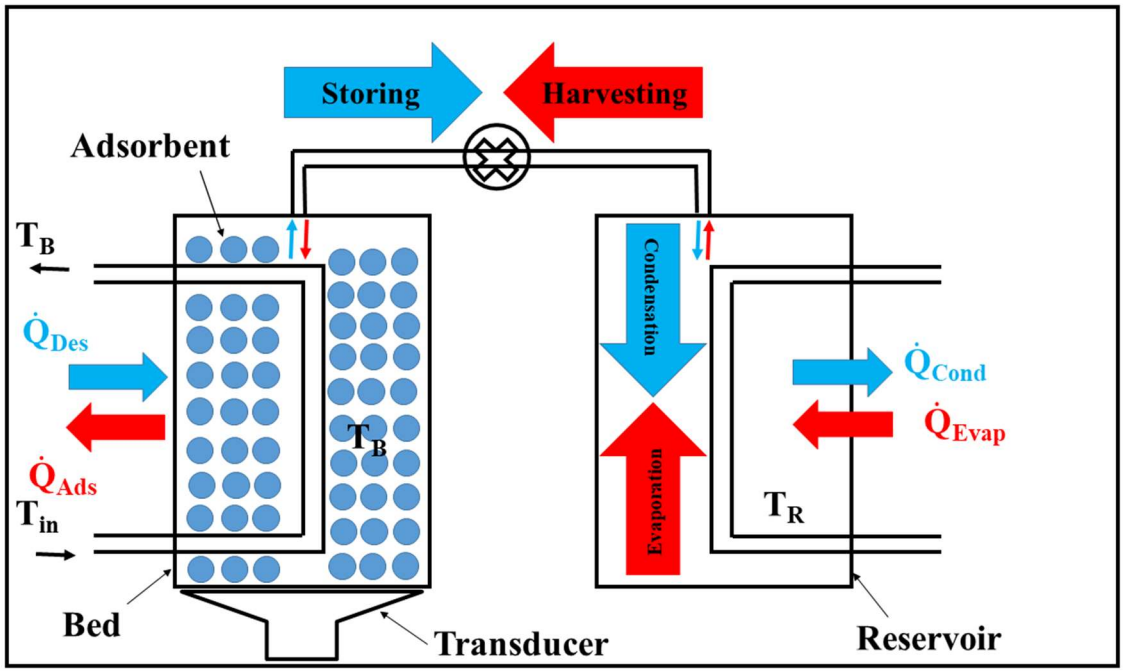

Figure 21. Schematic of an ultrasound-integrated sorption TES.

The differences in the regeneration time, the regeneration temperature and the required regeneration energy of the adsorption pairs necessitates the development of comparative models and metrics to estimate and compare the efficiency of desorption processes.

Modeling of adsorption thermal energy storage (TES) systems has been previously performed using a variety of assumptions and models [141]–[148]. As invaluable and contributory these works are, they apparently lack a figure of merit that enables the comparison and justification of the TES systems based on the desorption dynamics of the adsorption pair. Here, based on the overall energy recovery of the thermal storage process two models which introduce two distinct metrics related to efficiency are proposed: constant-time efficiency and constant-power efficiency. The novel proposed metrics can be employed to justify incorporating ultrasound and any other auxiliary energy along with or without low-grade heat. The constant-time model is useful when the quality of the heat source is at stake. This model and its metric apprise sorption TES systems based on the temperature of the stored heat. For instance, for a sorption TES system that is fed by solar heat at a certain temperature, this metric can justify the feasibility of increasing the feed temperature by any means without the trouble of experimentation or simulation. On the other hand, the constant-power model and its corresponding metric is beneficial when the intensity of the heat source is important which could be of interest when the heat source is of intermittent nature.

7.1. Constant-Time Model

For the constant-time model, the desorption bed is assumed to be a lumped system meaning there is no spatial temperature gradient and the variation of temperature is solely temporal.

The lumped-system adaptation has been previously utilized to describe sorption energy systems [49], [144], [149]. The model is considered as an open system consisting of a single bed. During the storing stage (desorption), the heat transfer fluid enters the bed at a

temperature higher than the bed temperature, thus supplying thermal energy to remove the adsorbate. In the harvesting stage (adsorption), the removed adsorbate is re-supplied to the adsorbate and the heat transfer fluid enters the bed at a temperature lower than the bed temperature, thus removing thermal energy from the bed. The input energy to the system is simulated to be transferred to the bed by a heat transfer fluid through a heat exchanger of such effectiveness that working fluid enters the bed at a temperature higher than the bed temperature and leaves the bed at the same temperature as the bed. A representation of the model is presented in Fig. 22. The assumptions that are made in this model are valid enough so that the model represents an actual system to an acceptable degree without risking its universality. The energy balance of the bed during the desorption process is

$$C_f(T_{in} - T_B)dt - (\Delta H_{Ads} + h)dm_{des} - (U_{loss} + C_{Al})dT_B = (m_s c_s)dT_B \quad (35)$$

where C_f is the heat capacity rate of the heat transfer fluid, T_{in} the heat transfer fluid inlet temperature, T_B the adsorbent temperature, m_{des} the mass of the removed adsorbate, ΔH_{Ads} the enthalpy of adsorption, h_{des} the enthalpy of the removed adsorbate (water vapor), U_{loss} the product of the convective heat transfer coefficient and area of the bed (inverse of heat loss resistance), C_{Al} the heat capacity of the aluminum bed m_s the adsorbent mass and c_s the adsorbent specific heat capacity. The energy balance equation here assumes that the rate of thermal and concentration diffusions are comparable since the desorption depends on the regeneration temperature. To verify this assumption the Lewis number *Le* is utilized [64]:

$$Le = \frac{\alpha}{D_{air\quad{}_2O}} \quad (36)$$

where α is the thermal diffusivity and D_{air-H_2O} is the mass diffusivity of water vapor in air and differs from the mass diffusivity of adsorbate in pores discussed earlier.

For an average regeneration temperature of 50 °C observed in this study, the magnitude of Le is ~ 5 meaning that the thermal and mass diffusions are comparable. The mass diffusivity depends on temperature by the power of $2^{2.072}$ and since in real-world TES systems the temperature can be much higher, Le would become noticeably smaller.

A closer look into Eq. (35) reveals that the input energy to the bed is $C_f(T_{in} - T_B)dt$ and the stored energy (harvestable portion) is $dm_w\,\Delta H_{Ads}$. Following the classical approach toward efficiency, the desorption efficiency is defined as:

$$\eta = \frac{E_{des}}{E_{input}} = \frac{\Delta m_{des}\Delta H_{ads}}{C_f(T_{in}-T_B)\Delta t} \tag{37}$$

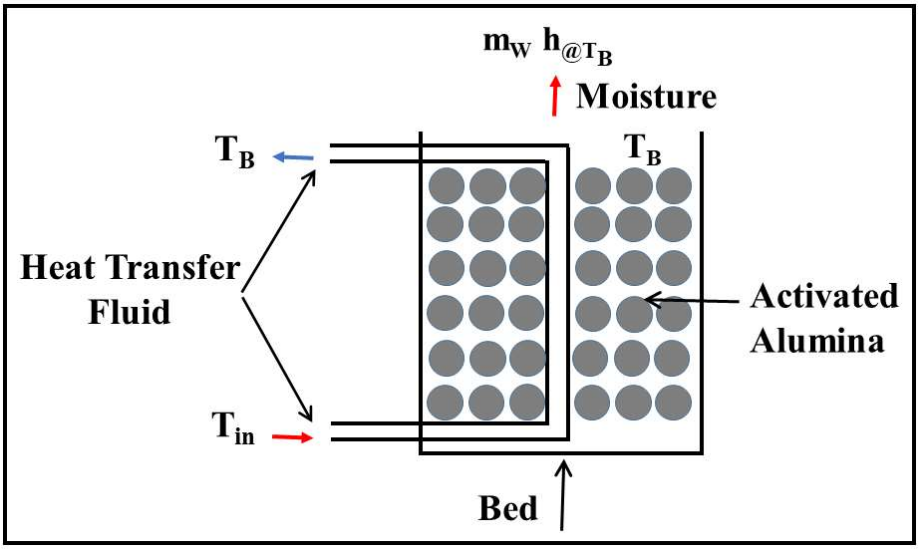

Figure 22. Schematic diagram of the constant-time model.

The desorption period (Δt) is assumed to be constant in this model. Since ΔH_{Des} and C_f remain unchanged, Eq. (37) can be rearranged to:

$$\eta_{\Delta t} = \frac{\Delta H_{ads}}{C_f \Delta t} \times \frac{\Delta m_{des}}{T_{in} - T_B} = K_{\Delta t} \frac{\Delta m_{des}}{T_{in} - T_B} \tag{38}$$

where $K_{\Delta t}$ is a product of constants and $\eta_{\Delta t}$ is the efficiency defined under a constant desorption period (Δt). For an infinitesimal increase in adsorbent temperature dT that causes the removal of dm adsorbate, Eq. (38) is simplified to:

$$\eta_{\Delta t} = K_{\Delta t} \frac{dm}{dT} \tag{39}$$

Since the mass of desiccant (m_s) is constant, using the definition of moisture ratio (MR) in Eq. (1) we have:

$$dm = m_s \, d(MR) \tag{40}$$

Combining Eq. (39) and Eq. (40), we can manifest the efficiency of the desorption process in terms of the variation of adsorbate content with respect to regeneration temperature $[d(MR)/dT]$:

$$\eta_{\Delta t} = K'_{\Delta t} \frac{d(MR)}{dT} \tag{41}$$

where $K'_{\Delta t}$ is also a product of constants. The metric $[d(MR)/dT]$, representing the variation of adsorbate content with adsorbent temperature, is the slope of the moisture ratio-temperature curve (Fig. 23). This metric is useful when comparing regeneration of adsorption pairs based on the regeneration temperature, especially for low-grade heat utilization in thermal energy storage and adsorption cooling systems.

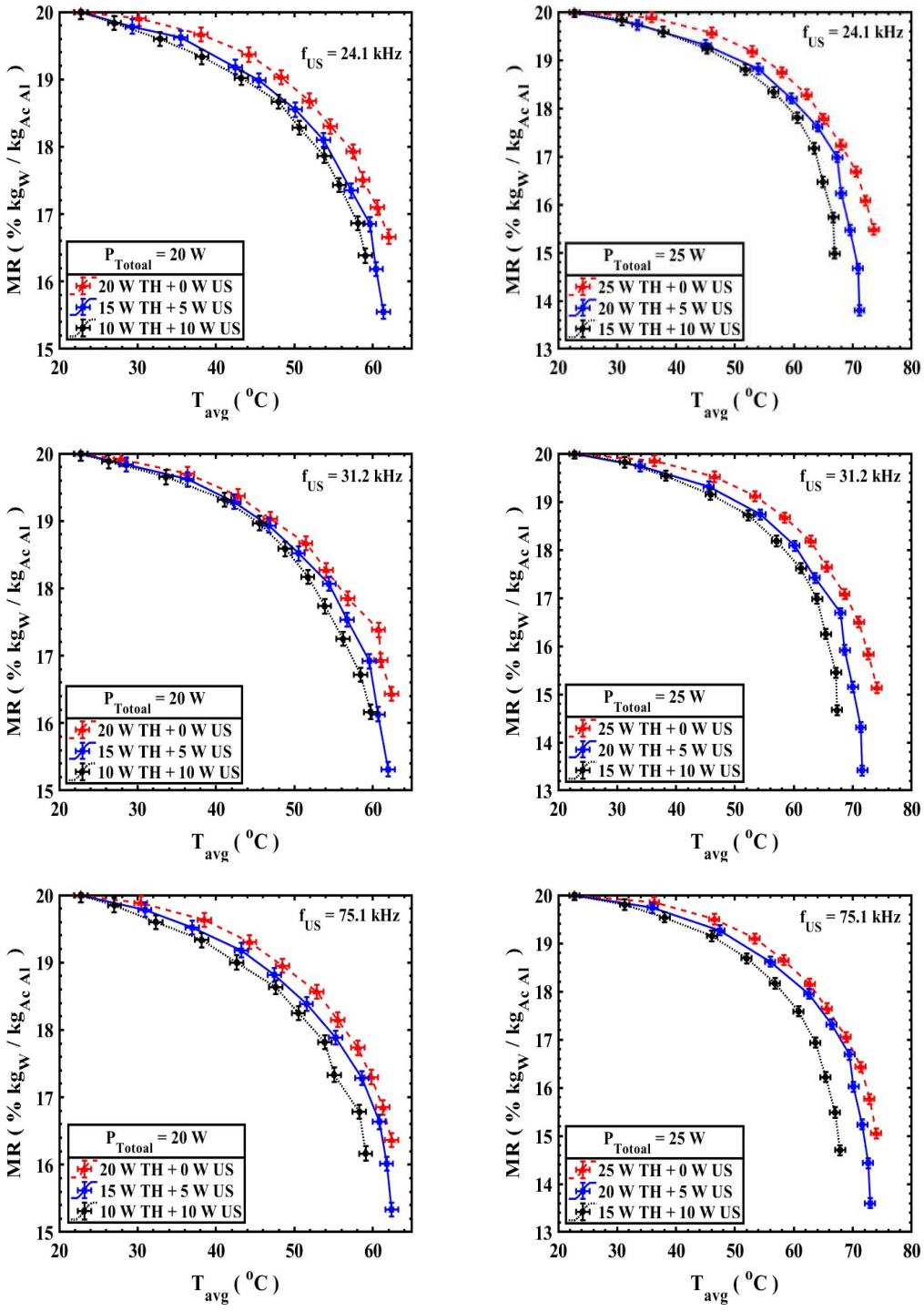

Figure 23. Moisture ratio variation with average regeneration temperature for activated alumina/water. P_{Total} =20 W (left) and P_{Total} =25 W (right). f_{US} =24.1 kHz (top), f_{US} =31.2 kHz (middle) and f_{US} =75.1 kHz (bottom).

7.2. Constant-Power Model

In the constant-power model like the constant-time model, the desorption bed is assumed to be a "lumped" system, meaning that the spatial temperature gradient is negligible compared to the temporal temperature variation. Although realistically there are axial and radial temperature gradients across the bed, the lumped system assumption seems reasonable enough as the maximum axial and radial temperature difference across the bed over a 65 °C temperature rise are 1°C and 6°C, respectively. The total input energy to the system, regardless of type and temperature, is simulated to be supplied by a heater. A schematic diagram of the model is presented in Fig. 24. The mathematical relations governing the model are the energy balance and the equation of state:

$$P_T dt - (\Delta H_{Ads} + h) dm_{des} - (U_{loss} + C_{Al}) dT_B = (m_s c_s) dT_B$$

$$MR(t) = MR_i \, exp\left[-k(1 - \frac{T(t)}{T_s})^{-n}\right] \tag{42}$$

where P_T is the total input power to the bed, MR_i the initial moisture ratio, k and n material-specific parameters of the revised Dubinin-Astakhov adsorption equation [150] and to be determined experimentally, and T_s the adsorbate saturation temperature. The desorption equation of state used here is a modified version of the Dubinin-Astakhov adsorption equation [71], [89]:

$$W = W_0 \exp\left[-\left(\frac{RT \ln(\frac{P_s}{P})}{E_c}\right)^{n_d}\right] \tag{43}$$

where W is the adsorption volume, E_c the characteristic energy and n_d the heterogeneity factor of the micropore size distribution. The desorption equation of state was not included in the constant-time model since the model could not be validated due to dissimilarities

between the model and the experimental part of this study. Teng et al. developed a temperature version of the Dubinin-Astakhov equation on the basis of T and T_s instead of P and P_s [151]:

$$x = x_0 \exp\left[-k_t\left(\frac{T}{T_s} - 1\right)^{n_t}\right] \tag{44}$$

where x is the adsorption capacity and k_t and n_t material-specific parameters.

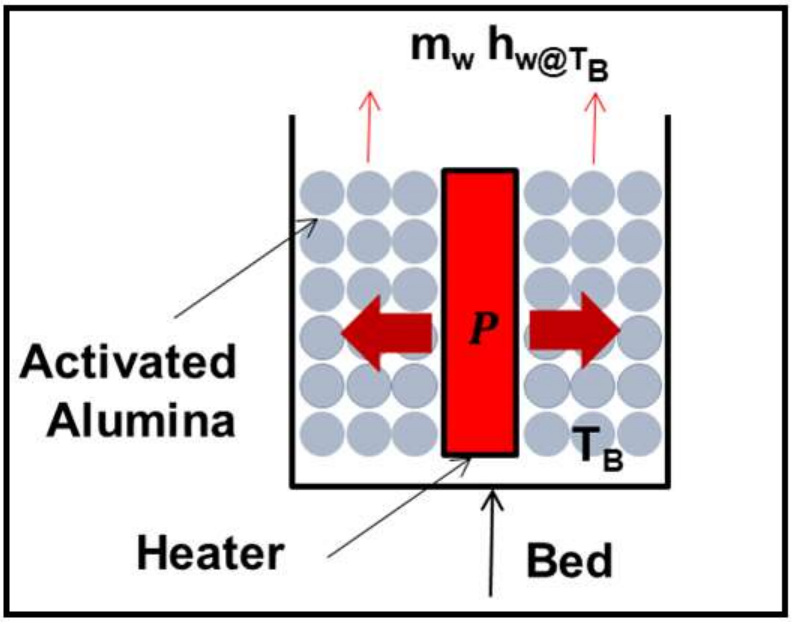

Figure 24. Schematic diagram of the constant-power model.

For desorption processes where temperatures are above the saturation temperature ($T > T_s$), Eq. (36) complies with experimental data [66]. However, for temperatures below the saturation temperature ($T < T_s$), the exponential part of the equation increases which no longer describes a desorption process but rather an adsorption process. The limitation of the Dubinin-Astakhov temperature equation of state necessitates a modification that enables the equation of state to describe desorption processes at temperatures below the saturation temperature. Following the approach from Teng et al. [151] we start with the Dubinin-Astakhov adsorption equation,

$$x = x_0 \exp\left[-C_1\left(RT\ln\left(\frac{P_s}{P}\right)\right)^{n_d}\right] = x_0 \exp[-C_1(A_{ads})^{n_d}] \quad (45)$$

where C_1 is a product of material-specific constants and A_{ads} the adsorption potential. Since desorption is the reverse of adsorption, it gives

$$A_{des} = -A_{ads} = -RT\ln\left(\frac{P_s}{P}\right) = RT\ln\left(\frac{P}{P_s}\right) \quad (46)$$

where A_{des} is the desorption potential. The inverse relationship between the pressure ratios of adsorption (P_s/P) and desorption (P/P_s) physically makes sense since the former favors pressures higher than P_s and the latter favors pressures lower than P_s which is the working principle of pressure-swing adsorption [152], [153]. Plugging Eq. (46) into Eq. (45), the desorption equation of state can be written as:

$$x = x_0 \exp\left[-C_1\left(RT\ln\left(\frac{P}{P_s}\right)\right)^{n_d}\right] \quad (47)$$

The Clausius-Clapeyron equation relates pressure and temperature for transition between a gas and a condensate phase [151]:

$$\ln P = -\frac{C_2}{T} + C_3 \quad (48)$$

where C_2 and C_3 are quantities depending on the adsorbate and its temperature and pressure. Substituting Eq. (48) into Eq. (47), the desorption equation of state can be re-written as:

$$x = x_0 \exp\left[-C_1\left(RTC_2(\frac{1}{T} - \frac{1}{T_s})\right)^{n_d}\right] \quad (49)$$

With some mathematical simplification, the desorption equation of state comes out as:

$$MR = MR_i \exp\left[-k\left((1 - \frac{T}{T_s})\right)^{n}\right] \quad (50)$$

A closer look into the energy balance equation (Eq. 42) reveals that the input energy to the bed is $E_{input} = P_T dt$ and the equivalent outcome in terms of energy is

$E_{des} = dm_{des}\,\Delta H_{Ads}$. Following the classical approach to define efficiency, the desorption efficiency η is defined as:

$$\eta = \frac{E_{des}}{E_{input}} = \frac{\Delta m_{des}\,\Delta H_{ads}}{P_T\,\Delta t} \tag{51}$$

In this approach, the total input power (P_T) is considered constant. Since ΔH_{ads} and P_T remain unchanged, Eq. (51) can be reduced to:

$$\eta_p = \frac{\Delta H_{ads}}{P_T} \times \frac{\Delta m_{des}}{\Delta t} = K_p \frac{\Delta m_{des}}{\Delta t} \tag{52}$$

where K_p is a product of constants and η_p is the efficiency defined under a constant total input power (P_T). For an infinitesimal time period *dt* that allows the removal of *dm* adsorbate, Eq. (52) is simplified to:

$$\eta_p = K_p \frac{dm_{des}}{dt} \tag{53}$$

Since the mass of adsorbent m_s is constant, using the definition of moisture ratio MR in Eq. (1) we have:

$$dm_{des} = m_s d(MR) \tag{54}$$

Using Eq. (54), we can express the efficiency of the desorption process in terms of the variation of adsorbate content with respect to time $[d(MR)/dt]$:

$$\eta_p = K_p' \frac{d(MR)}{dt} \tag{55}$$

where K_p' is also a product of constants. The metric $[d(MR)/dt]$, representing the variation of adsorbate content with time or in other words desorption speed, is the slope of the desorption curve. This metric can be helpful when comparing different regeneration methods based on cycle time and energy consumption. It should be emphasized that these newly defined constant-time and constant-power efficiencies are not the actual efficiencies

of the TES system, but rather are reliable tools to compare different adsorption thermal energy methods.

7.3. Constant-Power Model Validation

To test the accuracy of the constant-power model, the experimental data are compared with the model outputs. The analytical solution of the model equations in terms of bed temperature T as an implicit function of time is

$$P_T\ t = \left\{(\Delta H + h)m_{dry}MR_i\ \left\langle exp\left[-k(1-\frac{T_0}{T_s})^{-n}\right] - exp\left[-k(1-\frac{T(t)}{T_s})^{-n}\right]\right\rangle + \right.$$

$$\left.(m_s c_s + U_{loss} + C_{Al})\ \langle T(t) - T_0\rangle\right\} \quad (56)$$

The moisture ratio $MR(t)$ can be determined using the evaluated temperature $T(t)$ from Eq. (56) and the desorption equation of state (Eq. (50)).

Since the author could not find any values of k and n for activated alumina/water adsorption pair in the literature and these parameters are exclusive to the modified desorption equation of the state, it was decided to use the experimental data reported here to determine them. As ultrasound brings factors other than temperature in the desorption dynamic and consequently alters T_{reg}, two different values of heat-only and ultrasound-assisted k and n are considered. The heat-only related parameters were determined using six sets of heat-only experimental results and the ultrasound-assisted ones were determined using twelve sets of ultrasound-assisted experimental results. The values of the parameters k and n thus determined are provided in Table 10.

Table 10. Equation of state (Eq. (43)) constants determined from the present experimental data.

Parameter	Heat-only	Ultrasound-assisted
k	47.79×10^{-5}	31.31×10^{-5}
n	2.377	2.709

The experimental results and the model predictions for adsorbent temperature and moisture ratio for both power levels are shown in Fig. 25. The average deviation of bed temperatures predicted by the model from their corresponding experimental data are ≤ 9%. The model tends to be more accurate (≤4%) at lower total power level. This could be due to the lumped system assumption. Also, the enthalpy of removed adsorbate was averaged over the temperature range and the specific heat of adsorbent was assumed to remain constant and not vary with temperature and adsorbate loss.

The agreement between the adsorbent temperature and the moisture ratio predicted by the model and experimental results appears acceptable, and the metric $[d(MR)/dt]$ is thus a useful tool of comparison for the regeneration process.

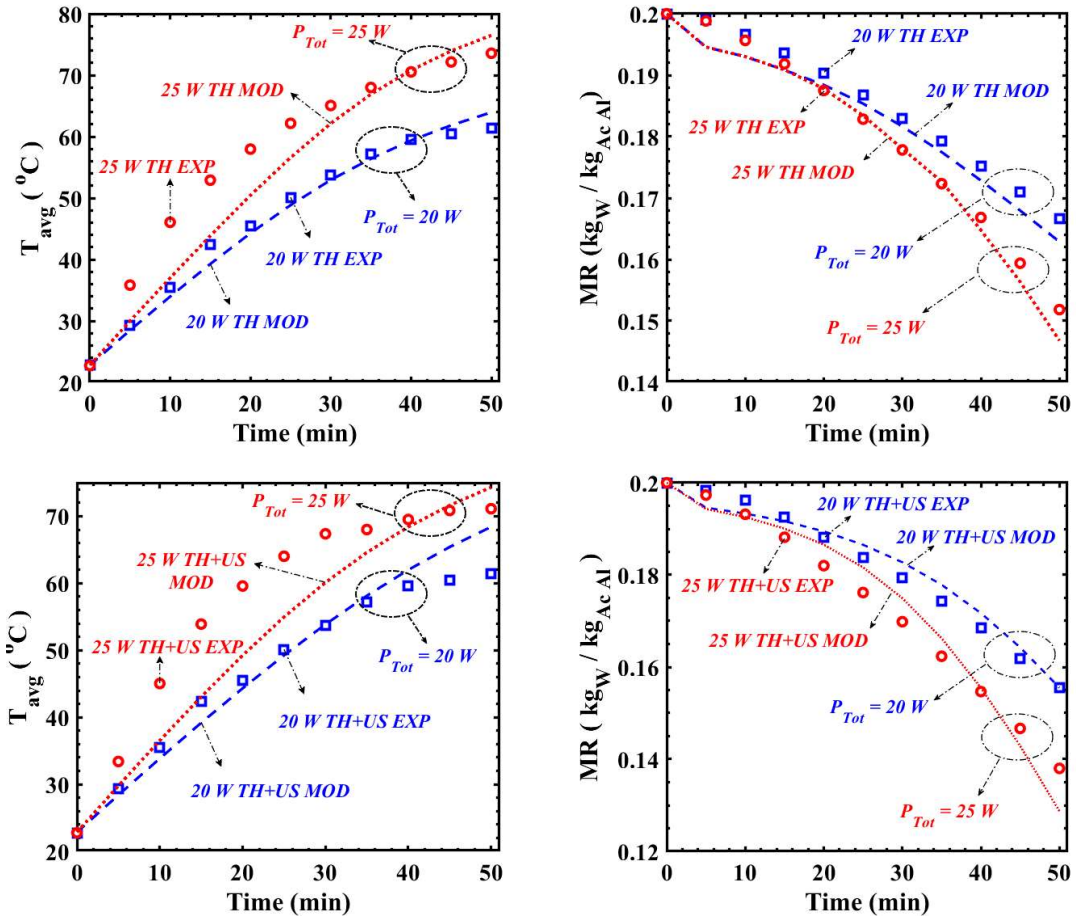

Figure 25. Comparison of activated alumina/water experimental data with constant-power model prediction: temperature (left) and moisture ratio (right). Heat-only regeneration (top) and ultrasound-assisted regeneration (bottom).

7.4. Constant-Time and Constant-Power Models Application

To test the applicability of the models, the activated alumina regeneration experimental results are employed. The average slope of moisture ratio-time and moisture ratio-temperature taken between the initial and final state of the experiments are plotted.

Figure 26 shows the averaged values of *d(MR)/dT* and *d(MR)/dt* for all six experiments. Utilizing the constant-time model, at any ultrasonic frequency and any power level, the

value of *d(MR)/dT* increased with application of ultrasound which indicates that the desorption occurs at lower temperature. Specifically, at 24.1 kHz frequency, for lower ultrasonic-to-total power ratios i.e. 0.2 and 0.25, the average values of *d(MR)/dT* increase by 44.2% and 27.8 % compared to their corresponding heat-only regeneration respectively. At higher ultrasonic-to-total-power ratios of 0.4 and 0.5, the increase in average magnitude of *d(MR)/dT* is still significant. It should be emphasized that when comparing between different regeneration methods based on regeneration temperature, for a given temperature, the magnitude of *d(MR)/dT* at that point should be considered, rather than the average value. The same trend is observed at other frequencies as well. Using the constant-power model, at all three ultrasonic frequencies and for both power levels, the value of *d(MR)/dt* increased with application of ultrasound which points out that a faster desorption occurs. Specifically, at 24.1 kHz frequency, for lower ultrasonic-to-total power ratios i.e. 0.2 and 0.25, the average values of *d(MR)/dt* increase by 37.2% and 33.6 % compared to their corresponding heat-only regeneration respectively. At higher ultrasonic-to-total-power ratios of 0.4 and 0.5, the increase in average magnitude of *d(MR)/dt* is not as significant.

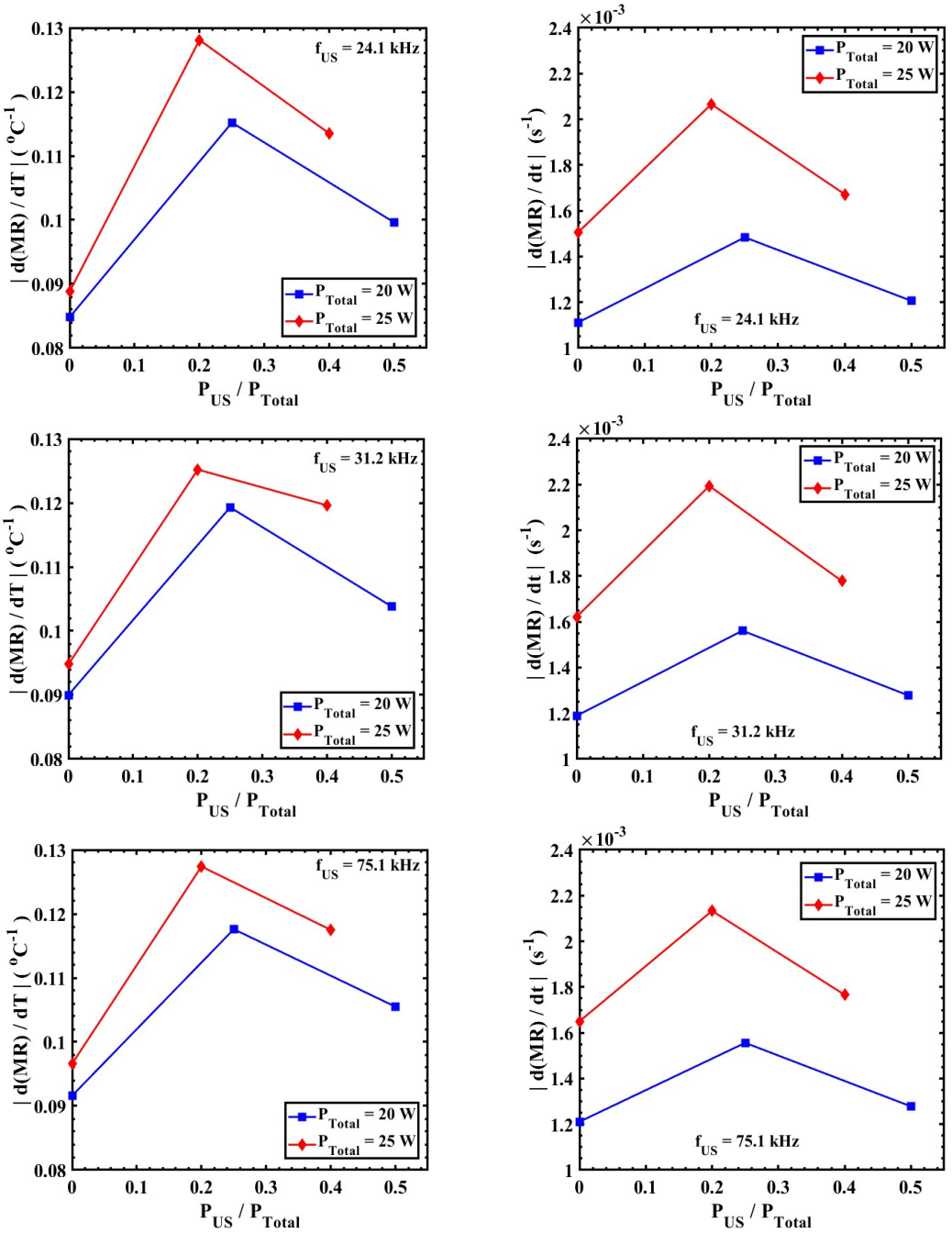

Figure 26. Variation of *d(MR)/dT* (left) and *d(MR)/dt* (right) with ultrasonic-to-total power ratio for activated alumina/water.

Since the validity of the constant-power model and consequently the proposed metric $[d(MR)/dt]$ is established, the metric is applied to the experimental results to investigate the efficiency of the ultrasound-assisted regeneration process compared to the conventional

heat-only regeneration process. The instantaneous and averaged values of $[d(MR)/dt]$ are presented in Fig. 27 and Fig. 28, respectively.

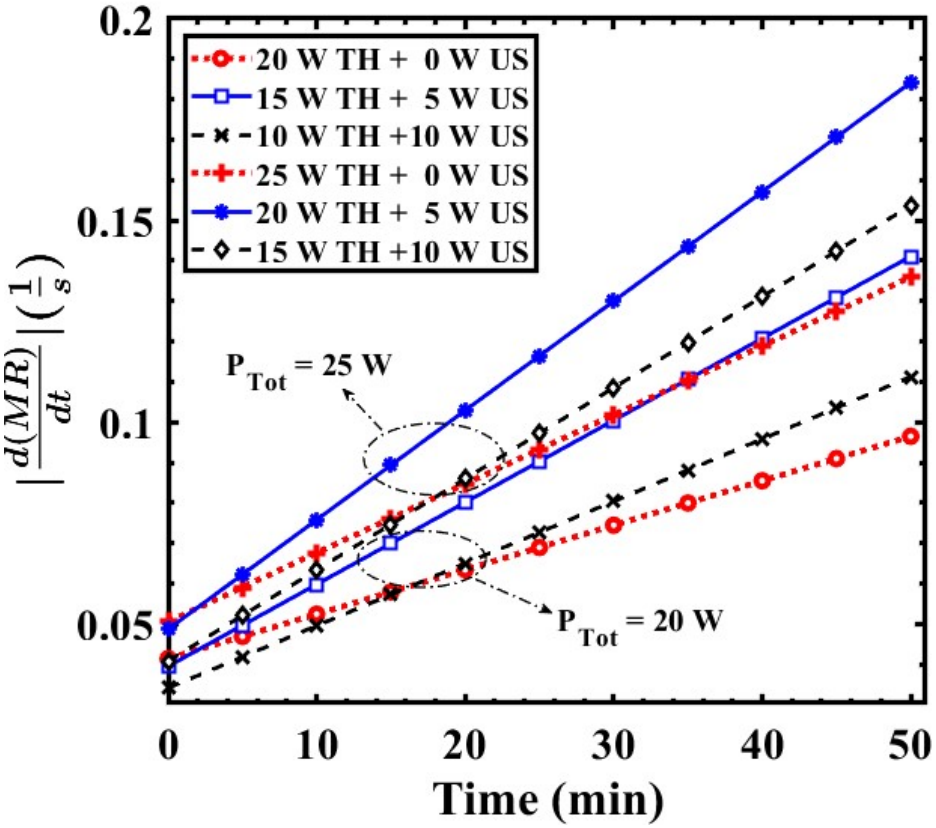

Figure 27. Instantaneous values of [d(MR)/dt] for activated alumina/water.

As can be seen from Fig. 27, at both power levels, the slope of the higher P_{US}/P_{Total} ratio regeneration is initially lower than that for heat-only regeneration, suggesting that although integration of ultrasound ultimately results in enhanced desorption, until some time passes allowing the regeneration temperature to reach a certain level, applying ultrasound would not be beneficial. Not surprisingly, greater desorption is achieved at higher total power input of 25 W. For each power level, regardless of the P_{US}/P_{Total} ratio, integration of ultrasound results in higher averaged $[d(MR)/dt]$ (Fig. 28) meaning that over the entire period of the experiments, higher desorption is obtained.

The nonlinear variation of averaged $[d(MR)/dt]$ with P_{US}/P_{Total} ratio suggests that there is an optimal P_{US}/P_{Total} that results in the most efficient desorption as hypothesized in Eq. (15).

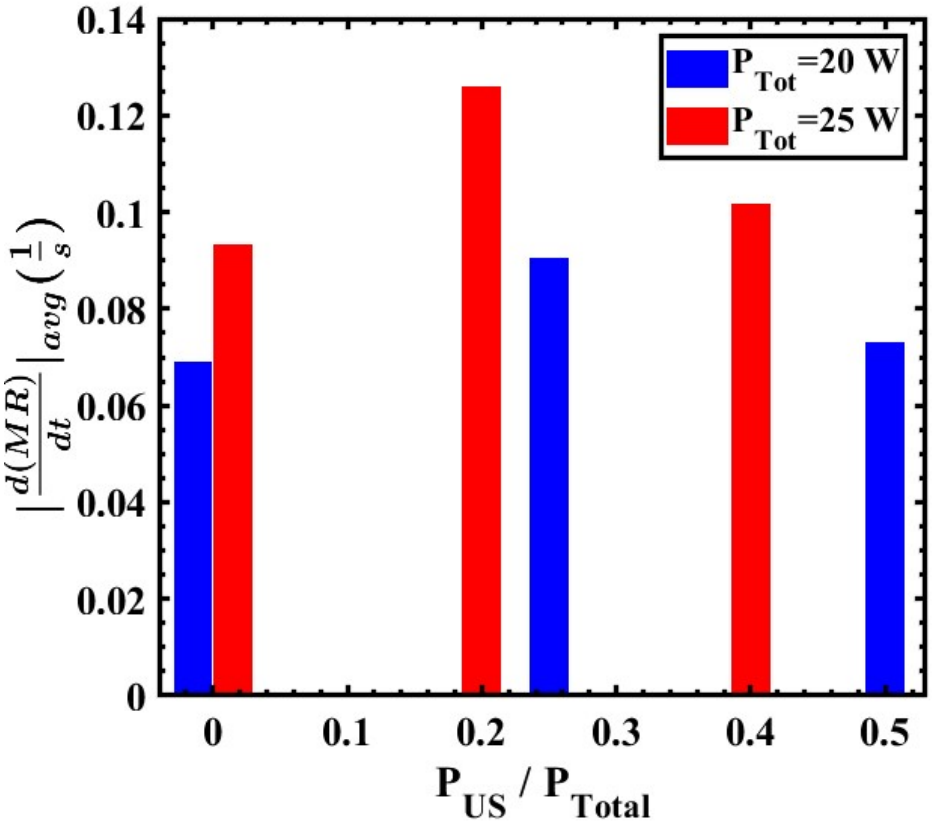

Figure 28.Averaged values of [d(*MR*)/d*t*] for activated alumina/water.

7.5. Summary

The constant-time and constant-power analytical models describing the charging stage of sorption thermal energy storage (TES) are developed. Based on each model a novel efficiency metric that can be utilized to justify different regeneration processes are defined. The metric *d(MR)/dT* evolved from the constant-time model assesses the regeneration process based on the quality of the heat source (regeneration temperature) during the charging stage of sorption TES systems.

On the other hand, the metric *d(MR)/dt* obtained from the constant-power model apprises the regeneration process based on the intensity of the heat source (thermal power) during the charging stage of sorption TES systems. The constant-power model was verified with the experimental results and the accuracy of the model was confirmed. Both models were applied to regeneration of activated alumina and based on both metrics, the feasibility of integration of ultrasound in the regeneration process was confirmed.

8. CONCLUSIONS

The ultrasound-integrated regeneration of adsorbents as a substitute to conventional heat-only regeneration is investigated. Three commercially available adsorbents namely zeolite 13X, activated alumina and silica gel are chosen and total constant-power sets of experiments are performed.

For the case of ultrasonic-assisted desorption of water from zeolite 13X, the extent to which application of ultrasound is effective was analyzed. To do so, the effects of ultrasonic power and ultrasonic frequency on moisture removal and regeneration temperature were investigated. Comparing the moisture ratio at different ultrasonic-to-total power ratios shows that using ultrasound at lower power ratios, i.e. 0.20 and 0.25, significantly improves desorption relative to using only heat for regeneration. Using the newly defined metric *ultrasonic desorption enhancement UDE*, the effects of ultrasonic frequency on moisture removal were analyzed and it was concluded that the effect of ultrasound on desorption is more significant at lower frequencies. Comparing the regeneration temperature for zeolite shows that ultrasonication increases the adsorbent temperature regardless of frequency, presumably due to the heat-transfer-enhancing nature of ultrasound. Not surprisingly, at all three frequencies the highest desorption was achieved at the highest regeneration temperature. Another defined indicator, the *ultrasonic desorption efficiency enhancement UDEE*, was used to justify the use of ultrasound in moisture removal from zeolite 13X. Comparing the values of *UDEE* indicates that with an optimized ratio of ultrasonic-to-total power a ~24 % reduction in energy and time required for desorption of water from zeolite 13X can be achieved, relative to using only heat.

The regeneration of activated alumina using a combination of heat and ultrasound was also extensively investigated. The experimental results clearly show that integration of ultrasound along with thermal power without increasing the total input power enhances the removal of water from activated alumina relative to heat-only desorption with the same total power input showing the same trend observed in ultrasound-assisted regeneration of zeolite. The effectiveness of applying ultrasound is strongly influenced by the ratio of ultrasonic-to-total power and amongst the measured power ratios of 0.2, 0.25, 0.4 and 0.5, the highest desorption was observed at 0.2 power ratio corresponding to about 27% energy savings. The effect of ultrasonic frequency on moisture removal was investigated and it was concluded that increasing the frequency reduces the effectiveness of ultrasound. In terms of regeneration temperature, experimental data show that integration of ultrasound at higher power ratios, i.e. 0.4 and 0.5, considerably lowers the regeneration temperature without jeopardizing the desorption process.

Furthermore, regeneration of silica gel under ultrasonic radiation was investigated. Analyzing the values of moisture content, it can be concluded the application of ultrasound, regardless of P_{Total} or P_{US}/P_{Total} where P_{US} is the ultrasonic power, results in higher moisture removal rate in silica gel as it was observed in ultrasound-assisted regeneration of zeolite and activated alumina. The water vapor diffusion regime in silica gel is investigated and a diffusion model that includes all likely transport modes in porous media is proposed, based on which an apparent diffusion coefficient that considers temperature and ultrasonic inputs is developed. Regarding the regeneration temperature, it is concluded that the regeneration temperature of the silica gel is not solely dictated by the thermal input and the ultrasound-

enhanced heat transfer and acoustic dissipation noticeably contribute to the temperature rise.

Comparing the values of *UDEE* in ultrasound-assisted and non-ultrasound regeneration processes of silica gel proves that application of ultrasound at any power level and all P_{US}/P_{Total} results in energy savings by as much as 26%. The lower P_{US}/P_{Total} are observed to be more effective in improving energy efficiency than higher P_{US}/P_{Total}. The variation of moisture content *MC* with T_{reg} was investigated and integration of ultrasound was observed to lower the regeneration temperature T_{reg}. The highest drop in T_{reg} was achieved at the highest P_{US}/P_{Total} with ~ 11% lower T_{reg}. The values of *UDEE* for all power ratios and frequencies for the three investigated adsorbents are provided in Fig. 29. As can be seen from the figure, with regard to frequency, there is a non-linear proportionality between f_{US} and *UDEE* for the cases of zeolite and activated alumina. With regard to ultrasonic power ratio, except for the case of zeolite, as P_{US}/P_{Total} increases, *UDEE* decreases in a non-linear fashion.

Amongst the proposed mechanisms behind ultrasound-assisted regeneration, based on the inverse proportionality between f_{US} and *UDEE*, acoustic dissipation as a sole mechanism is refuted. Additionally, due to the absence of bulk liquid or bulk-liquid-imitating adsorbate molecule clusters, postulated mechanisms such as acoustic cavitation, microstreaming and acoustic streaming are rejected. Instead, three mechanisms of reduced adsorbate adsorption potential, increased adsorbate surface energy and enhanced mass diffusion are proposed.

Two analytical models, namely constant-time and constant-power, are developed that allow improved understanding of the energy flows in the desorption process. Based on each model a novel metric that can be employed to assess and predict the feasibility of different thermal and ultrasonic energy sources and input power levels in any application involving a desorption process are developed.

Based on the constant-time model, the metric $[d(MR)/dT]$, which represents the variation of adsorbate content with adsorbent temperature and is the slope of the moisture ratio-temperature curve is developed. This metric is useful when comparing regeneration of adsorption pairs based on the regeneration temperature, especially for low-grade heat utilization in thermal energy storage and adsorption cooling systems.

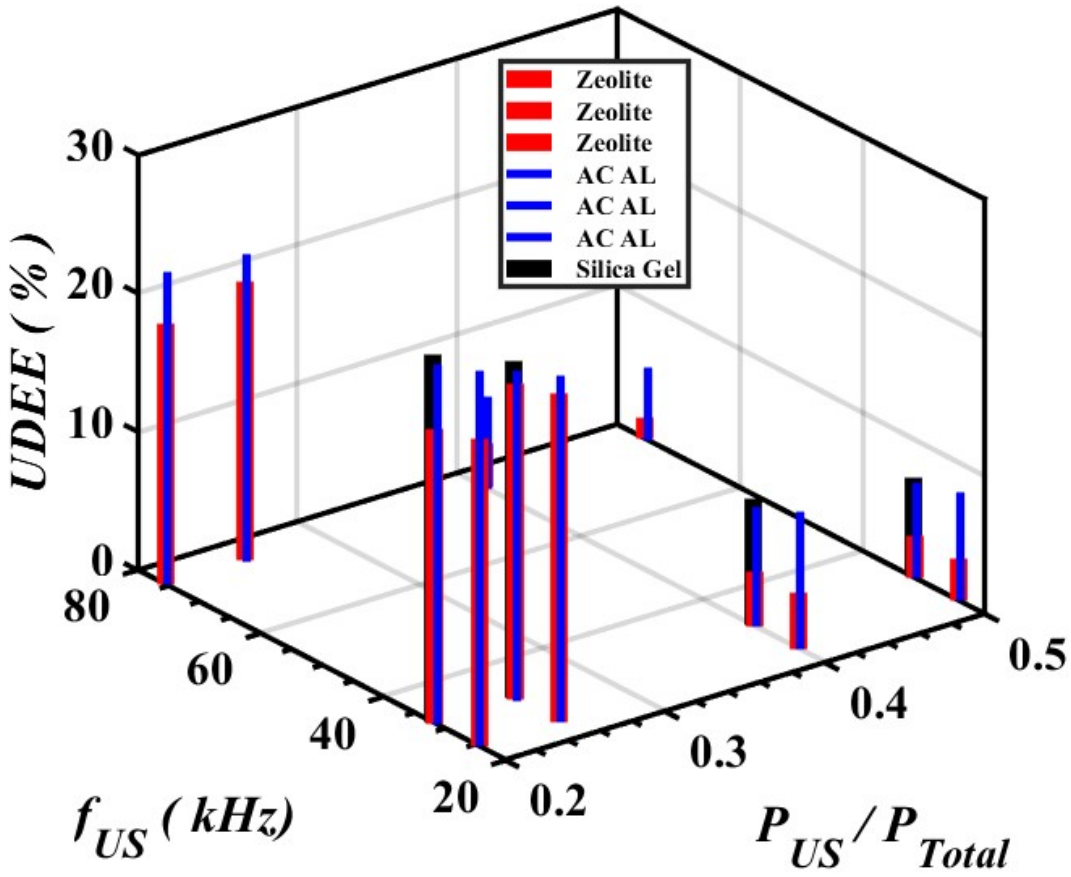

Figure 29. Ultrasonic desorption efficiency enhancement (*UDEE*) for the regeneration of silica gel, activated alumina and zeolite 13X.

8. FUTURE WORK

The experimental work presented here has shown some of the potential improvements afforded by integration of ultrasound in the regeneration process of various adsorbents. A variety of questions and further improvements still remain which should be addressed in future work to bring this concept to real-world applications:

1. Although three mechanisms of reduced adsorbate adsorption potential, increased adsorbate surface energy and enhanced mass diffusion all of which are induced by ultrasound have been proposed to explain the ultrasound-enhanced desorption phenomenon, none of them has been proven yet. Experimentation for the sole purpose of finding the possible mechanisms and the extent to which they contribute to the phenomenon appears necessary. The field could also benefit from simulation work that incorporates the high-paced alternating pressure induced by ultrasound into the regeneration regime.
2. Surface diffusion is reported to be the major mode of transport in porous media of high specific area such as silica gel and zeolite. Since ultrasound is observed to enhance diffusion in the regeneration process of adsorbents, the effects of ultrasonication on surface diffusion are worth further investigation.
3. Most or all of the previous research in the field of ultrasound-assisted regeneration of adsorbents has been conducted in the frequency range of 20 kHz - 80 kHz and an inverse proportionality between the observed enhancement and the frequency has been reported consistently. However, at high range frequencies (~ MHz), the mechanism by which ultrasound acts changes and

could potentially enhance the regeneration process, and thus is worth investigating.

REFERENCES

[1] D. Lefebvre and F. H. Tezel, "A review of energy storage technologies with a focus on adsorption thermal energy storage processes for heating applications," *Renewable and Sustainable Energy Reviews*, vol. 67, pp. 116–125, Jan. 2017, doi: 10.1016/j.rser.2016.08.019.

[2] A. LaPotin, H. Kim, S. R. Rao, and E. N. Wang, "Adsorption-Based Atmospheric Water Harvesting: Impact of Material and Component Properties on System-Level Performance," *Acc. Chem. Res.*, vol. 52, no. 6, pp. 1588–1597, Jun. 2019, doi: 10.1021/acs.accounts.9b00062.

[3] B. N. Bhadra, I. Ahmed, S. Kim, and S. H. Jhung, "Adsorptive removal of ibuprofen and diclofenac from water using metal-organic framework-derived porous carbon," *Chemical Engineering Journal*, vol. 314, pp. 50–58, Apr. 2017, doi: 10.1016/j.cej.2016.12.127.

[4] S. U. Rege, R. T. Yang, and C. A. Cain, "Desorption by ultrasound: Phenol on activated carbon and polymeric resin," *AIChE J.*, vol. 44, no. 7, pp. 1519–1528, Jul. 1998, doi: 10.1002/aic.690440706.

[5] H. Chen *et al.*, "Toward Design Rules of Metal–Organic Frameworks for Adsorption Cooling: Effect of Topology on the Ethanol Working Capacity," *Chem. Mater.*, vol. 31, no. 8, pp. 2702–2706, Apr. 2019, doi: 10.1021/acs.chemmater.9b00062.

[6] A. Pal, K. Uddin, K. Thu, and B. B. Saha, "Activated carbon and graphene nanoplatelets based novel composite for performance enhancement of adsorption cooling cycle," *Energy Conversion and Management*, vol. 180, pp. 134–148, Jan. 2019, doi: 10.1016/j.enconman.2018.10.092.

[7] J. Cot-Gores, A. Castell, and L. F. Cabeza, "Thermochemical energy storage and conversion: A-state-of-the-art review of the experimental research under practical conditions," *Renewable and Sustainable Energy Reviews*, vol. 16, no. 7, pp. 5207–5224, Sep. 2012, doi: 10.1016/j.rser.2012.04.007.

[8] J. Xu, R. Z. Wang, and Y. Li, "A review of available technologies for seasonal thermal energy storage," *Solar Energy*, vol. 103, pp. 610–638, May 2014, doi: 10.1016/j.solener.2013.06.006.

[9] C. W. Chan, J. Ling-Chin, and A. P. Roskilly, "Reprint of 'A review of chemical heat pumps, thermodynamic cycles and thermal energy storage technologies for low grade

heat utilisation,'" *Applied Thermal Engineering*, vol. 53, no. 2, pp. 160–176, May 2013, doi: 10.1016/j.applthermaleng.2013.02.030.

[10] S. M. Hasnain, "Review on sustainable thermal energy storage technologies, Part I: heat storage materials and techniques," *Energy Conversion and Management*, vol. 39, no. 11, pp. 1127–1138, Aug. 1998, doi: 10.1016/S0196-8904(98)00025-9.

[11] P. Tatsidjodoung, N. Le Pierrès, and L. Luo, "A review of potential materials for thermal energy storage in building applications," *Renewable and Sustainable Energy Reviews*, vol. 18, pp. 327–349, Feb. 2013, doi: 10.1016/j.rser.2012.10.025.

[12] A. N. Shmroukh, A. H. H. Ali, and S. Ookawara, "Adsorption working pairs for adsorption cooling chillers: A review based on adsorption capacity and environmental impact," *Renewable and Sustainable Energy Reviews*, vol. 50, pp. 445–456, Oct. 2015, doi: 10.1016/j.rser.2015.05.035.

[13] A. Al-Alili, Y. Hwang, and R. Radermacher, "Review of solar thermal air conditioning technologies," *International Journal of Refrigeration*, vol. 39, pp. 4–22, Mar. 2014, doi: 10.1016/j.ijrefrig.2013.11.028.

[14] J. Nastaj and B. Ambrożek, "Modeling of Drying of Gases Using Solid Desiccants," *Drying Technology*, vol. 27, no. 12, pp. 1344–1352, 2009, doi: 10.1080/07373930903383679.

[15] J. Nastaj and B. Ambrozek, "Modeling of Drying of Gaseous Mixtures in TSA System with Fixed Bed of Solid Desiccants," *Drying Technology*, vol. 30, no. 10, pp. 1062–1071, 2012, doi: 10.1080/07373937.2012.685138.

[16] P. Gandhidasan, A. A. Al-Farayedhi, and A. A. Al-Mubarak, "Dehydration of natural gas using solid desiccants," *Energy*, vol. 26, no. 9, pp. 855–868, 2001, doi: 10.1016/S0360-5442(01)00034-2.

[17] R. B. Chapas and J. A. Colwell, "Industrial Technologies Program Research Plan for Energy-Intensive Process Industries," *PNNL-17075*, 2007.

[18] M. Stakić, P. Stefanović, D. Cvetinović, and P. Škobalj, "Convective drying of particulate solids-Packed vs. fluid bed operation," *International Journal of Heat and Mass Transfer*, vol. 59, no. 1, pp. 66–74, 2013, doi: 10.1016/j.ijheatmasstransfer.2012.11.078.

[19] B. KINIGOMA and G. ANI, “Comparison of gas dehydration methods based on energy consumption,” *Journal of Applied Sciences and Environmental Management*, vol. 20, no. 2, pp. 253-258–258, 2016.

[20] A. E. Outlook, “Table 6. Industrial Sector Key Indicators and Consumption.”

[21] P. Netusil and M. Ditl, “Natural Gas Dehydration,” *Intech*, p. 13, 2012, doi: 10.1016/j.colsurfa.2011.12.014.

[22] S. Mokhatab and W. A. Poe, “Natural Gas Dehydration,” in *Handbook of Natural Gas Transmission and Processing*, Elsevier, pp. 317–352. doi: 10.1016/B978-0-12-386914-2.00009-1.

[23] A. Gurubalan, M. P. Maiya, and P. J. Geoghegan, “A comprehensive review of liquid desiccant air conditioning system,” *Applied Energy*, vol. 254, no. August, p. 113673, 2019, doi: 10.1016/j.apenergy.2019.113673.

[24] M. Djaeni, G. van Straten, P. V Bartels, J. P. M. Sanders, and A. J. B. van Boxtel, “Energy Efficiency of Multi-Stage Adsorption Drying for Low-Temperature Drying,” *Drying Technology*, vol. 27, no. 4, pp. 555–564, Mar. 2009, doi: 10.1080/07373930802715682.

[25] A. Yadav and V. K. Bajpai, “Experimental Comparison of Various Solid Desiccants for Regeneration by Evacuated Solar Air Collector and Air Dehumidification,” *Drying Technology*, vol. 30, no. 5, pp. 516–525, Apr. 2012, doi: 10.1080/07373937.2011.647997.

[26] M. Djaeni, D. Q. A’yuni, M. Alhanif, C. L. Hii, and A. C. Kumoro, “Air dehumidification with advance adsorptive materials for food drying: A critical assessment for future prospective,” *Drying Technology*, pp. 1–19, Feb. 2021, doi: 10.1080/07373937.2021.1885042.

[27] Y. Yao, S. Liu, and W. Zhang, “Regeneration of Silica Gel Using High-intensity Ultrasonic under Low Temperatures,” *Energy Fuels*, vol. 23, no. 1, pp. 457–463, Jan. 2009, doi: 10.1021/ef8000554.

[28] T. Yamamoto, G. Tanioka, M. Okubo, and T. Kuroki, “Water vapor desorption and adsorbent regeneration for air conditioning unit using pulsed corona plasma,” *Journal of Electrostatics*, vol. 65, no. 4, pp. 221–227, Apr. 2007, doi: 10.1016/j.elstat.2006.08.002.

[29] T. Chronopoulos, Y. Fernandez-Diez, M. M. Maroto-Valer, R. Ocone, and D. A. Reay, “Utilisation Of Microwave Energy for CO2 Desorption in Post-combustion Carbon Capture Using Solid Sorbents,” *Energy Procedia*, vol. 63, pp. 2109–2115, 2014, doi: 10.1016/j.egypro.2014.11.227.

[30] W. Zhang, Y. Yao, B. He, and R. Wang, “The energy-saving characteristic of silica gel regeneration with high-intensity ultrasound,” *Applied Energy*, vol. 88, no. 6, pp. 2146–2156, Jun. 2011, doi: 10.1016/j.apenergy.2010.12.023.

[31] Y. Yao, “Enhancement of mass transfer by ultrasound: Application to adsorbent regeneration and food drying/dehydration,” *Ultrasonics Sonochemistry*, vol. 31, pp. 512–531, Jul. 2016, doi: 10.1016/j.ultsonch.2016.01.039.

[32] M. Breitbach and D. Bathen, “Infuence of ultrasound on adsorption processes,” *Ultrasonics Sonochemistry*, p. 7, 2001.

[33] W. Zhang, Y. Yao, and R. Wang, “Influence of ultrasonic frequency on the regeneration of silica gel by applying high-intensity ultrasound,” *Applied Thermal Engineering*, vol. 30, no. 14–15, pp. 2080–2087, Oct. 2010, doi: 10.1016/j.applthermaleng.2010.05.016.

[34] O. Hamdaoui, E. Naffrechoux, L. Tifouti, and C. Pétrier, “Effects of ultrasound on adsorption–desorption of p-chlorophenol on granular activated carbon,” *Ultrasonics Sonochemistry*, vol. 10, no. 2, pp. 109–114, Mar. 2003, doi: 10.1016/S1350-4177(02)00137-2.

[35] J. A. Gallego-Juarez, G. Rodriguez-Corral, J. C. Gálvez Moraleda, and T. S. Yang, “A NEW HIGH-INTENSITY ULTRASONIC TECHNOLOGY FOR FOOD DEHYDRATION,” *Drying Technology*, vol. 17, no. 3, pp. 597–608, Mar. 1999, doi: 10.1080/07373939908917555.

[36] C. Peng, A. M. Momen, and S. Moghaddam, “An energy-efficient method for direct-contact ultrasonic cloth drying,” *Energy*, vol. 138, pp. 133–138, Nov. 2017, doi: 10.1016/j.energy.2017.07.025.

[37] J. Kroehnke, G. Musielak, and A. Boratynska, “Convective drying of potato assisted by ultrasound,” p. 9.

[38] M. Torki-Harchegani, D. Ghanbarian, A. Ghasemi Pirbalouti, and M. Sadeghi, “Dehydration behaviour, mathematical modelling, energy efficiency and essential oil yield of peppermint leaves undergoing microwave and hot air treatments,”

Renewable and Sustainable Energy Reviews, vol. 58, pp. 407–418, May 2016, doi: 10.1016/j.rser.2015.12.078.

[39] P. Comandini *et al.*, "Effects of power ultrasound on immersion freezing parameters of potatoes," *Innovative Food Science & Emerging Technologies*, vol. 18, pp. 120–125, Apr. 2013, doi: 10.1016/j.ifset.2013.01.009.

[40] J. A. Cárcel, J. V. García-Pérez, E. Riera, and A. Mulet, "Influence of High-Intensity Ultrasound on Drying Kinetics of Persimmon," *Drying Technology*, vol. 25, no. 1, pp. 185–193, Feb. 2007, doi: 10.1080/07373930601161070.

[41] S. J. Kowalski and A. Pawłowski, "Intensification of apple drying due to ultrasound enhancement," *Journal of Food Engineering*, vol. 156, pp. 1–9, Jul. 2015, doi: 10.1016/j.jfoodeng.2015.01.023.

[42] K. Schössler, H. Jäger, and D. Knorr, "Novel contact ultrasound system for the accelerated freeze-drying of vegetables," *Innovative Food Science & Emerging Technologies*, vol. 16, pp. 113–120, Oct. 2012, doi: 10.1016/j.ifset.2012.05.010.

[43] J. Szadzińska, S. J. Kowalski, and M. Stasiak, "Microwave and ultrasound enhancement of convective drying of strawberries: Experimental and modeling efficiency," *International Journal of Heat and Mass Transfer*, vol. 103, pp. 1065–1074, Dec. 2016, doi: 10.1016/j.ijheatmasstransfer.2016.08.001.

[44] E. Souza da Silva, S. C. Rupert Brandão, A. Lopes da Silva, J. H. Fernandes da Silva, A. C. Duarte Coêlho, and P. M. Azoubel, "Ultrasound-assisted vacuum drying of nectarine," *Journal of Food Engineering*, vol. 246, pp. 119–124, Apr. 2019, doi: 10.1016/j.jfoodeng.2018.11.013.

[45] Z. He, Y. Fei, Y. Peng, and S. Yi, "Ultrasound-Assisted Vacuum Drying of Wood: Effects on Drying Time and Product Quality," *BioResources*, vol. 8, no. 1, pp. 855–863, Jan. 2013, doi: 10.15376/biores.8.1.855-863.

[46] J. A. Gallego-Juarez and K. F. Graff, *Power Ultrasonics: Applications of High-Intensity Ultrasound*. Kent, UNITED KINGDOM: Elsevier Science & Technology, 2014. Accessed: Jul. 22, 2019. [Online]. Available: http://ebookcentral.proquest.com/lib/asulib-ebooks/detail.action?docID=1875322

[47] M. Legay, N. Gondrexon, S. Le Person, P. Boldo, and A. Bontemps, "Enhancement of Heat Transfer by Ultrasound: Review and Recent Advances,"

International Journal of Chemical Engineering, vol. 2011, pp. 1–17, 2011, doi: 10.1155/2011/670108.

[48] H. Daghooghi-Mobarakeh *et al.*, "Ultrasound-assisted regeneration of zeolite/water adsorption pair," *Ultrasonics Sonochemistry*, vol. 64, p. 105042, Jun. 2020, doi: 10.1016/j.ultsonch.2020.105042.

[49] H. Daghooghi Mobarakeh, K. Bandara, L. Wang, R. Wang, P. E. Phelan, and M. Miner, "Low-Grade Heat Utilization Through Ultrasound-Enhanced Desorption of Activated Alumina/Water for Thermal Energy Storage," ASME 2020 Power Conference, Aug. 2020. doi: 10.1115/POWER2020-16802.

[50] A. Bamasag, H. Daghooghi-Mobarakeh, T. Alqahtani, and P. Phelan, "Performance enhancement of a submerged vacuum membrane distillation (S-VMD) system using low-power ultrasound," *Journal of Membrane Science*, vol. 621, no. December 2020, pp. 119004–119004, 2021, doi: 10.1016/j.memsci.2020.119004.

[51] H. Daghooghi-Mobarakeh, M. Miner, L. Wang, R. Wang, and P. E. Phelan, "Application of ultrasound in regeneration of silica gel for industrial gas drying processes," *Drying Technology*, pp. 1–9, Jun. 2021, doi: 10.1080/07373937.2021.1929296.

[52] Y. Yao and S. Liu, *Ultrasonic Technology for Desiccant Regeneration*. Singapore, SINGAPORE: John Wiley & Sons, Incorporated, 2014. Accessed: Jul. 22, 2019. [Online]. Available: http://ebookcentral.proquest.com/lib/asulib-ebooks/detail.action?docID=1780042

[53] R. Penn, E. Yeager, and F. Hovorka, "Effect of Ultrasonic Waves on Concentration Gradients," *The Journal of the Acoustical Society of America*, vol. 31, no. 10, pp. 1372–1376, Oct. 1959, doi: 10.1121/1.1907637.

[54] R. S. Soloff, "Sonic Drying," *The Journal of the Acoustical Society of America*, vol. 36, no. 5, pp. 961–965, May 1964, doi: 10.1121/1.1919133.

[55] H. S. Muralidhara and D. Ensminger, "ACOUSTIC DRYING OF GREEN RICE," *Drying Technology*, vol. 4, no. 1, pp. 137–143, Feb. 1986, doi: 10.1080/07373938608916315.

[56] P. Greguss, "The mechanism and possible applications of drying by ultrasonic irradiation," *Ultrasonics*, vol. 1, no. 2, pp. 83–86, Apr. 1963, doi: 10.1016/0041-624X(63)90059-3.

[57] R. M. G. Boucher, “Drying by airborne ultrasonics,” *Ultrasonic news*, vol. 3, no. 2, pp. 8–16, 1959.

[58] H. S. Muralidhara, S. P. Chauhan, N. Senapati, R. Beard, B. Jirjis, and B. C. Kim, “Electro-Acoustic Dewatering (EAD) a Novel Approach for Food Processing, and Recovery,” *Separation Science and Technology*, vol. 23, no. 12–13, pp. 2143–2158, 1988.

[59] J. H. Moy and G. R. DiMARCO, “EXPLORING AIRBORNE SOUND IN A NONVACUUM FREEZE-DRYING PROCESS,” *J Food Science*, vol. 35, no. 6, pp. 811–817, Nov. 1970, doi: 10.1111/j.1365-2621.1970.tb02001.x.

[60] V. Fairbanks and W. I. Chen, “Influence of ultrasonics porous media,” p. 2.

[61] Kiran. A. Ramisetty, Aniruddha. B. Pandit, and Parag. R. Gogate, “Investigations into ultrasound induced atomization,” *Ultrasonics Sonochemistry*, vol. 20, no. 1, pp. 254–264, Jan. 2013, doi: 10.1016/j.ultsonch.2012.05.001.

[62] A. Arnau, Ed., *Piezoelectric transducers and applications*, 2nd ed. New York: Springer, 2008.

[63] J. P. Holman, *Experimental methods for engineers*, 7th ed.. Boston: McGraw-Hill, 2001.

[64] Y. A. Çengel and A. J. Ghajar, *Heat and mass transfer: fundamentals & applications*, Fifth edition. New York, NY: McGraw Hill Education, 2015.

[65] S. Vasta, A. Freni, A. Sapienza, F. Costa, and G. Restuccia, “Development and lab-test of a mobile adsorption air-conditioner,” *International Journal of Refrigeration*, vol. 35, no. 3, pp. 701–708, May 2012, doi: 10.1016/j.ijrefrig.2011.03.013.

[66] Y. Z. Lu, R. Z. Wang, M. Zhang, and S. Jiangzhou, “Adsorption cold storage system with zeolite–water working pair used for locomotive air conditioning,” *Energy Conversion and Management*, p. 11, 2003.

[67] Y. Hirasawa and W. Urakami, “Study on Specific Heat of Water Adsorbed in Zeolite Using DSC,” *Int J Thermophys*, vol. 31, no. 10, pp. 2004–2009, Oct. 2010, doi: 10.1007/s10765-010-0841-6.

[68] N. C. Srivastava and I. W. Eames, “A review of adsorbents and adsorbates in solid–vapour adsorption heat pump systems,” *Applied Thermal Engineering*, vol. 18, no. 9–10, pp. 707–714, Sep. 1998, doi: 10.1016/S1359-4311(97)00106-3.

[69] L. W. Wang, R. Z. Wang, and R. G. Oliveira, “A review on adsorption working pairs for refrigeration,” *Renewable and Sustainable Energy Reviews*, vol. 13, no. 3, pp. 518–534, Apr. 2009, doi: 10.1016/j.rser.2007.12.002.

[70] D. C. Wang, Z. Z. Xia, and J. Y. Wu, “Design and performance prediction of a novel zeolite–water adsorption air conditioner,” *Energy Conversion and Management*, vol. 47, no. 5, pp. 590–610, Mar. 2006, doi: 10.1016/j.enconman.2005.05.011.

[71] B. Mette, H. Kerskes, H. Drück, and H. Müller-Steinhagen, “Experimental and numerical investigations on the water vapor adsorption isotherms and kinetics of binderless zeolite 13X,” *International Journal of Heat and Mass Transfer*, vol. 71, pp. 555–561, Apr. 2014, doi: 10.1016/j.ijheatmasstransfer.2013.12.061.

[72] P. Tatsidjodoung, N. Le Pierrès, J. Heintz, D. Lagre, L. Luo, and F. Durier, “Experimental and numerical investigations of a zeolite 13X/water reactor for solar heat storage in buildings,” *Energy Conversion and Management*, vol. 108, pp. 488–500, Jan. 2016, doi: 10.1016/j.enconman.2015.11.011.

[73] S. Semprini *et al.*, “Numerical modelling of water sorption isotherms of zeolite 13XBF based on sparse experimental data sets for heat storage applications,” *Energy Conversion and Management*, vol. 150, pp. 392–402, Oct. 2017, doi: 10.1016/j.enconman.2017.08.033.

[74] Y. Yao, “Research and applications of ultrasound in HVAC field: A review,” *Renewable and Sustainable Energy Reviews*, vol. 58, pp. 52–68, May 2016, doi: 10.1016/j.rser.2015.12.222.

[75] D. D. Do and H. D. Do, “A model for water adsorption in activated carbon,” p. 7, 2000.

[76] T. Iiyama, K. Nishikawa, T. Otowa, and K. Kaneko, “An Ordered Water Molecular Assembly Structure in a Slit-Shaped Carbon Nanospace,” *J. Phys. Chem.*, vol. 99, no. 25, pp. 10075–10076, Jun. 1995, doi: 10.1021/j100025a004.

[77] K. Kaneko, Y. Hanzawa, T. Iiyama, T. Kanda, and T. Suzuki, “Cluster-Mediated Water Adsorption on Carbon Nanopores,” p. 7.

[78] S. Labouret and J. Frohly, “Determination of bubble size distributions in an ultrasonic cavitation field.,” *The Journal of the Acoustical Society of America*, vol. 127, no. 3, pp. 1984–1984, Mar. 2010, doi: 10.1121/1.3385105.

[79] S. Merouani, O. Hamdaoui, Y. Rezgui, and M. Guemini, “Energy analysis during acoustic bubble oscillations: Relationship between bubble energy and sonochemical parameters,” *Ultrasonics*, vol. 54, no. 1, pp. 227–232, Jan. 2014, doi: 10.1016/j.ultras.2013.04.014.

[80] H. Kiani, D.-W. Sun, and Z. Zhang, “The effect of ultrasound irradiation on the convective heat transfer rate during immersion cooling of a stationary sphere,” *Ultrasonics Sonochemistry*, vol. 19, no. 6, pp. 1238–1245, Nov. 2012, doi: 10.1016/j.ultsonch.2012.04.009.

[81] C. Bartoli and F. Baffigi, “Effects of ultrasonic waves on the heat transfer enhancement in subcooled boiling,” *Experimental Thermal and Fluid Science*, vol. 35, no. 3, pp. 423–432, Apr. 2011, doi: 10.1016/j.expthermflusci.2010.11.002.

[82] O. Bulliard-Sauret *et al.*, “Heat transfer intensification by low or high frequency ultrasound: Thermal and hydrodynamic phenomenological analysis,” *Experimental Thermal and Fluid Science*, vol. 104, pp. 258–271, Jun. 2019, doi: 10.1016/j.expthermflusci.2019.03.003.

[83] G. L. Lee, M. C. Law, and V. C.-C. Lee, “Modelling of liquid heating subject to simultaneous microwave and ultrasound irradiation,” *Applied Thermal Engineering*, vol. 150, pp. 1126–1140, Mar. 2019, doi: 10.1016/j.applthermaleng.2019.01.064.

[84] M. H. Entezari and P. Kruus, “Effect of frequency on sonochemical reactions II. Temperature and intensity effects,” *Ultrasonics Sonochemistry*, vol. 3, no. 1, pp. 19–24, Feb. 1996, doi: 10.1016/1350-4177(95)00037-2.

[85] G. Cum, G. Galli, R. Gallo, and A. Spadaro, “Role of frequency in the ultrasonic activation of chemical reactions,” *Ultrasonics*, vol. 30, no. 4, pp. 267–270, Jan. 1992, doi: 10.1016/0041-624X(92)90086-2.

[86] G. O. H. Whillock and B. F. Harvey, “Ultrasonically enhanced corrosion of 304L stainless steel II: The effect of frequency, acoustic power and horn to specimen distance,” *Ultrasonics Sonochemistry*, vol. 4, no. 1, pp. 33–38, Jan. 1997, doi: 10.1016/S1350-4177(96)00015-6.

[87] A. Weissler, “Sonochemistry: The Production of Chemical Changes with Sound Waves,” *The Journal of the Acoustical Society of America*, vol. 25, no. 4, pp. 651–657, Jul. 1953, doi: 10.1121/1.1907158.

[88] Z. Li, X. Li, H. Xi, and B. Hua, “Effects of ultrasound on adsorption equilibrium of phenol on polymeric adsorption resin,” *Chemical Engineering Journal*, vol. 86, no. 3, pp. 375–379, Apr. 2002, doi: 10.1016/S1385-8947(01)00301-1.

[89] D. D. Do, *Adsorption analysis: equilibria and kinetics*. London: Imperial College Press, 1998.

[90] R. T. Yang, “Adsorbents and Adsorption Isotherms,” in *Gas Separation by Adsorption Processes*, Elsevier, 1987, pp. 9–48. doi: 10.1016/B978-0-409-90004-0.50005-2.

[91] A. K. Meher, A. Jadhav, N. Labhsetwar, and A. Bansiwal, “Simultaneous removal of selenite and selenate from drinking water using mesoporous activated alumina,” *Appl Water Sci*, vol. 10, no. 1, p. 10, Jan. 2020, doi: 10.1007/s13201-019-1090-x.

[92] N. K. Mohammad, A. Ghaemi, and K. Tahvildari, “Hydroxide modified activated alumina as an adsorbent for CO2 adsorption: Experimental and modeling,” *International Journal of Greenhouse Gas Control*, vol. 88, pp. 24–37, Sep. 2019, doi: 10.1016/j.ijggc.2019.05.029.

[93] M. Dupont, B. Celestine, P. H. Nguyen, J. Merigoux, and B. Brandon, “Desiccant solar air conditioning in tropical climates: I—Dynamic experimental and numerical studies of silicagel and activated alumina,” *Solar Energy*, vol. 52, no. 6, pp. 509–517, Jun. 1994, doi: 10.1016/0038-092X(94)90658-0.

[94] A. Yadav and V. K. Bajpai, “Experimental Comparison of Various Solid Desiccants for Regeneration by Evacuated Solar Air Collector and Air Dehumidification,” *Drying Technology*, vol. 30, no. 5, pp. 516–525, Apr. 2012, doi: 10.1080/07373937.2011.647997.

[95] P. Gandhidasan, A. A. Al-Farayedhi, and A. A. Al-Mubarak, “Dehydration of natural gas using solid desiccants,” p. 14, 2001.

[96] S. Mokhatab, W. A. Poe, and J. Y. Mak, “Chapter 7 - Natural Gas Dehydration,” in *Handbook of Natural Gas Transmission and Processing (Third Edition)*, Third Edition., S. Mokhatab, W. A. Poe, and J. Y. Mak, Eds. Boston: Gulf Professional Publishing, 2015, pp. 223–263. doi: 10.1016/B978-0-12-801499-8.00007-9.

[97] *Handbook of Natural Gas Transmission and Processing*. Elsevier, 2015. doi: 10.1016/C2013-0-15625-5.

[98] H. Niazmand, H. Talebian, and M. Mahdavikhah, "Bed geometrical specifications effects on the performance of silica / water adsorption chillers ´ ome ´ triques du lit sur la performance Effets des spe ` adsorption au gel de silice / eau des refroidisseurs a," *International Journal of Refrigeration*, vol. 35, no. 8, pp. 2261–2274, 2012, doi: 10.1016/j.ijrefrig.2012.08.017.

[99] W. Chang, C. Wang, and C. Shieh, "Experimental study of a solid adsorption cooling system using flat-tube heat exchangers as adsorption bed," vol. 27, pp. 2195–2199, 2007, doi: 10.1016/j.applthermaleng.2005.07.022.

[100] G. L. Lee, M. C. Law, and V. C.-C. C. C. Lee, "Modelling of liquid heating subject to simultaneous microwave and ultrasound irradiation," *Applied Thermal Engineering*, vol. 150, no. October 2018, pp. 1126–1140, 2019, doi: 10.1016/j.applthermaleng.2019.01.064.

[101] O. Bulliard-Sauret *et al.*, "Heat transfer intensification by low or high frequency ultrasound: Thermal and hydrodynamic phenomenological analysis," *Experimental Thermal and Fluid Science*, vol. 104, no. July 2018, pp. 258–271, 2019, doi: 10.1016/j.expthermflusci.2019.03.003.

[102] T. L. Szabo, "Attenuation," in *Diagnostic Ultrasound Imaging: Inside Out*, Elsevier, 2014, pp. 81–119. doi: 10.1016/B978-0-12-396487-8.00004-5.

[103] J. Lee *et al.*, "Development and optimization of acoustic bubble structures at high frequencies," *Ultrasonics Sonochemistry*, vol. 18, no. 1, pp. 92–98, Jan. 2011, doi: 10.1016/j.ultsonch.2010.03.004.

[104] A. A. Gubaidullin, O. Y. Kuchugurina, D. M. J. Smeulders, and C. J. Wisse, "Frequency-dependent acoustic properties of a fluid/porous solid interface," *The Journal of the Acoustical Society of America*, vol. 116, no. 3, pp. 1474–1480, Sep. 2004, doi: 10.1121/1.1777856.

[105] "Ensminger, Dale, and Leonard J. Bond. Ultrasonics : Fundamentals, Technologies and Applications, Third Edition, CRC Press LLC, 2011. ProQuest Ebook Central, https://ebookcentral-proquest-com.ezproxy1.lib.asu.edu/lib/asulib-ebooks/detail.action?docID=767859.,"

[106] K. Urano, Y. Koichi, and Y. Nakazawa, “Equilibria for adsorption of organic compounds on activated carbons in aqueous solutions I. Modified Freundlich isotherm equation and adsorption potentials of organic compounds,” *Journal of Colloid and Interface Science*, vol. 81, no. 2, pp. 477–485, Jun. 1981, doi: 10.1016/0021-9797(81)90429-X.

[107] H. Ibach, “The relation between the strain-dependence of the heat of adsorption and the coverage dependence of the adsorbate induced surface stress,” *Surface Science*, vol. 556, no. 2–3, pp. 71–77, May 2004, doi: 10.1016/j.susc.2004.03.038.

[108] A. Burneau, J. Lepage, and G. Maurice, “Porous silica-water interactions. I. Structural and dimensional changes induced by water adsorption,” *Journal of Non-Crystalline Solids*, vol. 217, no. 1, pp. 1–10, Aug. 1997, doi: 10.1016/S0022-3093(97)00113-0.

[109] T. S. Jakubov and D. E. Mainwaring, “Adsorption-induced dimensional changes of solids,” *Phys. Chem. Chem. Phys.*, vol. 4, no. 22, pp. 5678–5682, Nov. 2002, doi: 10.1039/b206883d.

[110] G. Y. Gor, P. Huber, and N. Bernstein, “Adsorption-induced deformation of nanoporous materials—A review,” *Applied Physics Reviews*, vol. 4, no. 1, p. 011303, Mar. 2017, doi: 10.1063/1.4975001.

[111] G. Yu. Gor and A. V. Neimark, “Adsorption-Induced Deformation of Mesoporous Solids,” *Langmuir*, vol. 26, no. 16, pp. 13021–13027, Aug. 2010, doi: 10.1021/la1019247.

[112] G. Dolino, D. Bellet, and C. Faivre, “Adsorption strains in porous silicon,” *Phys. Rev. B*, vol. 54, no. 24, pp. 17919–17929, Dec. 1996, doi: 10.1103/PhysRevB.54.17919.

[113] A. A. Fomkin, “Adsorption of Gases, Vapors and Liquids by Microporous Adsorbents,” *Adsorption*, vol. 11, no. 3–4, pp. 425–436, Jul. 2005, doi: 10.1007/s10450-005-5636-x.

[114] C. Boissiere, D. Grosso, S. Lepoutre, L. Nicole, A. B. Bruneau, and C. Sanchez, “Porosity and Mechanical Properties of Mesoporous Thin Films Assessed by Environmental Ellipsometric Porosimetry,” *Langmuir*, vol. 21, no. 26, pp. 12362–12371, Dec. 2005, doi: 10.1021/la050981z.

[115] S. Ash and D. Everet, “Thermodynamics of the EEects of Adsorption on Interparticle Forces,” p. 22.

[116] D. H. Bangham and N. Fakhoury, “The Expansion of Charcoal accompanying Sorption of Gases and Vapours,” *Nature*, vol. 122, no. 3079, Art. no. 3079, Nov. 1928, doi: 10.1038/122681b0.

[117] D. D. Do, *Adsorption analysis: equilibria and kinetics*, no. v 2. Imperial College Press.

[118] Y. Yao and S. Liu, *Ultrasonic Technology for Desiccant Regeneration*. John Wiley & Sons, Incorporated.

[119] S. A. Reinecke and B. E. Sleep, “Knudsen diffusion, gas permeability, and water content in an unconsolidated porous medium,” *Water Resources Research*, vol. 38, no. 12, pp. 16-1-16–15, 2002, doi: 10.1029/2002wr001278.

[120] Y. Yao, “Enhancement of mass transfer by ultrasound: Application to adsorbent regeneration and food drying/dehydration,” *Ultrasonics Sonochemistry*, vol. 31, pp. 512–531, 2016, doi: 10.1016/j.ultsonch.2016.01.039.

[121] N. Kerabchi, S. Merouani, and O. Hamdaoui, “Depth effect on the inertial collapse of cavitation bubble under ultrasound: Special emphasis on the role of the wave attenuation,” *Ultrasonics Sonochemistry*, vol. 48, no. May, pp. 136–150, 2018, doi: 10.1016/j.ultsonch.2018.05.004.

[122] M. Amarillo *et al.*, “Impact of sound attenuation on ultrasound-driven yield improvements during olive oil extraction,” *Ultrasonics Sonochemistry*, vol. 53, no. October 2018, pp. 142–151, 2019, doi: 10.1016/j.ultsonch.2018.12.044.

[123] S. S. Rashwan, I. Dincer, and A. Mohany, “Investigation of acoustic and geometric effects on the sonoreactor performance,” *Ultrasonics Sonochemistry*, vol. 68, no. August 2019, p. 105174, 2020, doi: 10.1016/j.ultsonch.2020.105174.

[124] H. Daghooghi-Mobarakeh *et al.*, “Ultrasound-assisted regeneration of zeolite/water adsorption pair,” *Ultrasonics Sonochemistry*, vol. 64, no. February, p. 105042, 2020, doi: 10.1016/j.ultsonch.2020.105042.

[125] W. Zhang, Y. Yao, and R. Wang, “Influence of ultrasonic frequency on the regeneration of silica gel by applying high-intensity ultrasound,” vol. 30, no. 14, pp. 2080–2087, doi: 10.1016/j.applthermaleng.2010.05.016.

[126] R. E. Cunningham and R. J. J. Williams, *Diffusion in Gases and Porous Media*. 1980. doi: 10.1007/978-1-4757-4983-0.

[127] G. Chen, *Nanoscale energy transport and conversion: a parallel treatment of electrons, molecules, phonons, and photons*. Oxford ; New York: Oxford University Press, 2005.

[128] S. W. Webb and K. Pruess, "The use of Fick's law for modeling trace gas diffusion in porous media," *Transport in Porous Media*, vol. 51, no. 3, pp. 327–341, 2003, doi: 10.1023/A:1022379016613.

[129] I. Medveď and R. Černý, "Surface diffusion in porous media: A critical review," *Microporous and Mesoporous Materials*, vol. 142, no. 2–3, pp. 405–422, 2011, doi: 10.1016/j.micromeso.2011.01.015.

[130] K. Miyabe and G. Guiochon, "Surface diffusion in reversed-phase liquid chromatography," *Journal of Chromatography A*, vol. 1217, no. 11, pp. 1713–1734, 2010, doi: 10.1016/j.chroma.2009.12.054.

[131] K. Miyabe and G. Guiochon, "Influence of the modification conditions of alkyl bonded ligands on the characteristics of reversed-phase liquid chromatography," *Journal of Chromatography A*, vol. 903, no. 1–2, pp. 1–12, 2000, doi: 10.1016/S0021-9673(00)00891-8.

[132] E. R. Gilliland, R. F. Baddour, G. P. Perkinson, and K. J. Sladek, "Diffusion on Surfaces. I. Effect of Concentration on the Diffusivity of Physically Adsorbed Gases," *Industrial & engineering chemistry fundamentals*, vol. 13, no. 2, pp. 95–100, 1974.

[133] K. J. Sladek, E. R. Gilliland, R. F. Baddour, and K. J. Sladek, "Diffusion on Surfaces. II. Correlation of Diffusivities of Physically and Chemically Adsorbed Species," *Industrial and Engineering Chemistry Fundamentals*, vol. 13, no. 2, pp. 100–105, 1974, doi: 10.1021/i160050a002.

[134] A. J. Robell, E. V. Ballou, and M. Boudart, "Surface diffusion of hydrogen on carbon," *Journal of Physical Chemistry*, vol. 68, no. 10, pp. 2748–2753, 1964, doi: 10.1021/j100792a003.

[135] J. Gallego-Juarez and K. Graff, *Power Ultrasonics: Applications of High-Intensity Ultrasound*, 1st Editio. Woodhead Publishing, 2015.

[136] M. Breitbach and D. Bathen, “Influence of ultrasound on adsorption processes,” *Ultrasonics Sonochemistry*, vol. 8, no. 3, pp. 277–283, 2001, doi: 10.1016/S1350-4177(01)00089-X.

[137] H. Daghooghi Mobarakeh, K. Bandara, L. Wang, R. Wang, P. E. Phelan, and M. Miner, “Low-Grade Heat Utilization Through Ultrasound-Enhanced Desorption of Activated Alumina/Water for Thermal Energy Storage,” Aug. 2020. doi: 10.1115/POWER2020-16802.

[138] O. Naji, R. A. Al-juboori, L. Bowtell, A. Alpatova, and N. Ghaffour, “Direct contact ultrasound for fouling control and flux enhancement in air-gap membrane distillation,” *Ultrasonics Sonochemistry*, vol. 61, no. May 2019, 2020, doi: 10.1016/j.ultsonch.2019.104816.

[139] S. Labouret and J. Frohly, “Determination of bubble size distributions in an ultrasonic cavitation field.,” *The Journal of the Acoustical Society of America*, vol. 127, no. 3, p. 1984, 2010, doi: 10.1121/1.3385105.

[140] S. Merouani, O. Hamdaoui, Y. Rezgui, and M. Guemini, “Energy analysis during acoustic bubble oscillations: Relationship between bubble energy and sonochemical parameters,” *Ultrasonics*, vol. 54, no. 1, pp. 227–232, 2014, doi: 10.1016/j.ultras.2013.04.014.

[141] D. Dicaire and F. H. Tezel, “Regeneration and efficiency characterization of hybrid adsorbent for thermal energy storage of excess and solar heat,” *Renewable Energy*, vol. 36, no. 3, pp. 986–992, Mar. 2011, doi: 10.1016/j.renene.2010.08.031.

[142] T. Li, R. Wang, J. K. Kiplagat, and Y. Kang, “Performance analysis of an integrated energy storage and energy upgrade thermochemical solid–gas sorption system for seasonal storage of solar thermal energy,” *Energy*, vol. 50, pp. 454–467, Feb. 2013, doi: 10.1016/j.energy.2012.11.043.

[143] S. Hongois, F. Kuznik, P. Stevens, and J.-J. Roux, “Development and characterisation of a new MgSO4−zeolite composite for long-term thermal energy storage,” *Solar Energy Materials and Solar Cells*, vol. 95, no. 7, pp. 1831–1837, Jul. 2011, doi: 10.1016/j.solmat.2011.01.050.

[144] H. Schreiber, S. Graf, F. Lanzerath, and A. Bardow, “Adsorption thermal energy storage for cogeneration in industrial batch processes: Experiment, dynamic modeling and system analysis,” *Applied Thermal Engineering*, vol. 89, pp. 485–493, Oct. 2015, doi: 10.1016/j.applthermaleng.2015.06.016.

[145] J. Jänchen, D. Ackermann, H. Stach, and W. Brösicke, "Studies of the water adsorption on Zeolites and modified mesoporous materials for seasonal storage of solar heat," *Solar Energy*, vol. 76, no. 1–3, pp. 339–344, Jan. 2004, doi: 10.1016/j.solener.2003.07.036.

[146] Z.-J. Zheng, Y. He, and Y.-L. He, "Optimization for a Thermochemical Energy Storage-reactor based on Entransy Dissipation Minimization," *Energy Procedia*, vol. 75, pp. 1791–1796, Aug. 2015, doi: 10.1016/j.egypro.2015.07.144.

[147] D. Lefebvre, P. Amyot, B. Ugur, and F. H. Tezel, "Adsorption Prediction and Modeling of Thermal Energy Storage Systems: A Parametric Study," *Ind. Eng. Chem. Res.*, vol. 55, no. 16, pp. 4760–4772, Apr. 2016, doi: 10.1021/acs.iecr.5b04767.

[148] D. Dicaire and F. H. Tezel, "Use of adsorbents for thermal energy storage of solar or excess heat: improvement of energy density: Improvement of energy density for adsorption thermal energy storage," *Int. J. Energy Res.*, vol. 37, no. 9, pp. 1059–1068, Jul. 2013, doi: 10.1002/er.2913.

[149] Y. Gupta, L. Metchop, A. Frantzis, and P. E. Phelan, "Comparative analysis of thermally activated, environmentally friendly cooling systems," *Energy Conversion and Management*, vol. 49, no. 5, pp. 1091–1097, May 2008, doi: 10.1016/j.enconman.2007.09.016.

[150] M. M. Dubinin, E. D. Zaverina, L. V. Radushkevich, "Sorption and Structure of Active Carbons I. Adsorption of Organic Vapors," vol. 21, pp. 1351–1362, 1947.

[151] Y. Teng, R. Z. Wang, and J. Y. Wu, "Study of the fundamentals of adsorption systems," *Applied Thermal Engineering*, vol. 17, no. 4, pp. 327–338, Apr. 1997, doi: 10.1016/S1359-4311(96)00039-7.

[152] D. Ferreira, M. Boaventura, P. Bárcia, R. D. Whitley, and A. Mendes, "Two-Stage Vacuum Pressure Swing Adsorption Using AgLiLSX Zeolite for Producing 99.5+% Oxygen from Air," *Ind. Eng. Chem. Res.*, vol. 55, no. 3, pp. 722–736, Jan. 2016, doi: 10.1021/acs.iecr.5b03535.

[153] B. Besser *et al.*, "Hierarchical Porous Zeolite Structures for Pressure Swing Adsorption Applications," *ACS Appl. Mater. Interfaces*, vol. 8, no. 5, pp. 3277–3286, Feb. 2016, doi: 10.1021/acsami.5b11120.